UNIVERSITAT POLITÈCNICA DE VALÈNCIA

ETSI Aeroespacial y Diseño Industrial

UNIVERSITAT POLITÈCNICA DE VALÈNCIA

School of Aerospace Engineering and Industrial Design

Preliminary Analysis of thermonuclear propulsion for manned missions to Mars

End of Degree Project

Bachelor's Degree in Aerospace Engineering

AUTHOR: Santos Pino, Jose Enrique

Tutor: Moll López, Santiago Emmanuel

Cotutor: Moraño Fernández, José Antonio

External cotutor: Pino Ortega, Juan Manuel

ACADEMIC YEAR: 2023/2024

Abstract

The purpose of this project is to present a first approach to the possibilities of thermonuclear propulsion for transfer orbits between Earth and Mars.
Firstly, the method of patched conics will be employed. All Delta-V maneuvers will be considered instantaneous, and perturbations will be neglected.
Secondly, the different transfer orbits will be obtained by solving Lambert's problem, including the Hohmann transfer as the most energy efficient. The project will analyze the Delta-V requirements necessary to perform these transfer orbits. Data regarding the thermonuclear engine performance, reactor cinematics, and proportional controller will be based on the results achieved in the NERVA project.

Resumen

El propósito de este proyecto es presentar un primer enfoque sobre las posibilidades de la propulsión termonuclear para órbitas de transferencia entre la Tierra y Marte.
En primer lugar, se empleará el método de las cónicas enlazadas, todas las maniobras de Delta-V se considerarán instantáneas y se despreciarán las perturbaciones.
En segundo lugar, se obtendrán las diferentes órbitas de transferencia resolviendo el problema de Lambert, incluyendo la transferencia de Hohmann como la más eficiente en términos de energía. El proyecto analizará los requisitos de Delta-V necesarios para realizar estas órbitas de transferencia. Los datos sobre el rendimiento del motor termonuclear, la cinemática del reactor y el controlador proporcional se basarán en los resultados alcanzados en el proyecto NERVA.

Acknowledgments

En primer lugar, quiero darle las gracias a mi tutor, Santiago Emmanuel Moll López, y a mi co-tutor, Juan Manuel Pino Ortega. Sin la ayuda de ellos, este trabajo no habría sido posible.

Quiero también agradecer a mi madre, a Julián y a mi abuela, han sido ellos quienes me han acompañado y aguantado durante todo este proyecto.

Por último, quiero darles las gracias a mis amigos Javier y Jorge, por todos sus consejos y recomendaciones, sin ellos, todo este trabajo habría sido mucho más difícil.

Contents

List of Figures

List of Tables

Chapter 1

Introduction

The current aerospace industry faces large limitations in the propulsion field, especially when considering a manned mission to Mars. There is the need of a propulsion system capable of combining the large thrust-weight ratios obtained with chemical rocket engines but with a specific impulse comparable to ionic propulsion.

For this project, a stirling based thermonuclear propulsion is presented as a candidate for this concept of rocket engine and applied for a manned mission to Mars. Similarly to chemical engines, the propellant is heated and then, it exits through the nozzle. The difference arises in the heating process and the composition of the propellant.

The propellant is contained in a near adiabatic storage tank (to avoid heat losses to the exterior) and it is heated by the use of electric heaters based on induced magnetic fields. These heaters are powered by the nuclear reactor, based on a PWR (Pressurized Water Reactor) design, with the difference that the moderator and refrigerant is hydrogen gas instead of water. Once the propellant reaches the adequate temperature, a set of valves open and the working gas exits through the nozzle and, therefore, producing thrust in the process.

Stirling engines are employed to convert the thermal energy produced in the nuclear reactor, to mechanical energy. With the use of an alternator, this mechanical energy is converted into electricity with a relatively high efficiency.

Additionally, the scope of this project is also to expand the thermonuclear rocket engines developed in the NERVA project and study the possibilities of reaching similar specific impulses to the ones achieved in the NERVA project (800-900 s), with the concept of a thermonuclear propulsion rocket engine based on a hydrogen modified PWR power plant, using stirling engines coupled with alternators.

1.1 Project structure

The project is structured in 4 parts:

- Mission design: Chapters 2, 3 and 4. The second chapter sets the physical background of orbital mechanics, the third chapter defines a Hohmann transfer from Earth to Mars and the fourth chapter presents a total of 40,000 transfers from Earth to Mars by using the Lambert problem.

- Nuclear reactor and kinematics: Chapters 5 and 6. The fifth chapter is an introduction to pressurized water reactors (PWR) and their different working components, and chapter 6 presents the nuclear kinematics taking place inside the reactor.
- Aerospace thermonuclear propulsion history: Chapter 7. This chapter presents the historical background of the thermonuclear propulsion efforts in the aerospace industry along history.
- Stirling thermonuclear propulsion: Chapters 8 and 9. The eight chapter presents the thermodynamic background regarding stirling engines and the working principle of the electric heaters. Whereas, chapter 9 defines some important propulsive parameters, their relation with the Delta-V obtained in the mission design chapters and conclusions. Specifically, the conclusions include some important concepts such as the environmental impacts, an estimate cost, the percentage of propellant mass needed and a parametric study of some important parameters with some final thoughts.

Chapter 2

Orbit determination

2.1 Introduction

This chapter presents a method based on the universal variable formulation to calculate the position and velocity vectors of the Earth and Mars orbits for different time instants. Furthermore, an alternative method is also presented based on ode45, a matlab algorithm capable of solving differential equations.

Before presenting the methods, it is necessary to define the equation that describes the acceleration of an orbit:

$$\ddot{\boldsymbol{r}}_{abs} = \ddot{\boldsymbol{r}}_{rel} + \dot{\boldsymbol{\Omega}} \times \boldsymbol{r} + \boldsymbol{\Omega} \times (\boldsymbol{\Omega} \times \boldsymbol{r}) + 2\boldsymbol{\Omega} \times \dot{\boldsymbol{r}}_{rel} \tag{2.1}$$

where $\ddot{\boldsymbol{r}}_{abs}$ is the absolute acceleration, $\ddot{\boldsymbol{r}}_{rel}$ is the relative acceleration, $\boldsymbol{\Omega}$ and $\dot{\boldsymbol{\Omega}}$ are the angular velocity and angular acceleration respectively and $\boldsymbol{r}$ is the position vector.

Based on the hypothesis presented in chapter 1, the reference frame will be fixed and therefore the angular velocity and its acceleration will be zero. Therefore, equation (2.1) becomes:

$$\ddot{\boldsymbol{r}}_{abs} = \ddot{\boldsymbol{r}}_{rel} = -\frac{\mu}{r^3}\boldsymbol{r} \tag{2.2}$$

where μ is the gravitational parameter and r is the magnitude of the position vector.

Given the velocity and position of a point in a given orbit, equation (2.2) can be solved by employing the Lagrange coefficients or any differential equation solver such as ode45.

The starting points for both Earth and Mars trajectories are obtained from Horizons system [6] in heliocentric ecliptic coordinates (see Appendix A.1). The initial date has been chosen arbitrary, starting at first of January of 2030.

Position (km)	X	Y	Z
Earth	$-2.600 \cdot 10^7$	$1.448 \cdot 10^8$	$-9.532 \cdot 10^3$
Mars	$1.913 \cdot 10^8$	$-7.798 \cdot 10^7$	$-6.324 \cdot 10^6$

Table 2.1: Position(km) of Earth and Mars on 01/01/2030, from Horizons system [6].

Velocity (km/s)	X	Y	Z
Earth	$-2.982 \cdot 10$	-5.371	$-5.573 \cdot 10^{-4}$
Mars	$1.007 \cdot 10$	$2.451 \cdot 10$	$2.669 \cdot 10^{-1}$

Table 2.2: Velocity(km/s) of Earth and Mars on 01/01/2030, from Horizons system [6].

2.2 Ode 45

2.2.1 Algorithm

The ode45 solver is based on the Runge-Kutta method of order 4 and 5 with a variable time step. It is designed to solve equations in the form of:

$$\frac{dx}{dt} = f(t, x) \tag{2.3}$$

Equation (2.3) is a first order differential equation, it is needed to express equation (2.2) which is a second order differential equation in the form of a first order.

Equation (2.2) can be expressed as:

$$\frac{d}{dt}\begin{Bmatrix} x \\ \dot{x} \\ y \\ \dot{y} \\ z \\ \dot{z} \end{Bmatrix} = \begin{Bmatrix} \dot{x} \\ \frac{\mu}{r^3}x \\ \dot{y} \\ \frac{\mu}{r^3}y \\ \dot{z} \\ \frac{\mu}{r^3}z \end{Bmatrix} \tag{2.4}$$

The following change of variables can be applied to (2.4), obtaining (2.6):

$$\begin{Bmatrix} x \\ \dot{x} \\ y \\ \dot{y} \\ z \\ \dot{z} \end{Bmatrix} = \begin{Bmatrix} y(1) \\ y(2) \\ y(3) \\ y(4) \\ y(5) \\ y(6) \end{Bmatrix} \tag{2.5}$$

$$\frac{d}{dt}\begin{Bmatrix} y(1) \\ y(2) \\ y(3) \\ y(4) \\ y(5) \\ y(6) \end{Bmatrix} = \begin{Bmatrix} y(2) \\ \frac{\mu}{r^3}y(1) \\ y(4) \\ \frac{\mu}{r^3}y(3) \\ y(6) \\ \frac{\mu}{r^3}y(5) \end{Bmatrix} \tag{2.6}$$

Moreover, the magnitude of the position vector can be defined as:

$$r = \sqrt{y(1)^2 + y(3)^2 + y(5)^2} \tag{2.7}$$

2.2.2 Earth and Mars orbits

Once the equation (2.2) is expressed as a first order differential equation (2.6), the ode45 solver can be implemented.
Using the position and velocity obtained from JPL Horizons for Earth and Mars on the first of January of 2030, both orbits can be determined.

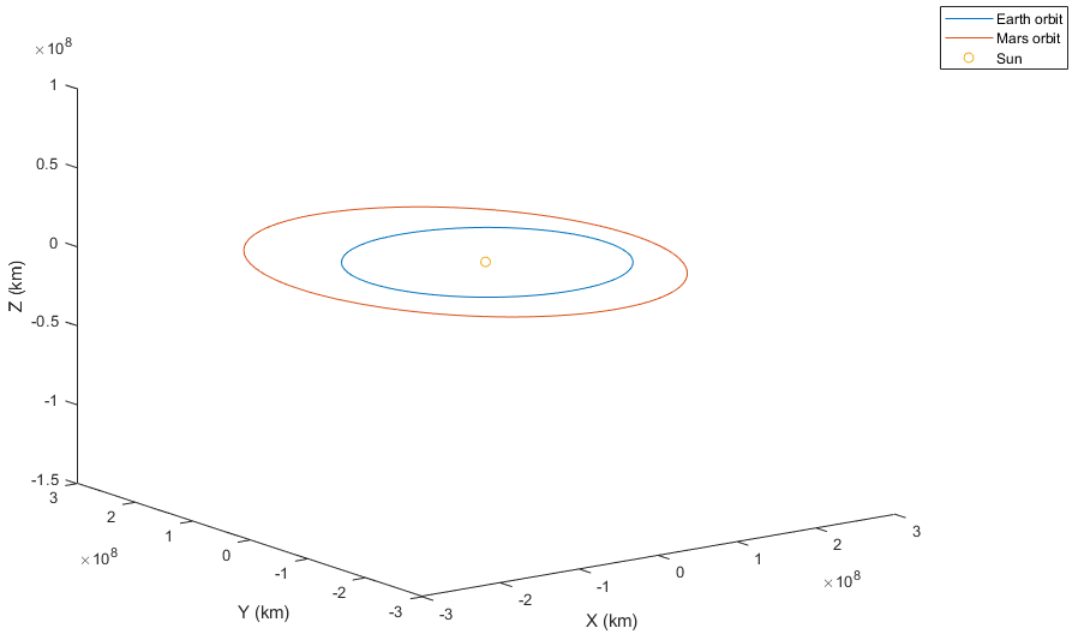

Figure 2.1: Mars and Earth orbits, obtained by ode45 solver.

2.3 Lagrange coefficients method

The following section will propose a step by step procedure of obtaining the Lagrange coefficients as a function of the universal anomaly χ and its implementation in an algorithm to determine the Earth and Mars orbital parameters, the procedure employed is based on the one presented in H.D. Curtis [30] and Vallado [58].

2.3.1 Lagrange coefficients

Given an elliptical orbit around the Earth, any point of the orbit has a velocity and a position vector that can be defined as:

$$\begin{aligned} \boldsymbol{r} &= x\hat{\boldsymbol{i}} + y\hat{\boldsymbol{j}} + z\hat{\boldsymbol{k}} \\ \boldsymbol{v} &= \dot{x}\hat{\boldsymbol{i}} + \dot{y}\hat{\boldsymbol{j}} + \dot{z}\hat{\boldsymbol{k}} \end{aligned} \tag{2.8}$$

Where $\hat{\boldsymbol{i}}, \hat{\boldsymbol{j}}, \hat{\boldsymbol{k}}$ are the unitary vectors in the X,Y,Z direction in geocentric coordinates.

However, a topocentric coordinate system will be selected as it allows to greatly simplify the process of obtaining the Lagrange coefficients.
Equation 2.8 for an initial point in topocentric coordinates now becomes:

$$\begin{aligned} \boldsymbol{r} &= x\hat{\boldsymbol{p}} + y\hat{\boldsymbol{q}} \\ \boldsymbol{v} &= \dot{x}\hat{\boldsymbol{p}} + \dot{y}\hat{\boldsymbol{q}} \end{aligned} \tag{2.9}$$

where now $\hat{\boldsymbol{p}}, \hat{\boldsymbol{q}}, \hat{\boldsymbol{w}}$ are the unitary vectors corresponding to the topocentric coordinates.
Defining equation (2.9) for an initial time interval, t_0:

$$\begin{aligned} \boldsymbol{r}_0 &= x_0\hat{\boldsymbol{p}} + y_0\hat{\boldsymbol{q}} \\ \boldsymbol{v}_0 &= \dot{x}_0\hat{\boldsymbol{p}} + \dot{y}_0\hat{\boldsymbol{q}} \end{aligned} \tag{2.10}$$

Equation (2.10) can be solved for $\hat{\boldsymbol{p}}, \hat{\boldsymbol{q}}$:

$$\begin{aligned} \hat{\boldsymbol{p}} &= -\frac{\boldsymbol{v}_0 y_0 + \boldsymbol{r}_0 \dot{y}_0}{\dot{x}_0 y_0 - x_0 \dot{y}_0} \\ \hat{\boldsymbol{q}} &= -\frac{\boldsymbol{v}_0 x_0 - \boldsymbol{r}_0 \dot{x}_0}{\dot{x}_0 y_0 - x_0 \dot{y}_0} \end{aligned} \tag{2.11}$$

Equation (2.11) can be simplified by introducing the specific angular momentum, which is constant along the orbit:

$$\boldsymbol{h} = \boldsymbol{r}_0 \times \boldsymbol{v}_0 = \begin{vmatrix} \hat{\boldsymbol{p}} & \hat{\boldsymbol{q}} & \hat{\boldsymbol{w}} \\ x_0 & y_0 & 0 \\ \dot{x}_0 & \dot{y}_0 & 0 \end{vmatrix} = \hat{\boldsymbol{w}}\left(x_0\dot{y}_0 - \dot{x}_0 y_0\right) \tag{2.12}$$

The magnitude of the specific angular momentum becomes:

$$h = \left(x_0\dot{y}_0 - \dot{x}_0 y_0\right) \tag{2.13}$$

The expression of specific angular momentum (2.13) can be solved for $\boldsymbol{x}_0$ and for $\boldsymbol{y}_0$:

$$\boldsymbol{x}_0 = \frac{-h + x_0\dot{y}_0}{y_0} \tag{2.14}$$

$$\boldsymbol{y}_0 = \frac{h + y_0\dot{x}_0}{x_0} \tag{2.15}$$

Substituting (2.14) in equation (2.11) for $\hat{\boldsymbol{p}}$ and respectively substituting (2.15) in $\hat{\boldsymbol{q}}$, yields:

$$\hat{\boldsymbol{p}} = \frac{\dot{y}_0\boldsymbol{r}_0 - y_0\boldsymbol{v_0}}{h} \tag{2.16}$$

$$\hat{\boldsymbol{q}} = \frac{-\dot{x}_0\boldsymbol{r}_0 + x_0\boldsymbol{v_0}}{h} \tag{2.17}$$

By substituting equations (2.16) and (2.17) in equation (2.9) and isolating the terms $\boldsymbol{r}_0$ and $\boldsymbol{v}_0$:

$$\begin{aligned} \boldsymbol{r} &= \left(\frac{x\dot{y}_0 - y\dot{x}_0}{h}\right)\boldsymbol{r}_0 + \left(\frac{-y_0 x + x_0 y}{h}\right)\boldsymbol{v}_0 = f\boldsymbol{r}_0 + g\boldsymbol{v}_0 \\ \dot{\boldsymbol{r}} &= \left(\frac{\dot{x}\dot{y}_0 - \dot{y}\dot{x}_0}{h}\right)\boldsymbol{r}_0 + \left(\frac{-y_0\dot{x} + x_0\dot{y}}{h}\right)\boldsymbol{v}_0 = \dot{f}\boldsymbol{r}_0 + \dot{g}\boldsymbol{v}_0 \end{aligned} \tag{2.18}$$

where $f, g, \dot{f}, \dot{g}$ are the Lagrange coefficients as a function of the velocity and position of an initial point at time t_0 and another point at time t:

$$\begin{aligned} f &= \frac{x\dot{y}_0 - y\dot{x}_0}{h} \\ g &= \frac{-y_0 x + x_0 y}{h} \\ \dot{f} &= \frac{\dot{x}\dot{y}_0 - \dot{y}\dot{x}_0}{h} \\ \dot{g} &= \frac{-y_0\dot{x} + x_0\dot{y}}{h} \end{aligned} \tag{2.19}$$

However, they are neither functions of the true anomaly, θ, nor the time, which will be needed later to determine the orbital parameters.

Therefore, the first step will be to obtain the coefficients as a function of the variation in the true anomaly. To do so, we start by defining the X and Y components and their time derivatives for a topocentric coordinate system:

$$x_0 = r_0 \cos(\theta_0) \tag{2.20}$$

$$y_0 = r_0 \sin(\theta_0) \tag{2.21}$$

$$\dot{x}_0 = \dot{r}_0 \cos(\theta_0) - r_0 \sin(\theta_0)\dot{\theta}_0 \tag{2.22}$$

$$\dot{y}_0 = \dot{r}_0 \sin(\theta_0) + r_0 \cos(\theta_0)\dot{\theta}_0 \tag{2.23}$$

To simplify equations (2.22) and (2.23), it is necessary to define the radial and perpendicular components of the velocity vector:

$$v_r = \dot{r} = \frac{d}{dt}\left(\frac{h^2}{\mu}\frac{1}{1 + e\cos(\theta)}\right) = \frac{\mu}{h} e \sin(\theta) \tag{2.24}$$

$$v_\perp = \dot{\theta} r = \frac{h}{r} = \frac{mu}{h}\left(1 + e\cos(\theta)\right) \tag{2.25}$$

Particularizing equations (2.24) and (2.25) for an initial time interval and solving for $\dot{r}$ and $\dot{\theta}$:

$$\dot{r} = \frac{\mu}{h} e \sin(\theta_0) \tag{2.26}$$

$$\dot{\theta}_0 = \frac{\mu^2}{h^3}\left(1 + e\cos(\theta_0)\right)^2 \tag{2.27}$$

Substuting the values of $\dot{r}$ and $\dot{\theta}$ in the equations (2.22) and (2.23) yields:

$$\dot{x}_0 = -\frac{\mu}{h}\sin(\theta_0) \tag{2.28}$$

$$\dot{y}_0 = \frac{\mu}{h}\left(e + \cos(\theta_0)\right) \tag{2.29}$$

Equations (2.22), (2.23), (2.28) and (2.29) can be particularized for any time interval:

$$x = r\cos(\theta) \tag{2.30}$$
$$y = r\sin(\theta) \tag{2.31}$$
$$\dot{x} = -\frac{\mu}{h}\sin(\theta) \tag{2.32}$$
$$\dot{y} = \frac{\mu}{h}\left(e + \cos(\theta)\right) \tag{2.33}$$

Finally, substituting by equations (2.30), (2.31), (2.32), (2.33) for a given time t and an initial time t_0 in (2.19) and applying trigonometric identities and equation (B.3) from appendix B.1, allows to obtain the Lagrange coefficients as a function of the variation in the true anomaly:

$$\begin{aligned} f &= 1 - \frac{\mu r\left(1 - \cos(\Delta\theta)\right)}{h^2} \\ g &= \frac{r r_0 \sin(\Delta\theta)}{h} \\ \dot{f} &= \frac{\mu}{h}\frac{1 - \cos(\Delta\theta)}{\sin(\Delta\theta)}\left(\frac{\mu\left(1 - \cos(\Delta\theta)\right)}{h^2} - \frac{1}{r_0} - \frac{1}{r}\right) \\ \dot{g} &= 1 - \frac{\mu r_0\left(1 - \cos(\Delta\theta)\right)}{h^2} \end{aligned} \tag{2.34}$$

The next step is to find the relationship between the true anomaly and time.
Equation (2.27) is particularized for any time interval t:

$$\dot{\theta} = \frac{d\theta}{dt} = \frac{h}{r^2} = \frac{\mu^2}{h^3}\left(1 + e\cos(\theta)\right)^2 \tag{2.35}$$

Separating the variables and integrating equation (2.35):

$$\int_{t_p}^{t} dt = \frac{h^3}{\mu^2}\int_{\theta_0}^{\theta} \frac{d\theta}{\left(1 + e\cos(\theta)\right)^2} \tag{2.36}$$

$$t - t_p = \frac{h^3}{\mu^2}\int_{\theta_0}^{\theta} \frac{d\theta}{\left(1 + e\cos(\theta)\right)^2} \tag{2.37}$$

where t_p is the time since the periapsis.

Equation (2.37) relates the true anomaly with time, this integration will allow to define the mean anomaly for the different conic sections.

2.3.2 Lagrange coefficient particularized for different conic sections

For this subsection, the mean anomaly for elliptic, parabolic and hyperbolic orbits will be defined as well as the eccentric anomaly. This will be achieved by employing equation (2.37), particularizing its solution based on the value of the eccentricity and employing the solution presented in D.Zwillinger [94], a mathematics book which contains standard tables and formulas.

The X and Y topocentric coordinates will be defined as a function of the eccentric anomaly, and following the same procedure presented in the last subsection, the Lagrange coefficients will

become a function of the variation in the eccentric anomaly for the different conic sections.

This will lead to the following scheme:

Figure 2.2: Relationship between time and the Lagrange coefficients.

Given an initial increment in time, dt, and knowing the initial position and velocity (and therefore the eccentricity of the orbit) another differential increment for the mean anomaly can be calculated from which the eccentric anomaly will be obtained, allowing to define the Lagrange coefficients for each specific conic section.
With this procedure the orbital parameters can be calculated.

Nevertheless, the Lagrange coefficients will be specific for each conic section, meaning that the eccentricity must be known in order to implement this process. In contrast, if a universal variable valid for all conic sections is defined, it is no longer needed to determine the type of orbit, as there will be only one set of equations covering all orbits, reducing computational costs.

2.3.2.1 Elliptic orbit

In the case of an elliptic orbit, the equation (2.37) becomes:

$$\begin{aligned} t - t_p = \frac{h^3}{\mu^2} \frac{1}{(1-e^2)^{\frac{3}{2}}} \Bigg[\Bigg[2 \arctan\left(\sqrt{\frac{1-e}{1+e}} \tan\left(\frac{\theta}{2}\right) \right) - \frac{e\sqrt{1-e^2}\sin(\theta)}{1+e\cos(\theta)} \Bigg] \\ - \left[2 \arctan\left(\sqrt{\frac{1-e}{1+e}} \tan\left(\frac{\theta_0}{2}\right) \right) - \frac{e\sqrt{1-e^2}\sin(\theta_0)}{1+e\cos(\theta_0)} \right] \Bigg] \end{aligned} \tag{2.38}$$

Equation (2.38) can be simplified if the starting point is considered to be the periapsis:

$$t = \frac{h^3}{\mu^2} \frac{1}{(1-e^2)^{\frac{3}{2}}} \left[2 \arctan\left(\sqrt{\frac{1-e}{1+e}} \tan\left(\frac{\theta}{2}\right) \right) - \frac{e\sqrt{1-e^2}\sin(\theta)}{1+e\cos(\theta)} \right] \tag{2.39}$$

As the objective is to calculate the Lagrange coefficients for any given initial point in the conic section, this simplification, equation (2.39), will not be considered.
From equation (2.38) the mean anomaly for an elliptic orbit, M_e, is defined:

$$M_e = \left[2 \arctan\left(\sqrt{\frac{1-e}{1+e}} \tan\left(\frac{\theta}{2}\right) \right) - \frac{e\sqrt{1-e^2}\sin(\theta)}{1+e\cos(\theta)} \right] \tag{2.40}$$

$$M_{e_0} = \left[2 \arctan\left(\sqrt{\frac{1-e}{1+e}} \tan\left(\frac{\theta_0}{2}\right) \right) - \frac{e\sqrt{1-e^2}\sin(\theta_0)}{1+e\cos(\theta_0)} \right] \tag{2.41}$$

Returning to equation (2.38) and introducing the mean anomaly:

$$t - t_p = \frac{h^3}{\mu^2} \frac{M_e - M_{e_0}}{(1-e^2)^{\frac{3}{2}}} \tag{2.42}$$

The mean anomaly is now a function of time, the next step is to determine the eccentric anomaly.

From figure (2.3), the eccentric anomaly can be defined as the angle between the apse line and a vector that goes from the origin towards any point of a circumference whose radius is the semi-major axis and is centered at the origin. Therefore:

$$a\cos(E) = ae + r\cos(\theta) \tag{2.43}$$

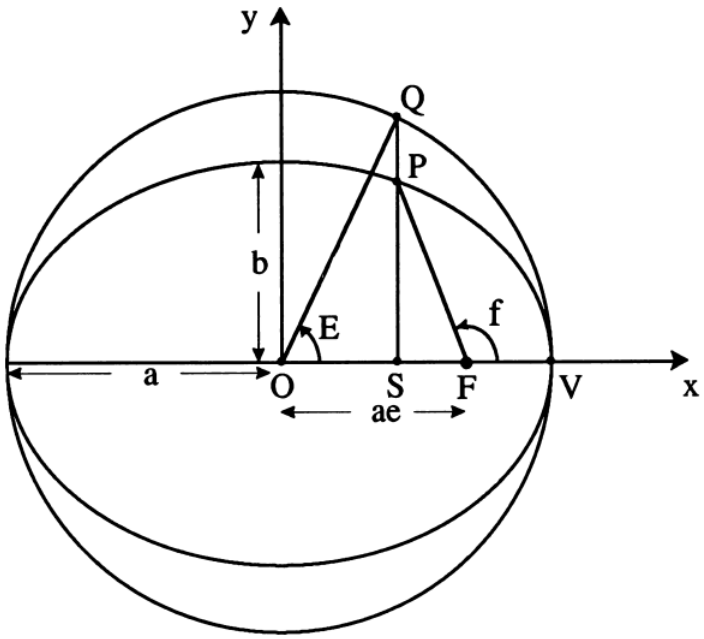

Figure 2.3: Eccentric anomaly. Source: Conway: [68].

The relationship between eccentric anomaly and mean anomaly is given by:

$$M_e = E - e\sin(E) \tag{2.44}$$

$$M_{e_0} = E_0 - e\sin(E_0) \tag{2.45}$$

Expressing the eccentric anomaly as a function of time:

$$(E - e\sin(E)) - (E_0 - e\sin(E_0)) = (t - t_p)\left(1 - e^2\right)^{\frac{3}{2}} \tag{2.46}$$

From equation (2.43) a set of relationships can be obtained:

$$r\cos(\theta) = a\left(\cos(E) - e\right) \tag{2.47}$$

$$\cos(E) = \frac{r\cos(\theta)}{a} + e = \frac{\cos(\theta + e}{1 + e\cos(\theta)} \tag{2.48}$$

$$\sin(E) = \frac{\sqrt{1 - e^2}\sin(\theta)}{1 + e\cos(\theta)} \tag{2.49}$$

Introducing equations (2.47) and (2.49) into the X and Y coordinates for the topocentric reference frame, it can be obtained:

$$x = a\left(\cos(E) - e\right) \tag{2.50}$$

$$y = \frac{h^2}{\mu}\frac{\sin(\theta)}{1 + e\cos(\theta)} = \frac{h^2}{\mu}\frac{\sin(E)}{\sqrt{1 - e^2}} \tag{2.51}$$

From equation (2.51), if the equation of the semi-major axis is introduced:

$$a = \frac{h^2}{\mu}\frac{1}{1 - e^2} \tag{2.52}$$

$$y = a\sqrt{1 - e^2}\sin(E) \tag{2.53}$$

Whereas, for the time derivatives of (2.50) and (2.53):

$$\dot{x} = -a\sin(E)\dot{E} \tag{2.54}$$

$$y = a\dot{E}\cos(E)\sqrt{1 - e^2} \tag{2.55}$$

$$\frac{dE}{dt} = \frac{1}{r}\sqrt{\frac{\mu}{a}} \tag{2.56}$$

Performing a similar procedure as for (2.34) and using equation (2.46), the Lagrange coefficients are obtained as a function of the variation in the eccentric anomaly:

$$\begin{aligned} f &= 1 - \frac{a\left(1 - \cos(\Delta E)\right)}{r_0} \\ g &= (t - t_p) - \sqrt{\frac{a^3}{\mu}}\left(\Delta E - \sin(\Delta E)\right) \\ \dot{f} &= \frac{-\sin(\Delta E)\sqrt{\mu a}}{r_0 r} \\ \dot{g} &= 1 - \frac{a}{r}\left(1 - \cos(\Delta E)\right) \end{aligned} \tag{2.57}$$

Given an initial point whose velocity and position are known, the orbit can be determined by using the set of Lagrange coefficients obtained in (2.57) and following the next steps:

- Step 1: Calculate the semi-major axis, the eccentricity, the initial true anomaly and the period of the orbit.
- Step 2: Calculate the initial mean anomaly and then the initial eccentric anomaly, with equations (2.41) and (2.45) respectively.
- Step 3: Define a time vector that goes from: $[t_0 : \Delta t : T]$, where Δt refers to the step increment and T is the period of the orbit.
- Step 4: Repeat Step 2 for each increment in time in an iterative process.
- Step 5: In each iteration of step 4 calculate the Lagrange coefficients and then employ the following equations:

$$\begin{aligned} r &= f r_0 + g v_0 \\ v &= \dot{f} r_0 + \dot{g} v_0 \end{aligned} \tag{2.58}$$

- Step 6: Store the values of the position and velocity in each iteration.

2.3.2.2 Parabolic orbit

For parabolic orbits, the procedure to obtain the mean anomaly is the same as in the elliptic orbits with the difference that now the eccentricity is 1, and the solution from (2.39) will be different.

$$t - t_p = \frac{h^3}{\mu^2}\left[\left[\frac{1}{2}\tan\left(\frac{\theta}{2}\right) + \frac{1}{6}\tan^3\left(\frac{\theta}{2}\right)\right] - \left[\frac{1}{2}\tan\left(\frac{\theta_0}{2}\right) + \frac{1}{6}\tan^3\left(\frac{\theta_0}{2}\right)\right]\right] \tag{2.59}$$

With the solution of the integral, equation (2.59), the mean anomaly for any given time in the orbit (M_p) and its initial value (M_{p_0}) are equal to:

$$M_p = \frac{1}{2}\tan\left(\frac{\theta}{2}\right) + \frac{1}{6}\tan^3\left(\frac{\theta}{2}\right) \tag{2.60}$$

$$M_{p_0} = \frac{1}{2}\tan\left(\frac{\theta_0}{2}\right) + \frac{1}{6}\tan^3\left(\frac{\theta_0}{2}\right) \tag{2.61}$$

$$t - t_p = \frac{h^3}{\mu^2}\left(M_p - M_{p_0}\right) \tag{2.62}$$

The parabolic anomaly (B), analogous to the eccentric anomaly for the ellipse, is calculated as a function of the true anomaly:

$$B = \tan\left(\frac{\theta}{2}\right) \tag{2.63}$$

$$\cos(\theta) = \frac{1 - B^2}{1 + B^2} \tag{2.64}$$

$$\sin(\theta) = \frac{2B}{1 + B^2} \tag{2.65}$$

The relationship between the parabolic anomaly and the mean anomaly is calculated by using equation (2.62):

$$\frac{h^3}{\mu^2}\left(M_p - M_{p_0}\right) = \frac{h^3}{\mu^2}\left[\left(\frac{1}{2}B + \frac{1}{6}B^3\right) - \left(\frac{1}{2}B_0 + \frac{1}{6}B_0^3\right)\right] = t - t_p \tag{2.66}$$

$$\left(\frac{1}{2}B + \frac{1}{6}B^3\right) - \left(\frac{1}{2}B_0 + \frac{1}{6}B_0^3\right) = M_p - M_{p_0} \tag{2.67}$$

The next step is to determine the Lagrange coefficients, this is achieved by expressing the X and Y coordinates as a function of the parabolic anomaly. To do so, equations (2.64) and (2.65) are substituted into (2.30), (2.31), (2.32) and (2.33).

$$x = \frac{h^2}{\mu 2}\left(1 - B^2\right) \tag{2.68}$$

$$y = \frac{h^2}{\mu} B \tag{2.69}$$

$$\dot{x} = -\sqrt{\frac{h^2}{\mu}}\frac{B}{r} \tag{2.70}$$

$$\dot{y} = \frac{h}{r} \tag{2.71}$$

Finally, with the same procedure employed in (2.34), the Lagrange coefficients are calculated as a function of the parabolic anomaly (B):

$$\begin{aligned} f &= \frac{1 - B^2 + 2BB_0}{1 + B_0^2} \\ g &= \frac{h^4}{\mu^2}\frac{\Delta B\left(1 + BB_0\right)}{2h} \\ \dot{f} &= \frac{\mu^2}{h^3}\frac{4\Delta B}{\left(1 + B^2\right)\left(1 + B_0^2\right)} \\ \dot{g} &= \frac{1 - B_0^2 + 2BB_0}{1 + B^2} \end{aligned} \tag{2.72}$$

2.3.2.3 Hyperbolic orbit

For a hyperbolic orbit, the eccentricity is greater than 1 and the integration in (2.39) yields a different results than in the two previous cases for the ellipse and the parabola:

$$\begin{aligned} t - t_p = \frac{1}{\left(e^2 - 1\right)^{\frac{3}{2}}}\Bigg[\Bigg[\frac{e\sqrt{e^2 - 1}\sin(\theta)}{1 + e\cos(\theta)} - \ln\left(\frac{\sqrt{e+1} + \sqrt{e-1}\tan\left(\frac{\theta}{2}\right)}{\sqrt{e+1} - \sqrt{e-1}\tan\left(\frac{\theta}{2}\right)}\right)\Bigg] \\ - \Bigg[\frac{e\sqrt{e^2 - 1}\sin(\theta_0)}{1 + e\cos(\theta_0)} - \ln\left(\frac{\sqrt{e+1} + \sqrt{e-1}\tan\left(\frac{\theta_0}{2}\right)}{\sqrt{e+1} - \sqrt{e-1}\tan\left(\frac{\theta_0}{2}\right)}\right)\Bigg]\Bigg] \end{aligned} \tag{2.73}$$

By expanding the terms in equation (2.73), the following expression is achieved:

$$\begin{aligned} t - t_p = \frac{1}{\left(e^2 - 1\right)}\Bigg[\Bigg[\frac{e\sin(\theta)}{1 + e\cos(\theta)} - \frac{1}{\sqrt{e^2 - 1}}\ln\left(\frac{\sqrt{e+1} + \sqrt{e-1}\tan\left(\frac{\theta}{2}\right)}{\sqrt{e+1} - \sqrt{e-1}\tan\left(\frac{\theta}{2}\right)}\right)\Bigg] \\ - \Bigg[\frac{e\sin(\theta_0)}{1 + e\cos(\theta_0)} - \frac{1}{\sqrt{e^2 - 1}}\ln\left(\frac{\sqrt{e+1} + \sqrt{e-1}\tan\left(\frac{\theta_0}{2}\right)}{\sqrt{e+1} - \sqrt{e-1}\tan\left(\frac{\theta_0}{2}\right)}\right)\Bigg]\Bigg] \end{aligned} \tag{2.74}$$

From equation (2.74) the mean anomaly for an hyperbolic orbit is defined.

$$M_h = \frac{e\sin(\theta)}{1+e\cos(\theta)} - \frac{1}{\sqrt{e^2-1}}\ln\left(\frac{\sqrt{e+1}+\sqrt{e-1}\tan\left(\frac{\theta}{2}\right)}{\sqrt{e+1}-\sqrt{e-1}\tan\left(\frac{\theta}{2}\right)}\right) \tag{2.75}$$

$$M_{h_0} = \frac{e\sin(\theta_0)}{1+e\cos(\theta_0)} - \frac{1}{\sqrt{e^2-1}}\ln\left(\frac{\sqrt{e+1}+\sqrt{e-1}\tan\left(\frac{\theta_0}{2}\right)}{\sqrt{e+1}-\sqrt{e-1}\tan\left(\frac{\theta_0}{2}\right)}\right) \tag{2.76}$$

$$t - t_p = \frac{1}{e^2-1}\left(M_h - M_{h_0}\right) \tag{2.77}$$

The hyperbolic anomaly (F), analogous to the eccentric anomaly for the elliptic orbit, is defined by:

$$\cos(\theta) = \frac{\cosh(F)-e}{1-e\cosh(F)} \tag{2.78}$$

$$\sin(\theta) = \frac{-a\sinh(F)\sqrt{e^2-1}}{a\left(1-e\cosh(F)\right)} \tag{2.79}$$

The relationship between the hyperbolic anomaly and the mean anomaly is given by the following relation:

$$M_h = e\sinh(F) - F \tag{2.80}$$

From which the hyperbolic anomaly can be obtained as a function of time:

$$\frac{1}{e^2-1}\left(e\sinh(F)-F\right) - \left(e\sinh(F_0)-F_0\right) = t - t_p \tag{2.81}$$

Substituting expressions (2.78) and (2.79) in the X and Y components of the position:

$$x = a\left(\cosh(F)-e\right) \tag{2.82}$$

$$y = -a\sinh(F)\sqrt{e^2-1} \tag{2.83}$$

$$\dot{x} = a\sinh(F)\dot{F} = -\frac{\mu a}{r}\sinh(F) \tag{2.84}$$

$$\dot{y} = a\cosh(F)\sqrt{e^2-1}\dot{F} = \frac{h}{r}\cosh(F) \tag{2.85}$$

The expressions (2.82), (2.82), (2.82) and (2.82) for a given time t and an initial time t_0 are substituted into the set of Lagrange coefficients in (2.19).
Using trigonometric relationships and with equation (2.81), the Lagrange coefficients are defined as a function of the hyperbolic anomaly (F):

$$\begin{aligned} f &= 1 - \frac{a\left(1-\cosh(\Delta F)\right)}{r_0} \\ g &= t - t_p - \sqrt{\frac{-a^3}{\mu}}\left(\sinh(\Delta F) - \Delta F\right) \\ \dot{f} &= -\frac{\sinh(\Delta F)\sqrt{-\mu a}}{r_0 r} \\ \dot{g} &= 1 - \frac{a}{r}\left(1-\cosh(\Delta F)\right) \end{aligned} \tag{2.86}$$

2.3.3 Universal variable formulation

As seen in the previous subsection, each type of conic had a different solution from the integral (2.37), which leads to different sets of Lagrange coefficient. In addition, the set of equations to solve an elliptic orbit have a major inconvenience, when the eccentricity is very close to that of a parabolic orbit, for instance: $e = 0.991$, there is a significant loss of accuracy.

One possible approach that allows the use of only one set of Lagrange coefficients without the loss of accuracy at near a parabolic orbit, is the definition of a universal anomaly, commonly named χ, through a change of variables known as the *Sundman transformation*. The only requirement is to know the initial position, $\boldsymbol{r}_0$, the initial velocity, $\boldsymbol{v}_0$, and provide a time interval.

The method employed in this section is based on Vallado [58] and the derivation presented in Bate, Mueller and White [24] and from Battin [25].

2.3.3.1 Derivation of the specific energy

The first step is to define the specific energy for an elliptic orbit:

$$\xi = \frac{v^2}{2} - \frac{\mu}{r} = -\frac{\mu}{2a} \tag{2.87}$$

The magnitude of the velocity, v, can be expressed as a function of the radial and perpendicular velocities:

$$v^2 = v_r^2 + v_\perp^2 = \dot{r}^2 + r^2\dot{\theta}^2 \tag{2.88}$$

The specific energy with the addition of the radial and perpendicular velocity, and solving for $\dot{r}$ becomes:

$$\frac{\dot{r}^2}{2} + \frac{h^2}{2 * r^2} - \frac{\mu}{r} = -\frac{\mu}{2a} \tag{2.89}$$

$$\dot{r}^2 = \frac{2\mu}{r} - \frac{h^2}{r^2} - \frac{\mu}{a} \tag{2.90}$$

$$\dot{r}^2 = \frac{2\mu}{r} - \frac{p\mu}{r^2} - \frac{\mu}{a} \tag{2.91}$$

where p is the semilatus rectum, $p = \dfrac{h^2}{\mu}$

Now, we introduce the universal anomaly with the following change of variables:

$$\dot{\chi} = \frac{\sqrt{\mu}}{r} \tag{2.92}$$

Adding χ in equation (2.91), and solving the differential expression yields:

$$\dot{r}^2 = \dot{\chi}^2 \left(-\frac{r^2}{a} + 2r - p \right) \tag{2.93}$$

$$\int_r \frac{dr}{\sqrt{-\frac{r^2}{a} + 2r - p}} = \int_0^\chi d\chi \tag{2.94}$$

$$\chi + d_0 = \sqrt{a} \arcsin \left(\frac{\frac{r}{a} - 1}{\sqrt{1 - \frac{h^2}{\mu a}}} \right) = \sqrt{a} \arcsin \left(\frac{\frac{r}{a} - 1}{e} \right) \tag{2.95}$$

where d_0 is a constant of integration.

In order to find a suitable expression that relates the universal anomaly and time, the following steps are needed:

- Step 1: Solve equation (2.95) for the magnitude of the position, r:

$$r = a\left[1 + e\sin\left(\frac{\chi + d_0}{\sqrt{a}}\right)\right] \tag{2.96}$$

- Step 2: Substitute the new expression of r in equation (2.92):

$$\dot{\chi} = \frac{d\chi}{dt} = \frac{\sqrt{\mu}}{a\left[1 + e\sin\left(\frac{\chi+d_0}{\sqrt{a}}\right)\right]} \tag{2.97}$$

- Step 3: Solve the first order differential equation (2.98) for $t \in [0, \Delta t]$ and $\chi \in [0, \chi]$

$$\sqrt{\mu}\Delta t = a\left[\chi - e\sqrt{a}\cos\left(\frac{\chi + d_0}{\sqrt{a}}\right) + e\sqrt{a}\cos\left(\frac{d_0}{\sqrt{a}}\right)\right] \tag{2.98}$$

- Step 4: Expand the previous equation (2.98) by using the trigonometric identity: $\cos(A+B) = \cos(A)\cos(B) - \sin(A)\sin(B)$.

$$\begin{aligned}\sqrt{\mu}\Delta t = a\Bigg[&\chi - e\sqrt{a}\cos\left(\frac{\chi}{\sqrt{a}}\right)\cos\left(\frac{d_0}{\sqrt{a}}\right) + e\sqrt{a}\sin\left(\frac{\chi}{\sqrt{a}}\right)\sin\left(\frac{d_0}{\sqrt{a}}\right)\\ &+ e\sqrt{a}\cos\left(\frac{d_0}{\sqrt{a}}\right)\Bigg]\end{aligned} \tag{2.99}$$

- Step 5: Define the integration constant, d_0.
  This will be achieved by defining equation (2.96) for an initial time, $t_0 = 0$, in which the universal anomaly is zero, $\chi_{t=0} = 0$,

$$\sin\left(\frac{d_0}{\sqrt{a}}\right) = \frac{1}{e}\left(\frac{r_0}{a} - 1\right) \tag{2.100}$$

  It is also convenient to define the cosine of the integration constant, this can be done by calculating the time derivative of equation (2.96) for the initial time:

$$\left.\frac{dr}{dt}\right|_{t=0} = \dot{r}_0 = a\frac{e}{\sqrt{a}}\cos\left(\frac{d_0}{\sqrt{a}}\right)\left.\dot{\chi}\right|_{t=0} = \frac{e\sqrt{\mu a}}{r_0}\cos\left(\frac{d_0}{\sqrt{a}}\right) \tag{2.101}$$

  And solving for the integration constant, yields:

$$\cos\left(\frac{d_0}{\sqrt{a}}\right) = \frac{1}{e}\frac{\dot{r}_0 r_0}{\sqrt{\mu a}} = \frac{1}{e}\frac{\boldsymbol{v}_{r_0}\boldsymbol{r}_0}{\sqrt{\mu a}} \tag{2.102}$$

- Step 6: Substitute expressions (2.101) and (2.102) in equation (2.99):

$$\sqrt{\mu}\Delta t = a\left[\chi - \cos\left(\frac{\chi}{\sqrt{a}}\right)\frac{\boldsymbol{v}_{r_0}\boldsymbol{r}_0}{\sqrt{\mu}} + \sqrt{a}\sin\left(\frac{\chi}{\sqrt{a}}\right)\left(\frac{r_0}{a} - 1\right) + \frac{\boldsymbol{v_{r_0}}\boldsymbol{r_0}}{\sqrt{\mu}}\right] \tag{2.103}$$

  Rearranging terms in the equation:

$$\sqrt{\mu}\Delta t = a\chi + a\frac{\boldsymbol{v}_{r_0}\boldsymbol{r}_0}{\sqrt{\mu}}\left(1 - \cos\left(\frac{\chi}{\sqrt{a}}\right)\right) + a\sqrt{a}\sin\left(\frac{\chi}{\sqrt{a}}\right)\left(\frac{r_0}{a} - 1\right) \tag{2.104}$$

- Step 7: Apply the following change of variables, $z = \frac{\chi^2}{a}$, in equation (2.104):

$$\sqrt{\mu}\Delta t = \frac{\chi^3}{z} + \frac{\chi^2}{z}\frac{\boldsymbol{v}_{r_0}\boldsymbol{r}_0}{\sqrt{\mu}}\left(1-\cos\left(\sqrt{z}\right)\right) + \frac{\chi^3}{\sqrt{z^3}}\sin\left(\sqrt{z}\right)\left(\frac{r_0 z}{\chi^2}-1\right) \tag{2.105}$$

Reorganizing the terms in the right hand side of the equation leads to:

$$\sqrt{\mu}\Delta t = \chi^3\left(\frac{\sqrt{z}-\sin(\sqrt{z})}{\sqrt{z^3}}\right) + \chi^2\frac{\boldsymbol{v}_{r_0}\boldsymbol{r}_0}{\sqrt{\mu}}\left(\frac{1-\cos\left(\sqrt{z}\right)}{z}\right) + \chi\frac{r_0}{\sqrt{z}}\sin(\sqrt{z}) \tag{2.106}$$

Finally, equation (2.106) provides a relation between the universal anomaly and time.

However, equation (2.106) presents a set of problems that have to be assessed:

- Equation (2.106) becomes indeterminate when the variable z acquires a value of zero.
- Equation (2.106) was defined by means of the specific energy particularized for an elliptic orbit. Therefore, an expression that is valid for parabolas and hyperbolas is needed.
- It is required to define a method that allows to calculate the universal anomaly, χ.

2.3.3.2 General expression for the universal anomaly

The first two problems can be solved by defining two series, $C(z)$ and $S(z)$, known as the Stumpff functions:

$$C(z) = \begin{cases} \dfrac{1-cos(\sqrt{z})}{z} & \text{if } z > 0 \\ \dfrac{\cosh(\sqrt{-z})-1}{-z} & \text{if } z < 0 \\ \dfrac{1}{2} & \text{if } z = 0 \end{cases} \tag{2.107}$$

$$S(z) = \begin{cases} \dfrac{\sqrt{z}-sin(\sqrt{z})}{\sqrt{z^3}} & \text{if } z > 0 \\ \dfrac{\sinh(\sqrt{-z})-\sqrt{-z}}{\sqrt{z^3}} & \text{if } z < 0 \\ \dfrac{1}{6} & \text{if } z = 0 \end{cases} \tag{2.108}$$

$$\text{Type of conic section } = \begin{cases} \text{Elliptic orbit} & \text{if } z > 0 \\ \text{Hyperbolic orbit} & \text{if } z < 0 \\ \text{Parabolic orbit} & \text{if } z = 0 \end{cases} \tag{2.109}$$

Equation (2.106) with the addition of the stumpff functions, now becomes:

$$\sqrt{\mu}\Delta t = \chi^3\left(1-\alpha r_0\right)S(z) + \chi^2\left(\frac{\boldsymbol{r}_0\boldsymbol{v}_{r_0}}{\sqrt{\mu}}\right)C(z) + \chi r_0 \tag{2.110}$$

Before assessing the third problem and presenting the algorithm to determine the orbit, it is necessary to define the Lagrange coefficients as a function of the universal variable, χ.

The starting point is the topocentric coordinates, that can be related to the universal anomaly. First, the X and Y position and their time derivatives will be calculated and particularized for an elliptic orbit, which later with the addition of the Stumpff functions will be also valid for parabolas and hyperbolas.

The X component is defined as:

$$x = r\cos(\theta) = \frac{1}{e}\left(\frac{h^2}{\mu} - r\right) = \frac{1}{e}\left(a\left(1-e^2\right) - r\right) \tag{2.111}$$

Substituting in the right hand side of equation (2.111) by the definition of r, which was obtained in (2.96):

$$x = -ae - a\sin\left(\frac{\chi + d_0}{\sqrt{a}}\right) \tag{2.112}$$

Calculating the time derivative of X yields:

$$\dot{x} = -\frac{\sqrt{a\mu}}{r}\cos\left(\frac{\chi + d_0}{\sqrt{a}}\right) \tag{2.113}$$

The time derivative of X can also be expressed as:

$$\dot{x} = \frac{d\left(r\cos(\theta)\right)}{dt} = \dot{r}\cos(\theta) + r\sin(\theta)\frac{h}{r^2} = -\frac{\sqrt{a\mu}}{r}\cos\left(\frac{\chi + d_0}{\sqrt{a}}\right) \tag{2.114}$$

Multiplying equation (2.114) by r and dividing by $\sqrt{a\mu}$:

$$\frac{\dot{r}r}{\sqrt{a\mu}}\cos(\theta) + \sin(\theta)\frac{h}{\sqrt{a\mu}} = -\cos\left(\frac{\chi + d_0}{\sqrt{a}}\right) \tag{2.115}$$

Applying equation (2.102) for any time interval t in the left hand side of (2.115) and reorganizing the terms:

$$\cos\left(\frac{\chi + d_0}{\sqrt{a}}\right)e\cos(\theta) + \sin(\theta)\sqrt{1-e^2} = -\cos\left(\frac{\chi + d_0}{\sqrt{a}}\right) \tag{2.116}$$

$$\cos\left(\frac{\chi + d_0}{\sqrt{a}}\right) = -\frac{\sin(\theta)\sqrt{1-e^2}}{1+e\cos(\theta)} = -\frac{\sin(\theta)\sqrt{1-e^2}}{\frac{h^2}{\mu r}} = -\frac{r\sin(\theta)}{a\sqrt{1-e^2}} \tag{2.117}$$

Finally, the Y position becomes a function of the universal anomaly:

$$y = r\sin(\theta) = a\sqrt{1-e^2}\cos\left(\frac{\chi + d_0}{\sqrt{a}}\right) \tag{2.118}$$

Calculating the time derivative of Y:

$$\dot{y} = \sqrt{1-e^2}\frac{\sqrt{a\mu}}{r}\sin\left(\frac{\chi + d_0}{\sqrt{a}}\right) = \frac{h}{r}\sin\left(\frac{\chi + d_0}{\sqrt{a}}\right) \tag{2.119}$$

Similarly as presented in the previous chapters, once the topocentric coordinates are a function of the universal anomaly, they are substituted in the set of equations (2.19). To simplify the terms, equations (2.100) and (2.102) are employed, and to define the new Lagrange coefficients for parabolas and hyperbolas, the Stumpff functions will also be added.

Finally, the set of Lagrange coefficients dependant on the universal variable are equal to:

$$\begin{aligned} f &= 1 - \frac{\chi^2}{r_0} C(z) \\ g &= \Delta t - \frac{\chi^3}{\sqrt{\mu}} S(z) \\ \dot{f} &= \frac{\sqrt{\mu}}{r r_0} \chi \left(z S(z) - 1 \right) \\ \dot{g} &= 1 - \frac{\chi^2}{r} C(z) \end{aligned} \tag{2.120}$$

In addition, there is an important property that can be derived from the Lagrange coefficients, that later will be employed in the Lambert problem. We start by defining the cross product of the velocity and position vectors:

$$\boldsymbol{r} \times \boldsymbol{v} = (f \boldsymbol{r}_0 + g \boldsymbol{v}_0) \times \left(\dot{f} \boldsymbol{r}_0 + \dot{g} \boldsymbol{v}_0 \right) \tag{2.121}$$

Developing the terms of equation (2.121):

$$\boldsymbol{h} = f \dot{g} \boldsymbol{h} - \dot{f} g \boldsymbol{h} \tag{2.122}$$

Equation (2.122) leads to:

$$1 = f \dot{g} - \dot{f} g \tag{2.123}$$

2.3.4 Algorithm

To define the universal variable an iterative method is necessary, the one presented in this subsection will be based on the Newton-Raphson method.
The first step is to move the left-hand side term of equation (2.110) to the right-hand side and denoting the expression as $f(\chi)$:

$$f(\chi) = -\sqrt{\mu} \Delta t + \chi^3 \left(1 - \alpha r_0\right) S(z) + \chi^2 \left(\frac{\boldsymbol{r}_0 \boldsymbol{v}_{r_0}}{\sqrt{\mu}} \right) C(z) + \chi r_0 = 0 \tag{2.124}$$

The next step is to calculate the time derivative of equation (2.124):

$$\dot{f}(\chi) = r_0 + \chi^2 \left(1 - \alpha r_0\right) C(z) + \chi \left(\frac{\boldsymbol{r}_0 \boldsymbol{v}_{r_0}}{\sqrt{\mu}} \right) \left(1 - z S(z)\right) \tag{2.125}$$

Then, the universal anomaly will be expressed as:

$$\chi_{i+1} = \chi_i - \frac{f(\chi_i)}{\dot{f}(\chi_i)} \tag{2.126}$$

For the initial guess, χ_0, it will be considered the one suggested in the orbital mechanics book of Chobotov [27]:

$$\chi_0 = \sqrt{\mu}\frac{\Delta t}{|a|} \tag{2.127}$$

The criteria of convergence will be given by the ratio of $\frac{f(\chi_i)}{\dot{f}(\chi_i)}$, where the tolerance is set to 10^{-8}.

Finally, the structure of the algorithm to determine the Mars and Earth orbit using the Lagrange coefficients is the following:

- Step 1: Define an initial position and velocity vector, $\boldsymbol{r}_0$ and $\boldsymbol{v}_0$
- Step 2: Calculate the semi-major axis, a and the period of the orbit, T.
- Step 3: Define a time vector that starts at t_0 and finishes at T in increments of Δt.
- Step 4: For each time increment, Δt, the universal anomaly is calculated.
  To do so, the previous method is employed:
  - Set a loop where the initial guess is equation (2.127).
  - Define equation (2.126) in the loop.
  - The loop breaks when ratio $\frac{f(\chi_i)}{\dot{f}(\chi_i)}$ is lower than the tolerance, 10^{-8}.
- Step 5: In each iteration of Step 4, the Lagrange coefficients are calculated using the set of equations (2.120).
- Step 6: With the Lagrange coefficients the position and velocity vectors at a time Δt are calculated:

$$r = fr_0 + gv_0 \tag{2.128}$$

$$v = \dot{f}r_0 + \dot{g}v_0 \tag{2.129}$$

- Step 7: The values obtained in step 6 are stored for each iteration.

2.3.5 Earth and Mars orbits

The values used for the initial position and velocity for both Earth and Mars orbits, are the same as the ones employed in the ode45 algorithm, which dates to the first of January of 2030. See Tables (2.1) and (2.2).
With the previously presented algorithm for universal variables, the orbit of Mars and Earth are determined. See Figure (2.4).

2.3.5.1 Validation

In order to validate the orbits from figure (2.4), an arbitrary point has been selected and its corresponding position and velocity has been compared with the ones obtained from Horizons system [6] for the same date:

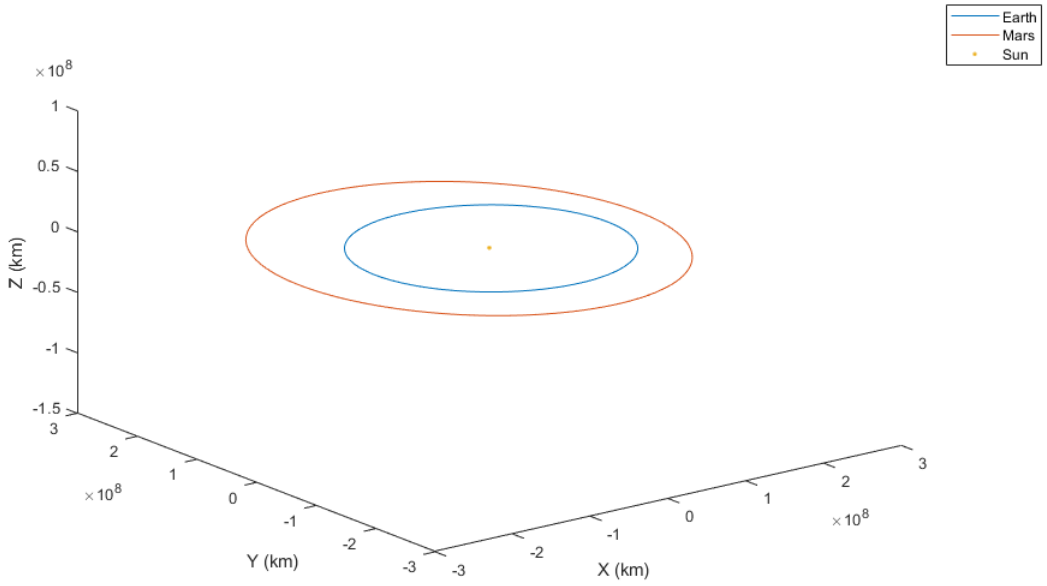

Figure 2.4: Earth and Mars orbits calculated by universal variable formulation.

Position (km)	X	Y	Z
Earth JPL Horizons	$7.7705 \cdot 10^7$	$-1.3061 \cdot 10^8$	$8.4426 \cdot 10^3$
Earth Universal variable	$7.438 \cdot 10^7$	$-1.3265 \cdot 10^8$	$10.229 \cdot 10^3$

Table 2.3: Position(km) of the Earth on 24/07/2030, from Horizons system [6] and the universal variable method.

Position (km)	X	Y	Z
Mars JPL Horizons	$-1.7258 \cdot 10^7$	$2.3561 \cdot 10^8$	$5.3609 \cdot 10^6$
Mars Universal variable	$-1.5258 \cdot 10^7$	$2.3556 \cdot 10^8$	$5.3111 \cdot 10^6$

Table 2.4: Position(km) of Mars on 24/07/2030, from Horizons system [6] and the universal variable method.

Velocity (km/s)	X	Y	Z
Earth JPL Horizons	$2.5124 \cdot 10$	$1.5111 \cdot 10$	$-2.5327 \cdot 10^{-4}$
Earth Universal variable	$2.5477 \cdot 10$	$1.452 \cdot 10$	$-1.247 \cdot 10^{-4}$

Table 2.5: Velocity (km/s) of the Earth on 24/07/2030, from Horizons system [6] and the universal variable method.

Velocity (km/s)	X	Y	Z
Mars JPL Horizons	$-2.3251 \cdot 10$	$2.896 \cdot 10^{-1}$	$5.761 \cdot 10^{-1}$
Mars Universal variable	$-2.3266 \cdot 10$	$4.9209 \cdot 10^{-1}$	$5.8071 \cdot 10^{-1}$

Table 2.6: Velocity (km/s) of Mars on 24/07/2030, from Horizons system [6] and the universal variable method

The universal variable formulation, does not take into account the effect produced by other planets, it is derived from the two-body-problem. Whereas, JPL Horizons is based on the N-Body problem, as it takes into account the eight planets of the Solar System, leading to a more precise result.

Chapter 3

Hohmann transfer orbit

3.1 Introduction

There exit two variables that for any preliminary design of a transfer orbit, must be taken into account: the required **Delta-V** and the **time of flight**.

Starting with the first variable, the Delta-V is related to the specific impulse. As it can be easily deduced, the lower the required Delta-V, the lower the mass of fuel needed to perform a certain maneuver. This relation will be later presented in detail in chapter 9.

However, minimizing Delta-V does not necessarily means minimizing the time of flight, nor does it always results in a proportional decrease in the fuel consumption. The first point, can be seen when comparing a Hohmann transfer with a Bi-elliptic transfer, the latest for certain applications allows a lower Delta-V than the Hohmann transfer, but at the cost of increasing the flight time.

The flight time will condition the mission design, especially for manned missions, as a longer flight time would involve more resources for sustaining the crew which also leads to a decrease in the available payload and may condition the thrust weight ratio needed.

An ideal transfer orbit from point A to point B, should fulfill the following characteristics:

- The transfer orbit must be coplanar, meaning that the initial and final orbits are in the same plane. If the orbits were non-coplanar, a plane change maneuver would be needed which is undesirable as it will greatly increase the required Delta-V.
- The flight path angle should be ideally zero degrees. This can be seen with the following equation applied for two coplanar orbits with the same apse line:

$$\Delta V = \sqrt{(\boldsymbol{v}_2 - \boldsymbol{v}_1)^2} = \sqrt{v_2^2 + v_1^2 - 2v_1 v_2 \cos(\Delta\gamma)} \tag{3.1}$$

  where $\Delta\gamma$ is the variation in the flight path angle, the Delta-V becomes minimum when the variation in the flight angle is zero.

Generally, the most efficient transfer orbit, in terms of fuel consumption, is the Hohmann transfer. It can be defined as a coplanar elliptic orbit with two tangential burns at the apoapsis and periapsis of the transfer orbit, where the radial component of the velocity is zero. The flight time for any Hohmann transfer is half the period of the transfer orbit.

3.2 Method of patched conics

Any interplanetary transfer is subjected to the gravitational effects from not only the departure or arrival planet and the Sun, but also the different planets in the solar system. This lead to the N-body problem, for which there is currently no analytic solution, but it can be solved numerically with approximations such as the Euler's method or the Heun's method.

In order to simplify the complexity of the problem and work in the two-body frame, it is convenient to employ a well-known approximation, the method of patched conics. This method allows to not only consider a two body unperturbed Kepler orbit but also not calculating directly the sphere of influence of both the departure and arrival planets. The foundation of this method is based on the large distances between planets and the Sun in the heliocentric frame, leading to consider that the distance between the center of a given planet and its sphere of influence is such a small scale in the heliocentric frame that the sphere of influence can be considered as a single point coincident with the center of the respective planet. This approximation has a relatively adequate accuracy for interplanetary transfers.

With the method of patched conics, a Hohmann transfer from Earth to Mars is divided in three phases:

- Departure from a parking Earth orbit: A geocentric coordinate system is employed, where the departure orbit is hyperbolic.
- Transfer orbit: The heliocentric coordinate system is used, where the transfer orbit is an ellipse.
- Arrival to Mars: A mars centered coordinate system with a hyperbolic arrival orbit.

3.3 Previous considerations

From Figure (2.4), presented in chapter 2, it can be seen that the Mars orbit is not contained in the ecliptic plane. In fact, it has an inclination that can be calculated with the following equation:

$$\boldsymbol{h}_{Mars} \cdot \boldsymbol{u}_z = h_{Mars} \cos(i) \tag{3.2}$$

$$i_{Mars} = 1.8474^\circ \tag{3.3}$$

where $\boldsymbol{u}_z$ is the unitary vector in the z direction for heliocentric coordinates, $\boldsymbol{h}$ is the specific angular momentum in its vector form and i is the inclination.

Therefore, any transfer between Earth and Mars is a transfer between two non-coplanar orbits. This would require to perform a plane change maneuver, which ideally it should be performed during launch rather than in the parking orbit, as performing it in the parking orbit would increase greatly the required delta-V.

In addition, the change in the true anomaly over time, the angular velocity, it is not constant for celestial bodies. This variation for a perfect elliptic orbit can be calculated by using the next procedure:

$$n = \frac{d\theta}{dt} = \frac{d\theta}{dM_e}\frac{dM_e}{dt} \tag{3.4}$$

where M_e is the mean anomaly and n the angular velocity.

Starting with the first partial derivative of equation (3.4), the mean anomaly as a function of the true anomaly is given by equation (2.40). For the Earth and Mars orbit, the effect that the true anomaly has over the mean anomaly can be observed in Figure (3.1).

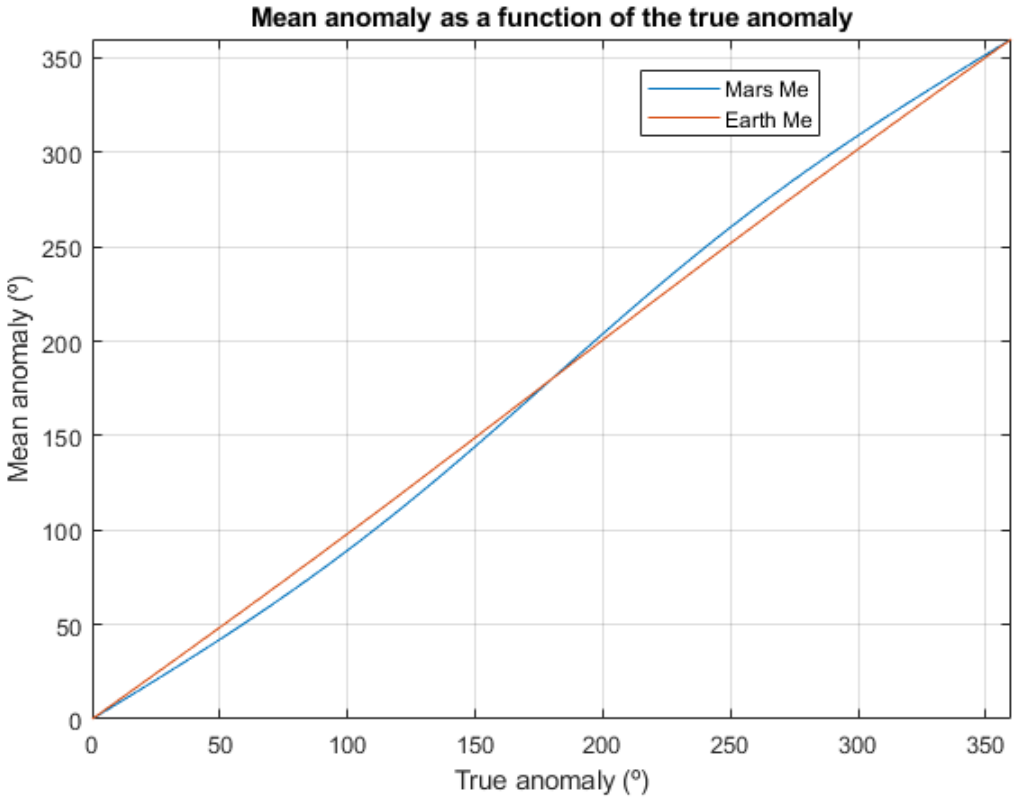

Figure 3.1: Earth and Mars mean anomaly as a function of the true anomaly.

Calculating the partial derivative of the mean anomaly with respect to the true anomaly, yields:

$$\frac{dM_e}{d\theta} = -\frac{e\sqrt{1-e^2}\cos(\theta)}{1+e\cos(\theta)} - \frac{e^2\sqrt{1-e^2}\sin(\theta)^2}{(1+e\cos(\theta))^2} + \frac{\sqrt{\frac{1-e}{1+e}}\sec\left(\frac{\theta}{2}\right)^2}{1+\frac{(1-e)\tan\left(\frac{\theta}{2}\right)^2}{1+e}} \tag{3.5}$$

Particularizing equation (2.43) for the periapsis as the starting point, provides the relation between the mean anomaly and the orbital time, t:

$$M_e = \frac{\mu^2}{h^3}\left(1-e^2\right)^{3/2} t \tag{3.6}$$

$$\frac{dM_e}{dt} = \frac{\mu^2}{h^3}\left(1-e^2\right)^{3/2} \tag{3.7}$$

Finally, with equations (3.5) and (3.7), the orbital angular velocity becomes a function of the true anomaly, the eccentricity and the specific angular momentum. For a Mars and Earth orbit, during a complete revolution, the angular velocity becomes:

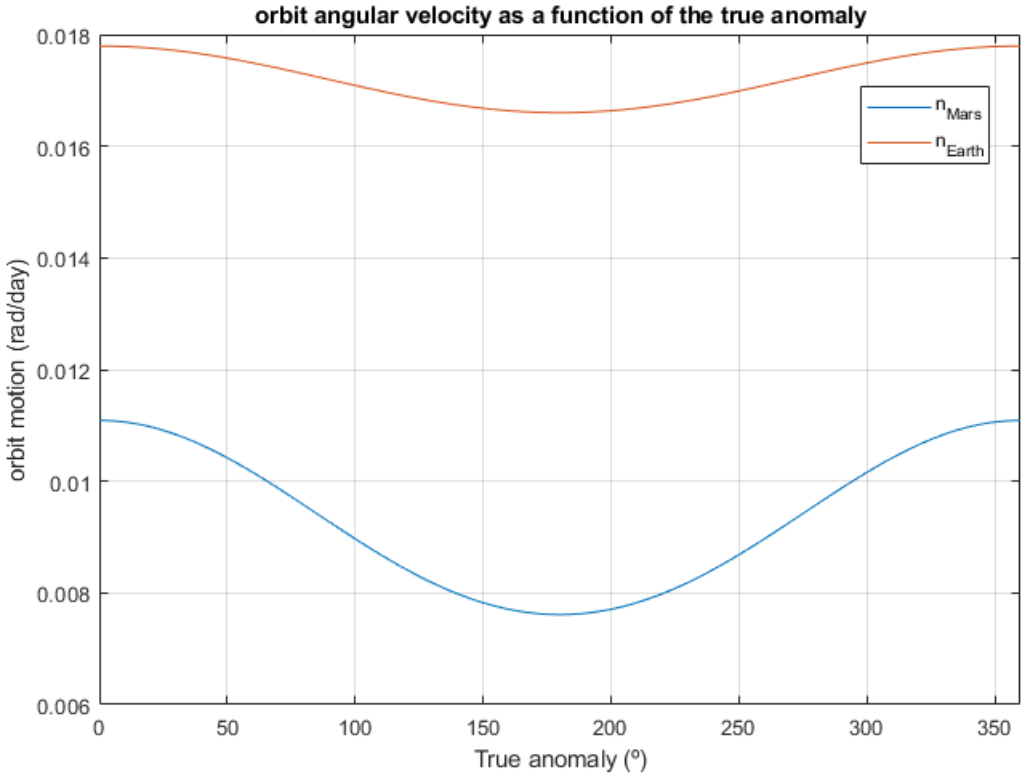

Figure 3.2: Earth and Mars orbital angular velocity for one revolution.

In order to apply a Hohmann transfer from Earth to Mars and reduce the computational complexity of the problem at hand, the Mars orbit will be contained in the ecliptic plane, or in other words, it will be considered coplanar with the Earth orbit. In addition, both orbits have an eccentricity close to zero, but they are still elliptic, to simplify calculations, they will be considered circular orbits with the following radius:

$$r_{Earth} = 1.4973 \times 10^8 \tag{3.8}$$

$$r_{Mars} = 2.2892 \times 10^8 \tag{3.9}$$

As presented before, the angular velocity of both Mars and Earth orbits, is not constant. It is convenient to work with a single value for each orbit, therefore the mean motion will be used by means of the orbit period:

$$n = \frac{2\pi}{T} \tag{3.10}$$

$$n_{Earth} = 0.0172\, rad/day \tag{3.11}$$

$$n_{Mars} = 0.0091\, rad/day \tag{3.12}$$

Lastly, the selection of the parking orbit for both the departure from Earth and the orbit to rendezvous during the arrival to Mars is a trade-off between mission requirements and fuel expenditure. To simplify the Hohmann transfer, the Earth parking orbit will be assumed to be a circular orbit with an altitude of 200 km. Whereas for the Mars parking orbit, an elliptical orbit will be studied for different eccentricities taking only into account its impact on fuel expenditure.

3.4 Departure hyperbola

A parabolic trajectory will allow the spacecraft to leave the Earth sphere of influence, but it will have the same orbit as the Earth. In order to transition from a parking orbit to the transfer orbit, it is necessary to overcome the Earth sphere of influence with an excess speed. This speed is calculated by the difference between the speed at the periapsis of the transfer ellipse and the Earth orbit speed, assuming a circular orbit:

$$V_{Earth} = \sqrt{\frac{\mu}{r_{Earth}}} \tag{3.13}$$

$$V_{Departure} = h_1/r_p = h_1/r_{Earth} \tag{3.14}$$

$$V_{Excess} = V_\infty = V_{Departure} - V_{Earth} \tag{3.15}$$

where h_1 is the specific angular momentum for the transfer orbit and r_p is the radius of the perigee, which is the distance from the Earth to the Sun.

For the Earth orbital velocity, equation (3.13), all the parameters are known. Whereas, for the velocity at the perigee of the transfer orbit, the specific angular momentum and eccentricity are unknown. They can be obtain by defining the orbit position, equation (B.3), for the periapsis and apoapsis, knowing that the true anomaly is 0 and 180^{o} respectively, and solving the system of equations yields:

$$e_{transfer} = \frac{r_a - r_p}{r_a + r_p} \tag{3.16}$$

$$h_{transfer} = \sqrt{r_p\,\mu\,(1 + e_{transfer})} \tag{3.17}$$

Once the excess speed has been defined, the hyperbolic velocity is calculated by using the energy equation particularized for a hyperbola:

$$\epsilon = \frac{V^2}{2} - \frac{\mu}{r} = \frac{\mu}{2a} \tag{3.18}$$

$$V^2 - 2V_c^2 = V_\infty^2 \tag{3.19}$$

$$V_{Hyperbolic} = \sqrt{2V_c^2 + V_\infty^2} \tag{3.20}$$

where V_c is the velocity for the parking orbit, $V_c = \dfrac{\mu}{r}$.

The difference between the hyperbolic velocity and the parking orbit speed is the required delta-V that the engine needs to provide in order for the spacecraft to reach the transfer orbit:

$$\Delta V = V_{Hyperbolic} - V_c \tag{3.21}$$

Summarizing all the previous equations and substituting the different terms:

Heliocentric frame	
V_{Earth} (km/s)	29.772
$V_{Departure}$ (km/s)	32.738
V_{∞} (km/s)	2.966
$e_{Transfer}$	0.209
$h_{Transfer}$ km^2/s	$4.902 \cdot 10^9$

Table 3.1: Velocities and transfer orbit parameters in the heliocentric frame.

Geocentric frame	
$V_{Hyperbolic}$ (km/s)	11.401
$V_{Parking}$ (km/s)	7.784
$h_{Parking}$ (km)	200
$\Delta V_{Departure}$ (km/s)	3.617

Table 3.2: Velocities and departure hyperbola parameters in the geocentric frame.

Finally, the required Delta-V to transition from a 200 km circular parking orbit to the departure hyperbola is 3.617 km/s.

3.5 The transfer orbit

The objective of the transfer is to rendezvous with Mars, this will only be achieved for certain launch opportunities. The key principle to determine the launch windows, it is the fact that the time of flight during the transfer orbit is half of its period. In other words, the spacecraft will arrive at Mars when it is at the apogee of the transfer ellipse. This leads to an initial condition, the angle between the departing and arrival point is 180 degrees.

From Figure (3.3), it can be seen that Mars must be ahead of Earth during the departure, and at the arrival, Earth is now ahead of Mars. The phase angle between both planets at departure, ϕ_0, will determine when to launch, whereas the phase angle at arrival, ϕ_f, will be needed when calculating the launch opportunities for the return trip.

The first step is to create a mathematical model to define the phase angle between Earth and Mars for a time interval. From chapter 2, the Earth and Mars orbit where defined from 2030 to 2040, with each position vector associated with a specific date. By performing the dot product of Mars and Earth position vectors, the angle between both vectors can be calculated.

$$\boldsymbol{r}_{Earth} \cdot \boldsymbol{r}_{Mars} = r_{Earth} r_{Mars} \cos(\phi) \tag{3.22}$$

where ϕ is the phase angle between both planets.

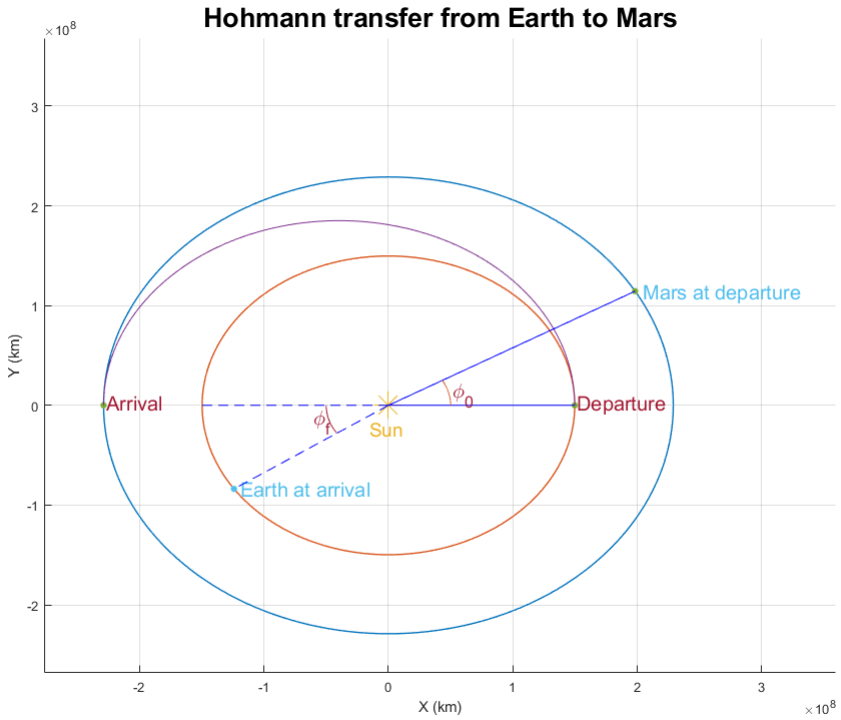

Figure 3.3: Earth and Mars Hohmann transfer.

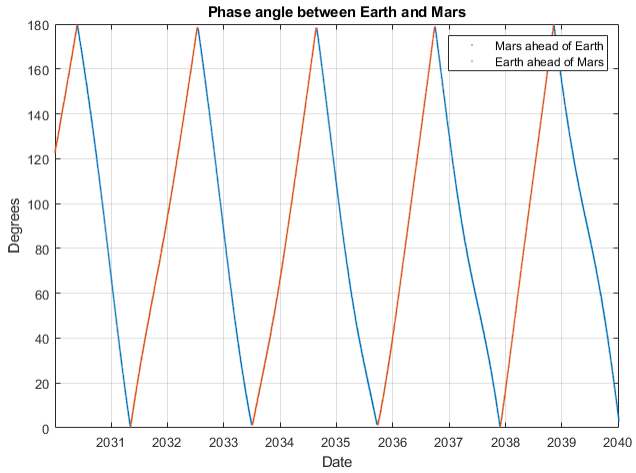

Figure 3.4: Earth and Mars Phase angle from 2030 to 2040.

In order to successfully rendezvous with Mars, during the departure, Mars must be ahead of Earth with a specific initial angle. It can be calculated by using the mean orbital motion and taking

into account that from the departure point to the arrival point there are 180 degrees.

$$\phi_0 = \pi - n_{Mars} t_{12} \tag{3.23}$$

$$t_{12} = \frac{\pi}{\sqrt{\mu}} a^{\frac{3}{2}} \tag{3.24}$$

where ϕ_0 is the initial phase angle, t_{12} is half the orbit period and a is the semi-major axis of the transfer orbit.

With the previous equation the initial phase angle is determined. The next step, it is to obtain the phase angle between Earth and Mars at arrival. For this purpose, the following relation is employed:

$$\phi_f + \pi = n_{Earth} t_{12} \tag{3.25}$$

Rearranging the terms of equation (3.25) and considering the counterclockwise direction positive for angles:

$$\phi_f = \pi - n_{Earth} t_{12} \tag{3.26}$$

During the return trip, Mars must be ahead of Earth with an specific phase angle, ϕ_{return}, needed for a successfully rendezvous with Earth . The required phase angle is equal to the previously calculated ϕ_f but with a different sign and the transfer ellipse is the same that for the transfer to Mars with the opposite direction, as now, it is a transfer from an outer planet to an inner planet.

$$\phi_{return} = -\phi_f \tag{3.27}$$

ϕ_0	43.738°
t_{12}	260 $days$
ϕ_{return}	75.998°

Table 3.3: Phase angles and time of flight.

Departure from Earth	Arrival to Mars	Return window	t_{wait} $(days)$
12/02/2031	30/10/2031	21/01/2033	449
23/03/2033	8/12/2033	04/03/2035	451
18/05/2035	2/02/2036	02/05/2037	455
08/08/2037	25/04/2038	26/07/2039	457
17/10/2039	03/07/2040	28/09/2041	452

Table 3.4: Launch opportunities.

3.6 Arrival hyperbola

Once at the apogee of the transfer orbit, the spacecraft velocity reaches its minimum value, which is lower than the heliocentric velocity of Mars. If no additional change is performed the spacecraft will follow a hyperbolic orbit relative to Mars, see Figure (3.5), from which depending on its perigee radius three scenarios can occur:

- Collide with the planet, if the perigee radius equals the radius of the planet.
- If the perigee radius is different from the radius of the planet and no engines are fired, the spacecraft will perform a fly-by maneuver, changing its velocity vector.
- Transition from the arrival hyperbola to a parking orbit around Mars, this can be achieved by firing the engines at the periapsis of the hyperbola which coincide with the parking orbit periapsis. The increment in the heliocentric velocity will depend on the perigee radius of the parking orbit.

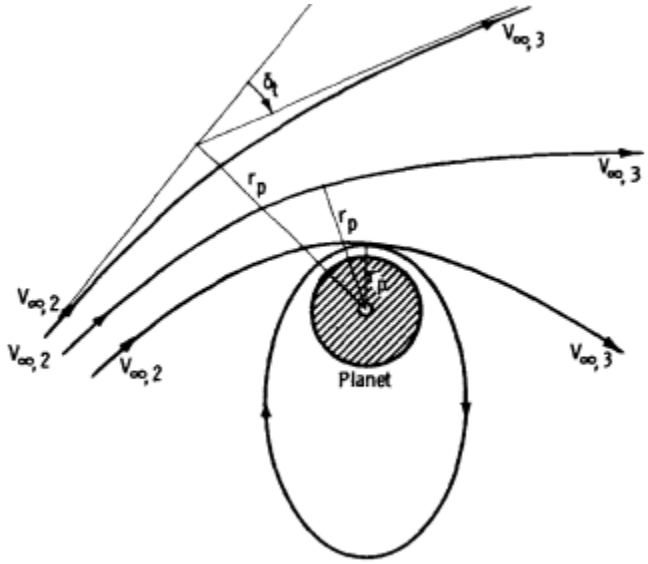

Figure 3.5: Arrival Hyperbola for fly-by and capture orbit scenarios with varying perigee radius. Source [56]

Before defining the parking orbit, the excess speed of the arrival hyperbola can be calculated as it is independent of the perigee radius. It only depends on the Mars velocity and the spacecraft speed at the arrival in heliocentric coordinates.

$$V_\infty = V_{Mars} - V_A \tag{3.28}$$

$$V_{Mars} = \sqrt{\frac{\mu}{r_{Mars}}} \tag{3.29}$$

$$V_{Arrival} = \frac{h_{Transfer}}{r_{Mars}} \tag{3.30}$$

$V_\infty\ (km/s)$	2.666
$V_{Mars}\ (km/s)$	24.077
$V_{Arrival}\ (km/s)$	21.412

Table 3.5: Excess speed of the arrival hyperbola.

To properly define the parking orbit based only on fuel consumption, it is necessary to obtain an expression of the required delta-V as a function of the perigee radius and the eccentricity of the parking orbit. First, the hyperbolic velocity at the perigee is defined by using the energy equation:

$$V_{Hyp}^2 - V_{Esc}^2 = V_\infty^2 \tag{3.31}$$

$$V_{Hyp}(r_p) = \sqrt{V_\infty^2 + 2\frac{\mu_{Mars}}{r_p}} \tag{3.32}$$

where, $V_{Esc} = \sqrt{2}\sqrt{\frac{\mu}{r}}$ is the escape velocity at the perigee and r_p is the perigee radius.

The next step is to find the expression for the velocity at the perigee of the parking orbit. This can be easily done by knowing that at the perigee the true anomaly is 0 degrees and the velocity has only a tangential component.

$$r_p = \frac{h^2}{\mu_{Mars}}\frac{1}{1+e} \tag{3.33}$$

$$V_p = \frac{h}{r_p} = \frac{\mu\,(1+e)}{r_p V_p} \tag{3.34}$$

$$V_p(r_p, e) = \sqrt{\frac{\mu\,(1+e)}{r_p}} \tag{3.35}$$

Finally, the require delta-V becomes a function of the perigee radius and the eccentricity:

$$\Delta V(r_p, e) = V_{Hyp}(r_p) - V_p(r_p, e) \tag{3.36}$$

To find the perigee radius that minimizes the ΔV for a given eccentricity, the derivative is calculated and then it is equaled to zero.

$$\frac{d\Delta V}{dr_p} = 0 \tag{3.37}$$

$$r_p'(e) = \frac{2\mu}{v_\infty^2}\frac{(1-e)}{(1+e)} \tag{3.38}$$

The optimum perigee radius, r_p', becomes a function of the parking orbit eccentricity and the excess speed. By performing a parametric study varying the eccentricity, Figures (3.6) and (3.7), a set of tendencies can be observed:

- A highly eccentric parking orbit allows a lower delta-V, effectively reducing the fuel consumption.
- The optimal perigee radius follows an inversely proportional relation with the eccentricity. The lower the optimal perigee radius, the higher the eccentricity and the lower the required delta-V.

$V_{hyp}\ (km/s)$	5.619
$V_{parking_{perigee}}\ (km/s)$	4.355
$e_{parking}$	0.55
$r_p - r_{Mars}\ (km)$	104.14
$r_p\ (km)$	$3.5 \cdot 10^3$
$\Delta V_{arrival}\ (km/s)$	1.264

Table 3.6: Arrival hyperbola and parking orbit.

$\Delta V_{Departure}$ (km/s)	3.617
$\Delta V_{arrival}\ (km/s)$	1.264
$\Delta V_{Total}\ (km/s)$	4.881

Table 3.7: Total ΔV for an Earth to Mars Hohmann transfer.

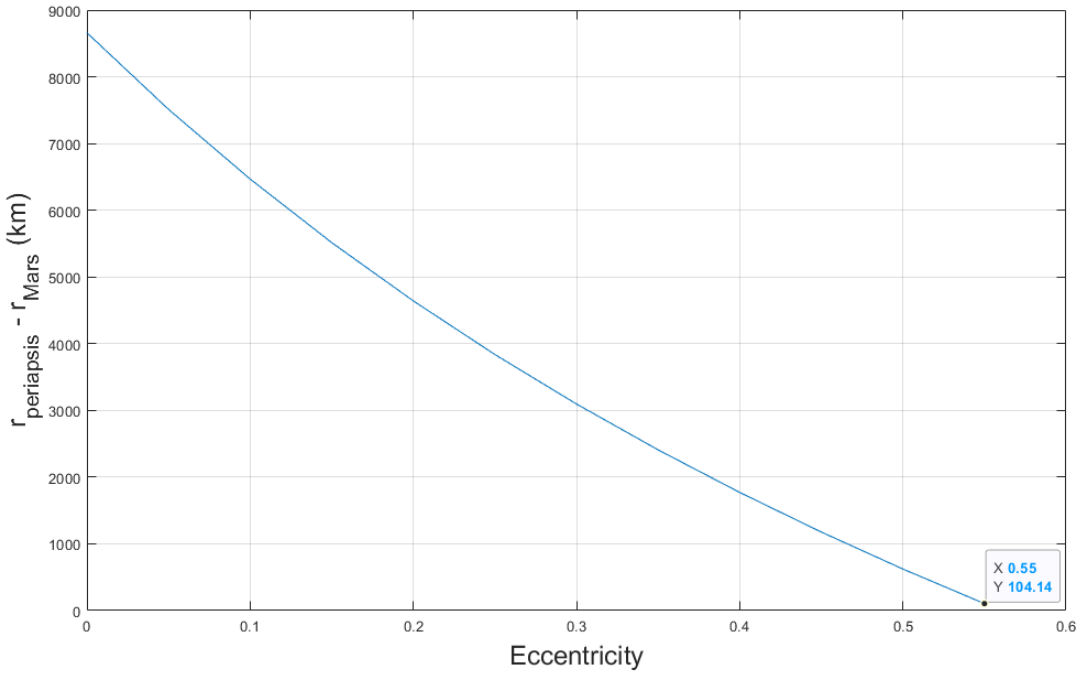

Figure 3.6: Parking orbit perigee distance from Mars surface vs Parking orbit eccentricity.

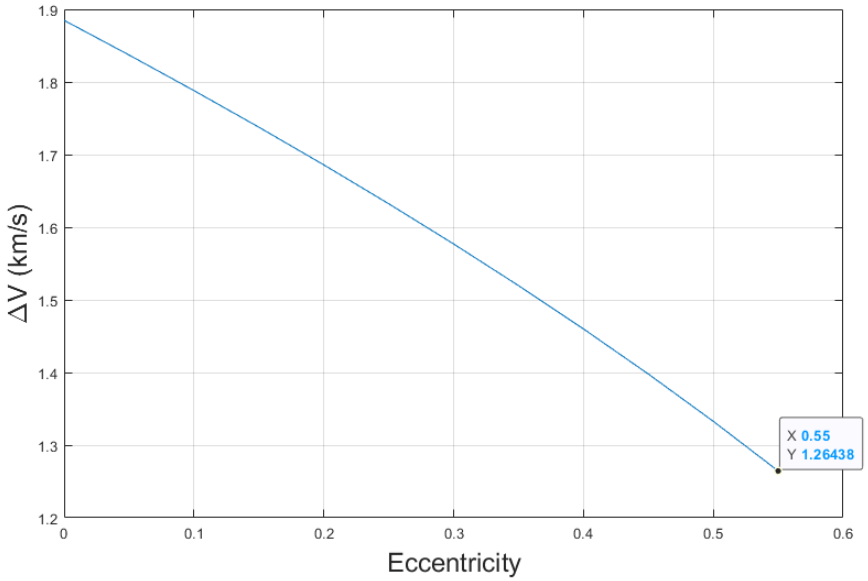

Figure 3.7: Require ΔV vs Parking orbit eccentricity.

Chapter 4

The Lambert problem

4.1 Introduction

As seen in the previous chapter, a Hohmann transfer from Earth to Mars takes around 250 days with the launch windows taking place at approximately two years time intervals. In addition, the required delta-V obtained was not realistic, as a plane change maneuver would take place due to Mars and Earth orbits being non-coplanar. All of this circumstances rises the need of an alternative method with more flexible launch opportunities as well as shorter transfer time while trying to minimize the required delta-V taking into account the changes in inclination.

The Lambert's problem allows to achieve these objectives, it consists on a boundary condition problem where two initial position vectors are known as well as the transfer time between both vectors. Lambert allows to find the orbit that connects both points with the respective transfer time. Nevertheless, there exist multiple solutions depending on different scenarios:

- Based on the revolutions, we find two types:
  - Single revolution: The phase angle between the initial and the final points is less than 360 degrees. Hyperbolic, parabolic and elliptic solutions can be found. They can be type I or II transfers.
  - Multiple revolutions: The phase angle is greater than 360 degrees, only elliptical solutions are found. They are named type III transfer.
- Based on the type of transfer, see Figure (4.1), we find:

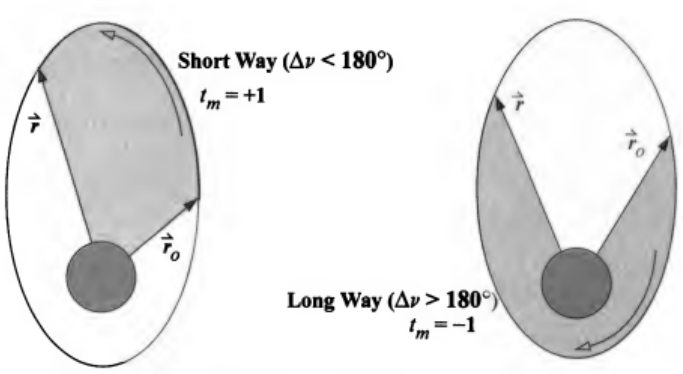

Figure 4.1: Prograde and retrograde transfer orbits. Source: Vallados [58].

  - Prograde transfer. It is the shortest transfer connecting both points. The inclination is between 0 and 90 degrees.
  - Retrograde transfer. It is the longest transfer connecting both points. The inclination is between 90 and 180 degrees.

- Another classification based on the type of transfer orbit is the following:
  - Type I : Variation in the true anomaly lower than 180 degrees.
  - Type II : Variation in the true anomaly between 180 degrees and 360 degrees.
  - Type III: Variation in the true anomaly greater than 360 degrees.

4.2 Universal variable solution

A solution for the Lambert problem that works for all orbits and allows to consider the prograde and retrograde solutions, is calculated by using the universal variables formulation. If the Lagrange coefficients, $f, g, \dot{f}, \dot{g}$ are known, the velocity vectors can be easily obtained:

$$\boldsymbol{V}_1 = \frac{\boldsymbol{r}_2 - f\boldsymbol{r}_1}{g} \tag{4.1}$$

$$\boldsymbol{V}_2 = \frac{1}{g}\left(g\boldsymbol{r}_2 - \boldsymbol{r}_1\right) \tag{4.2}$$

From the previous equations, $\boldsymbol{V}_1$ and $\boldsymbol{V}_2$ are the velocity vectors for the initial and final position vectors. These equations are obtain by using the set of equations (2.18) and the property (2.123).

Therefore, the problem consists on finding the value of $f, g, \dot{f}, \dot{g}$. This process can be achieved by using different types of solvers which require to perform iterations. One of these solvers, it is the one based on the Newton Raphson's iterative method used by Bate, Mueller and White, which works for most type of transfer orbits. Nevertheless, for highly hyperbolic transfers there exists convergence issues. A solution is to employ an alternative method based on the bisection technique presented by Vallado, which makes use of the Stumpff functions, $C(z)$ and $S(z)$, and an upper and lower value of z, as well as an initial guess.

The first step is to define the Lagrange coefficients as a function of the variation in the true anomaly and the variable z:

$$\begin{aligned}
&f = 1 - \frac{\mu r\,(1-\cos(\Delta\theta))}{h^2} \qquad g = \frac{r r_0 \sin(\Delta\theta)}{h} \\
&\dot{f} = \frac{\mu}{h}\frac{1-\cos(\Delta\theta)}{\sin(\Delta\theta)}\left(\frac{\mu\,(1-\cos(\Delta\theta))}{h^2} - \frac{1}{r_0} - \frac{1}{r}\right) \qquad \dot{g} = 1 - \frac{\mu r_0\,(1-\cos(\Delta\theta))}{h^2} \\
&f = 1 - \frac{\chi^2}{r_0}C(z) \qquad g = \Delta t - \frac{\chi^3}{\sqrt{\mu}}S(z) \qquad z = \frac{\chi^2}{a} \\
&\dot{f} = \frac{\sqrt{\mu}}{r r_0}\chi\,(zS(z)-1) \qquad \dot{g} = 1 - \frac{\chi^2}{r}C(z)
\end{aligned} \tag{4.3}$$

To solve the algorithm it is necessary to find an equation that relates the variation in time, Δt, with the variable z. To achieve this, we start by equaling the coefficient f from both terms, in (4.3), and solving for the universal anomaly, χ:

$$\chi = \sqrt{\frac{r_1 r_2\,(1-\cos(\Delta\theta))}{\frac{h^2}{\mu}C(z)}} \tag{4.4}$$

The cosine of the variation in the true anomaly can be calculated by using the two position vectors:

$$\cos(\Delta\theta) = \frac{\boldsymbol{r}_1 \cdot \boldsymbol{r}_1}{r_1\, r_2} \tag{4.5}$$

With the universal anomaly defined, by equaling both terms of $\dot{f}$ and applying a change of variables, the next expression can be obtained:

$$y = r_1 + r_2 + \frac{A\,(zS(z)-1)}{\sqrt{C(z)}} \tag{4.6}$$

Where the variables y and A are equal to:

$$y = \frac{\mu r_1 r_2\,(1-\cos(\Delta\theta))}{h^2} \tag{4.7}$$

$$A = \pm\sqrt{r_1 r_2\,(1+\cos(\Delta\theta))} \tag{4.8}$$

Defining equation (4.4) with the new variables:

$$\chi = \sqrt{\frac{y}{C(z)}} \tag{4.9}$$

Analogous to the previous case, equaling both terms of g and implementing the previous equations, it allows to find the relationship between the variable z and the transfer time:

$$\Delta t = \frac{\chi^3 S(z) + A\sqrt{y}}{\sqrt{\mu}} \tag{4.10}$$

4.2.1 Algorithm

The algorithm has as inputs the initial and final position vectors, the transfer time, the gravitational constant and the type of transfer orbit (Prograde or retrograde solution) based on the sign of equation (4.8). Its output are the velocity vectors, $\boldsymbol{V}_1$ and $\boldsymbol{V}_2$.

- Step 1. Define the following parameters:
  - Tolerance.
  - Upper and lower limit for z. If the transfer orbit is highly hyperbolic a lower limit is needed.
  - An initial guess for z.
  - Maximum number of iterations.
- Step 2. Calculate equation (4.5).
- Step 3. Calculate the value of A, equation (4.8). Positive sign for prograde or short transfer and negative sign for retrograde or long transfer. If A is equal to 0, then there is no solution for the transfer.
- Step 4. Start the loop with a maximum number of iterations.
  - Step 4.1. Start by defining the variable y, equation (4.6).
  - Step 4.2. If A is greater than 0 and y is negative: increase the lower limit and recalculate z by using the next equation:

$$z = \frac{z_{lower} + z_{upper}}{2} \tag{4.11}$$

  - Step 4.3. Calculate the universal anomaly, χ, with equation (4.9).
  - Step 4.4 Calculate the Δt with equation (4.10).
  - Step 4.5. If the value of Δt is greater than the transfer time, set the upper limit as the value of z. Otherwise, define the lower limit as the value of z.
  - step 4.6. Calculate z with equation (4.11).
  - Step 4.7. If the difference between Δt and the transfer time is lower than the tolerance break the loop.
- Step 5. Calculate the Lagrange coefficients with the following equations:

$$f = 1 - \frac{y}{r_1} \tag{4.12}$$

$$g = A\sqrt{\frac{y}{\mu}} \tag{4.13}$$

$$\dot{g} = 1 - \frac{y}{\mu} \tag{4.14}$$

$$\dot{f} = \frac{f\dot{g} - 1}{g} \tag{4.15}$$

- Step 6. Calculate the velocity vectors.

4.3 Improved Lambert solver

A second Lambert solver has been selected to validate the results obtained with the bisection method. This new solver is a modified version of Lancaster and Blanchard by Dr. Dario Izzo from the European Space Agency, ESA. This algorithm does not use the universal variables nor the Stumpff functions. In addition, the solver works for single and multiple revolution transfers.

The main characteristic of this solver is the use of the household iteration method. It consist of a series of differential equations in the form of:

$$x_{n+1} = x_n + \frac{f(x_n)}{\dot{f}(x_n)} \left(1 + \frac{f(x_n)\ddot{f}(x_n)}{2\left(\dot{f}(x_n)\right)^2} \right) \tag{4.16}$$

$$f = T(x) - T^* \tag{4.17}$$

Where T is the dimensionless flight time, which is a function of the semi-major axis particularized for the minimum energy ellipse, a_m.

4.4 Porkchop plots

The porkchop plots allow to study different parameters such as the kinetic energy or the required Delta-V for different departure and arrival dates. To create these plots, the method of patched conics will be considered as well as circular parking orbits.

Each departure and arrival date is associated with a position vectors $\boldsymbol{R}_1$ and $\boldsymbol{R}_2$ respectively, and the transfer time is the difference in days between the departure and arrival dates. The velocity vectors are calculated with the previous Lambert solvers.

For the departure and arrival dates, the following ranges are selected:

- Departures: From 01-01-2031 to 20-07-2031.
- Arrivals: From 20-07-2031 to 05-02-2032.

4.4.1 Departure and arrival hyperbola characteristic energy

The excess velocity vector is calculated as the difference between the planet speed and the transfer velocity vectors obtained with the Lambert solver:

$$\boldsymbol{V}_{\infty_{Departure}} = \boldsymbol{V}_1 - \boldsymbol{V}_{Earth} \tag{4.18}$$

$$\boldsymbol{V}_{\infty_{Arrival}} = \boldsymbol{V}_{Mars} - \boldsymbol{V}_2 \tag{4.19}$$

The characteristic energy is equal to twice the kinetic energy of the hyperbola. For the departure and arrival is equal to:

$$C_{3_{Departure}} = V^2_{\infty_{Departure}} \tag{4.20}$$

$$C_{3_{Arrival}} = V^2_{\infty_{Arrival}} \tag{4.21}$$

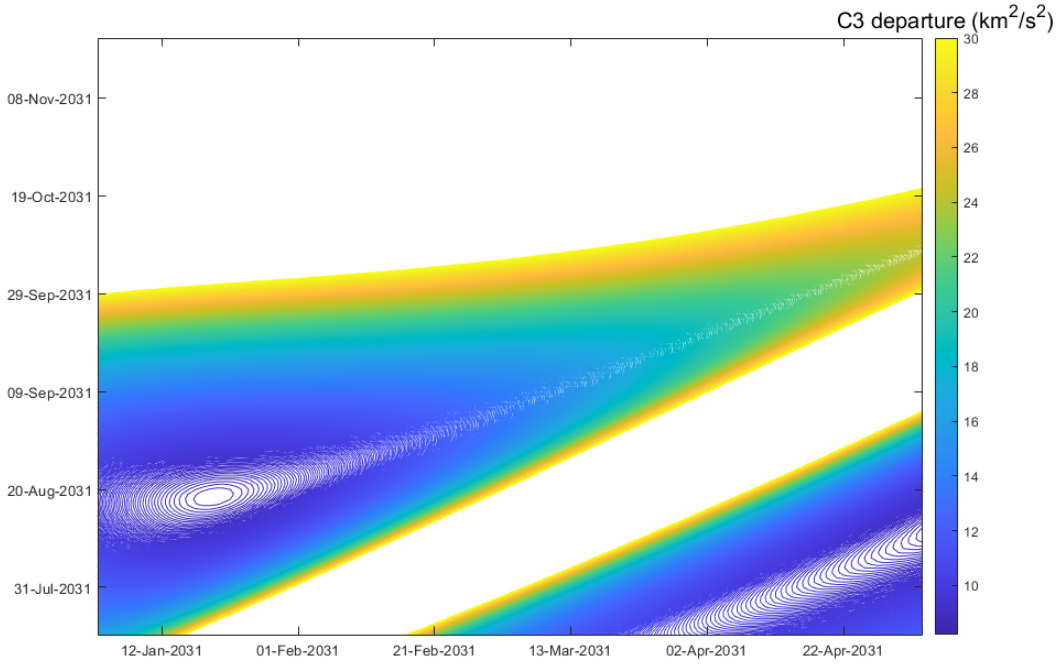

Figure 4.2: Porkchop plot: C3 departure solved with the bisection method.

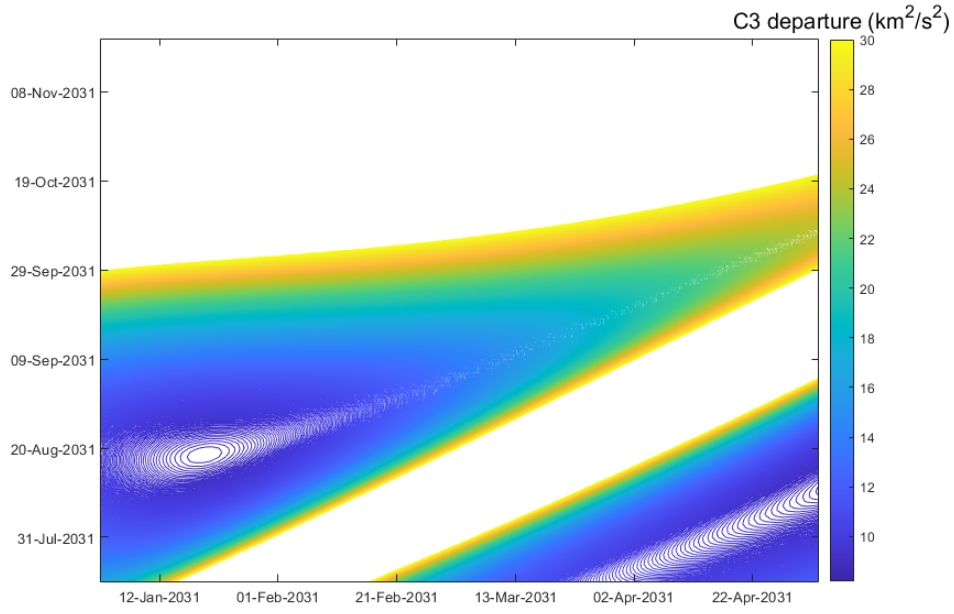

Figure 4.3: Porkchop plot: C3 departure solved with the robust Lambert solver.

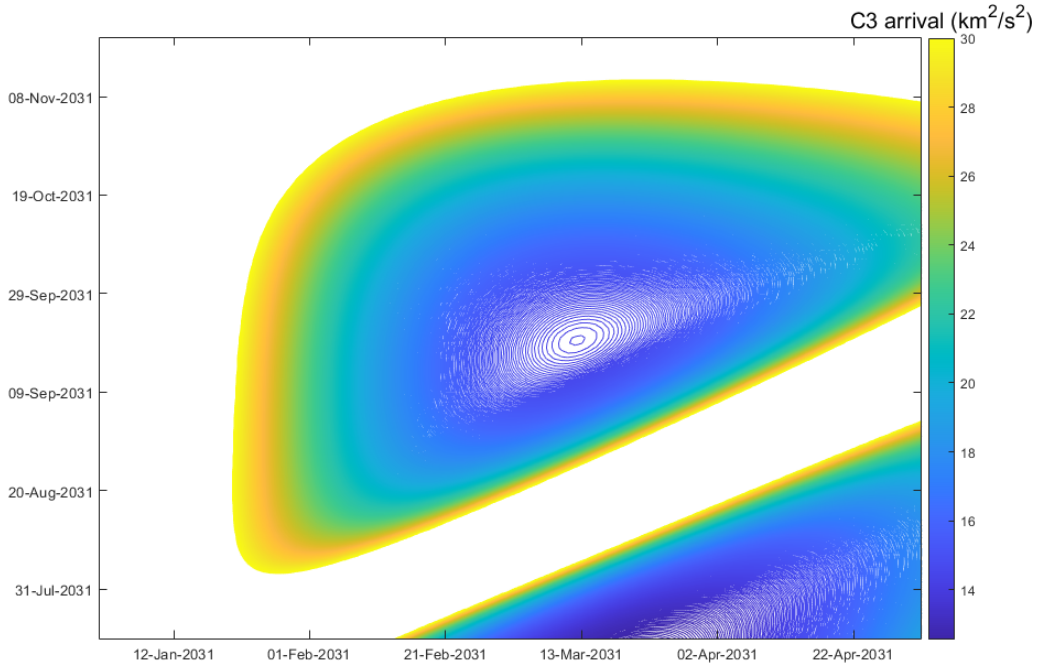

Figure 4.4: Porkchop plot: C3 Arrival solved with the bisection method.

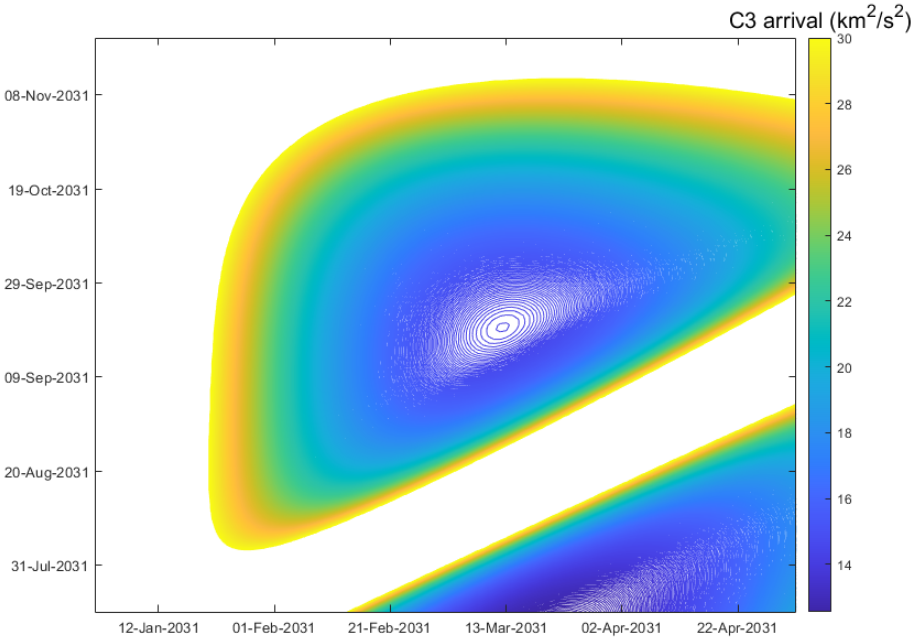

Figure 4.5: Porkchop plot: C3 Arrival solved with the robust Lambert solver.

4.4.2 Required ΔV

The parking orbit altitude for departure and arrival is 100 and 200 km respectively. The required delta-V for departure and arrival is calculated with the following equation:

$$\Delta V_{Departure} = \sqrt{\frac{2\mu_{Earth}}{r_{Parking}} + (|\boldsymbol{V}_1 - \boldsymbol{V}_{Earth}|)^2} - \sqrt{\frac{\mu_{Earth}}{r_{Parking}}} \tag{4.22}$$

$$\Delta V_{Arrival} = \sqrt{\frac{2\mu_{Mars}}{r_{Parking}} + (|\boldsymbol{V}_{Mars-\boldsymbol{V}_2}|)^2} - \sqrt{\frac{\mu_{Mars}}{r_{Parking}}} \tag{4.23}$$

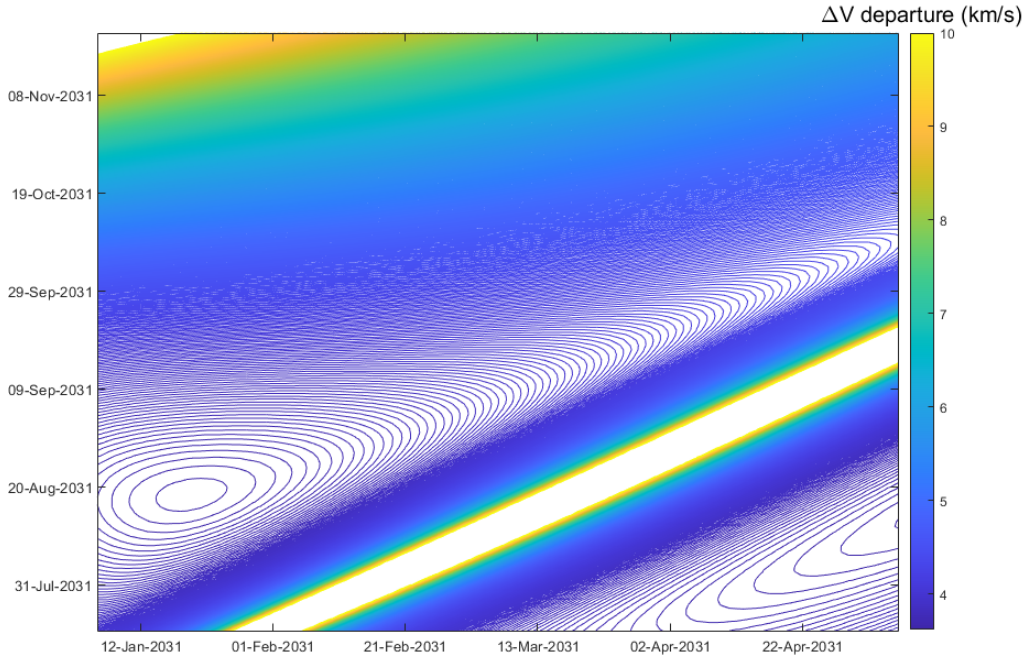

Figure 4.6: Porkchop plot: $\Delta V_{Departure}$ solved with the Bisection method.

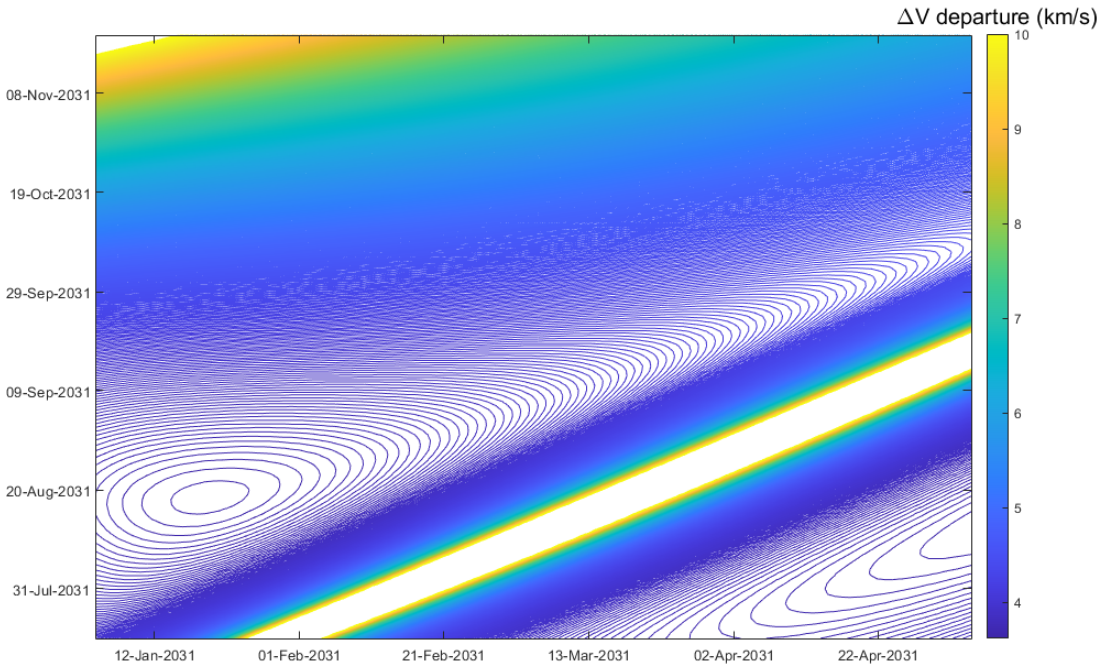

Figure 4.7: Porkchop plot: $\Delta V_{Departure}$ solved with the robust Lambert solver.

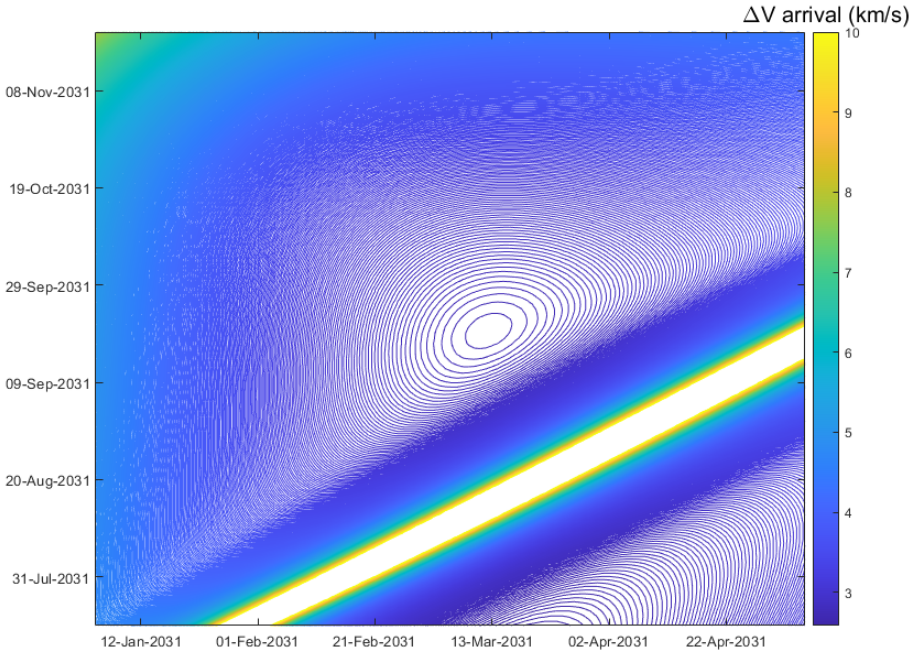

Figure 4.8: Porkchop plot: $\Delta V_{Arrival}$ solved with the Bisection method.

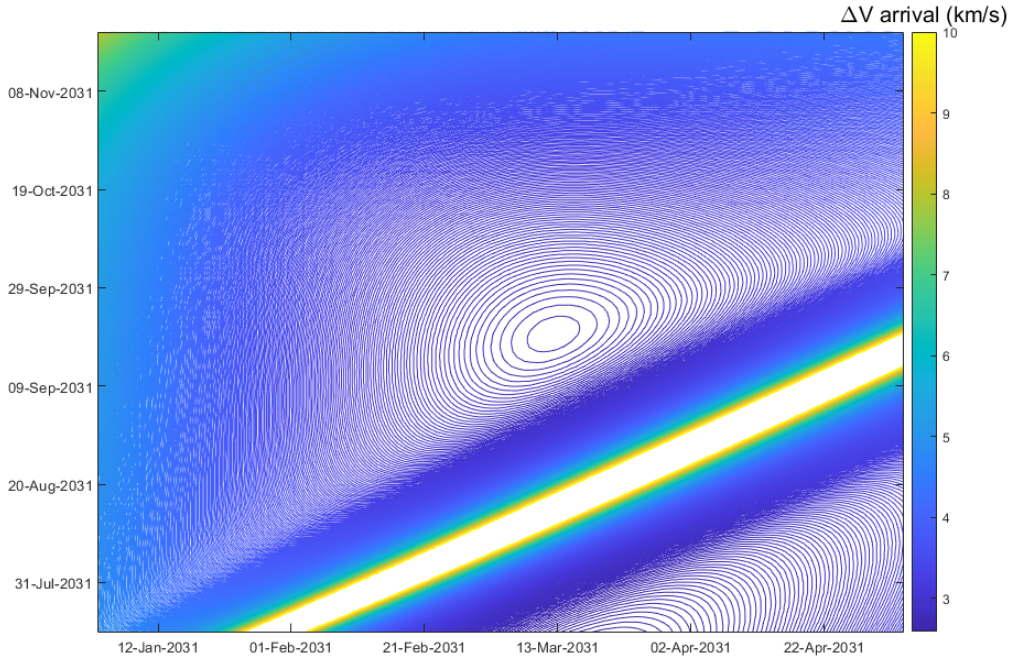

Figure 4.9: Porkchop plot: $\Delta V_{Arrival}$ solved with the robust Lambert solver.

Finally, the total ΔV is obtained as the sum of the Delta-V for departure and arrival.

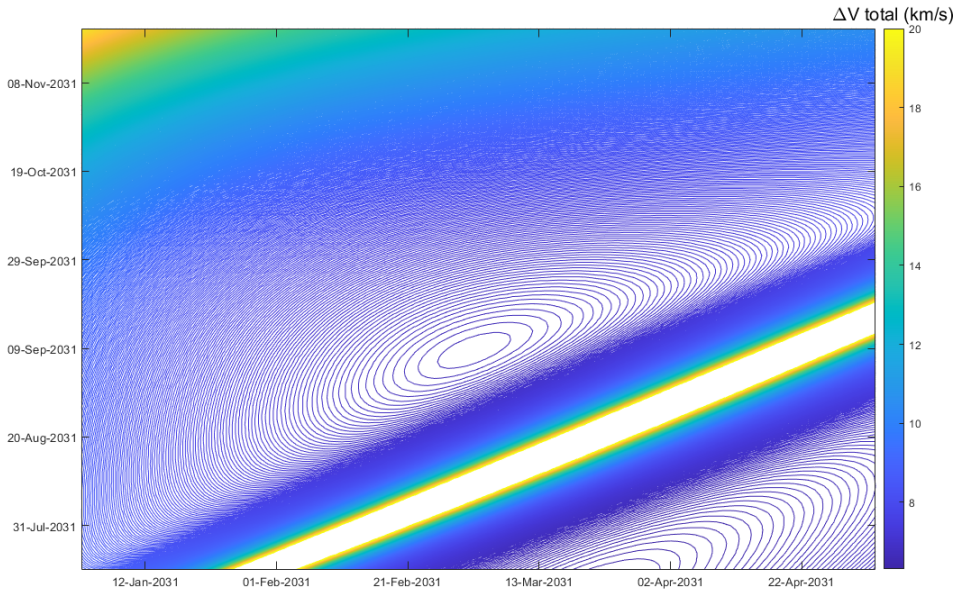

Figure 4.10: Porkchop plot: ΔV solved with the Bisection method.

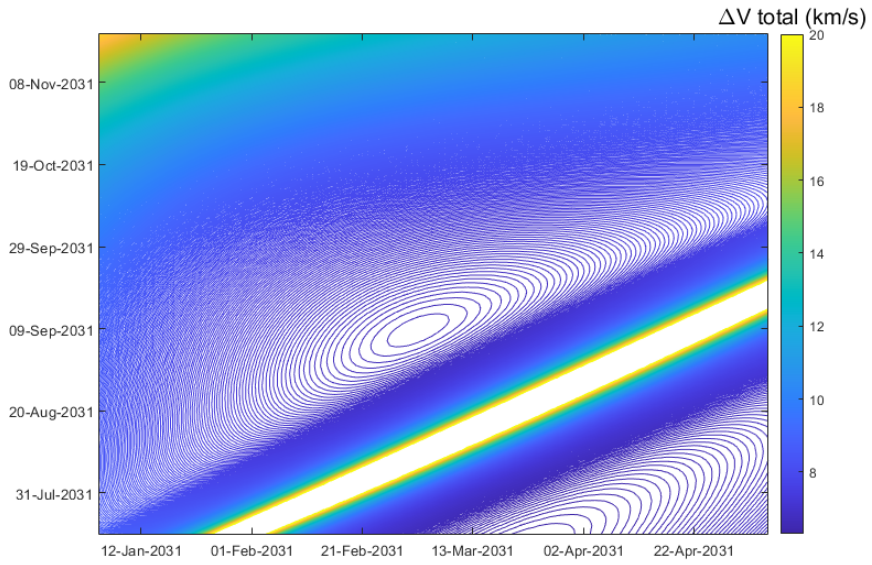

Figure 4.11: Porkchop plot: ΔV solved with the robust Lambert solver.

4.4.3 Earth-Mars transfer for different flight times with optimum ΔV

For this next subsection a set of different transfer times have been study for a minimum ΔV. The data used to create the porkchop plots was stored in a matrix of 200 by 200, where each row correspond to a departure date in intervals of 1 day and each column correspond to an arrival date in the same time interval. The minimum energy transfer can be easily obtained by finding the minimum value inside the matrix and its position allows to define the departure and arrival dates.

ΔV (km/s)	6.64
Transfer time (days)	210
Departure date (dd-mm-yyyy)	21/02/2031
Arrival date (dd-mm-yyyy)	19/09/2031

Table 4.1: Optimum energy transfer.

To find the minimum energy for a defined time transfer a search algorithm was create, which has the following structure:

- Define a lower and upper limits based on the acceptable range for ΔV.
- Start two loops to search each position of the ΔV matrix.
- Create a temporal matrix of the same size as the ΔV matrix to store the following values:
  - If the ΔV value for a given position is in the tolerance range, store the value in the temporal matrix.
  - If the ΔV is outside the tolerance range, store a value of 1000 in the temporal matrix.

- Find the minimum value in the temporal matrix and store it with its position.
- The stored row position correspond to a departure date and the column position correspond to the arrival date.

With the previous algorithm the minimum delta-V is obtained for a transfer time of 45 ,80, 90 and 100 days:

ΔV (km/s)	43.87	18.46	15.38	13.19
Transfer time (days)	45	80	90	100
Departure date (dd-mm-yyyy)	06/06/2031	02/05/2031	22/04/2031	12/04/2031
Arrival date (dd-mm-yyyy)	21/07/2031	21/07/2031	21/07/2031	21/07/2031

Table 4.2: Optimum energy transfer for different flight times.

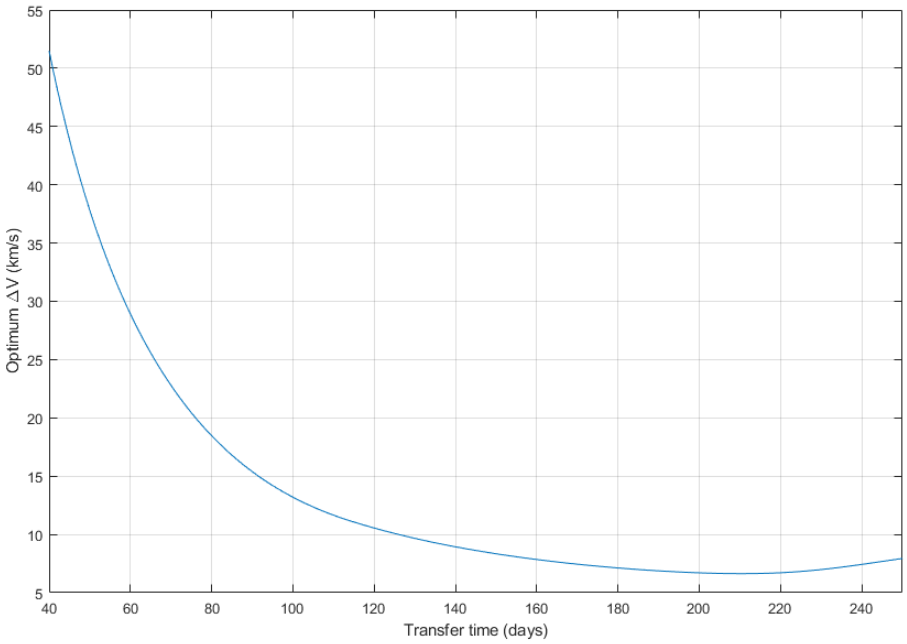

Figure 4.12: Optimum ΔV as a function of the transfer time.

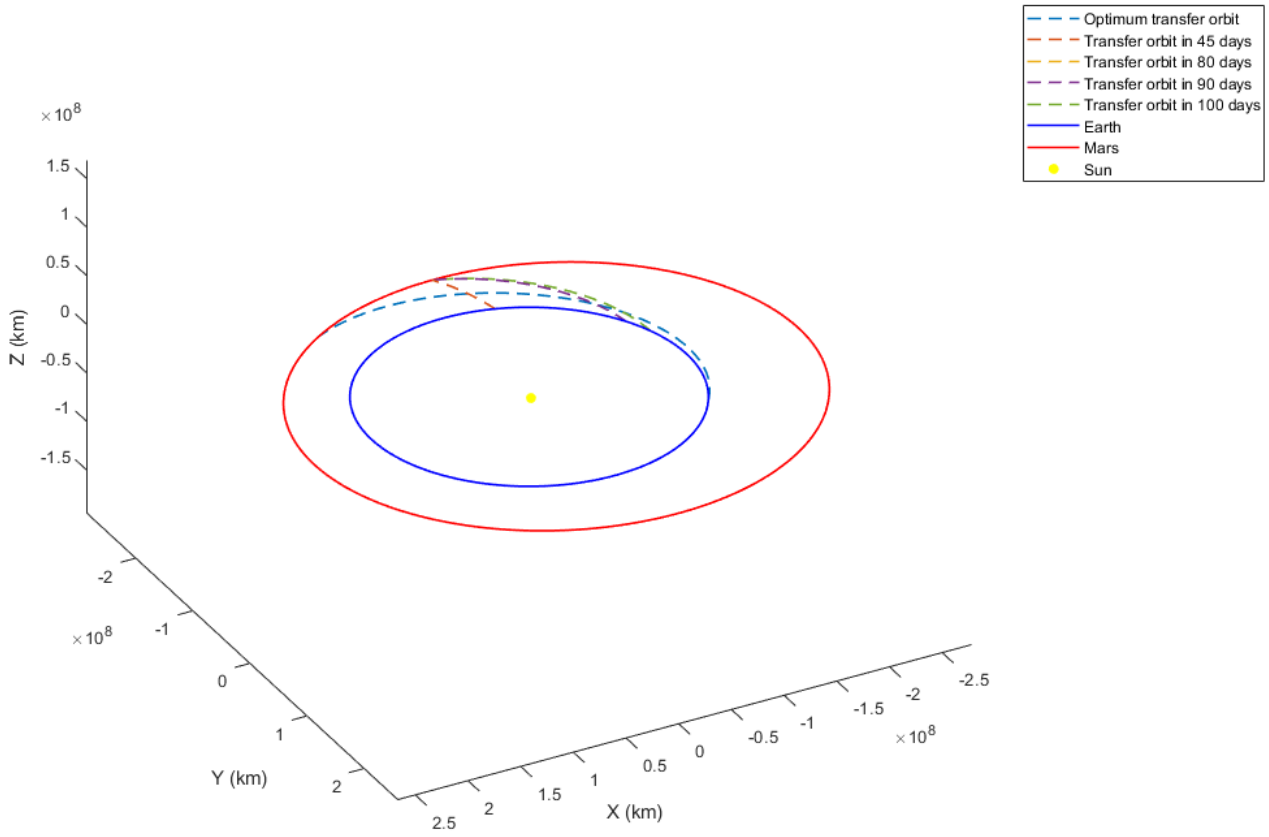

Figure 4.13: Orbit propagator for Earth-Mars transfers with different transfer times for optimum ΔV.

Chapter 5

Thermonuclear energy

5.1 Introduction

This chapter is an introduction to thermonuclear reactors to concisely show how this equipment work. Therefore, the content of these paragraphs constitutes an approach to describe the thermonuclear technology from a qualitative point of view, and at the same time to slightly quantify the most important thermonuclear reactions which happen in the core of the reactor.

Due to the complexity of this matter the description focusses the attention on one of the most known technologies, the Pressurized Water Reactors (PWR), which could be classified as nuclear reactors of third generation. Belonging to the third generation of nuclear reactors, it can be found technologies such as the Canadian CANDU with pressurized heavy water or the Boiling Water Reactors BWR from General Electric.

The fourth generation of thermonuclear reactors are complex technologies which let to reach high temperature of the refrigeration fluid such as those reactors with melted Lead as refrigerant or other with melted salts.

The main concepts included in this chapter are valid for other technologies of thermonuclear reactors, although the scope of the chapter is to decipher a complex technology with the intention to evaluate the feasibility of small thermonuclear reactors for application in aerospace propulsion.

The advantage of thermonuclear reactors as energy sources in aerospace vehicles is the high capability of portable energy in the nuclear reactor, which allows guaranteed travel for long periods of time due to its possibility to supply thermal and electric energy.

5.2 Pressurized water reactors, PWR

Figure (5.1) shows a thermonuclear conventional reactor PWR (pressurized water reactor) with three loops because the architecture is composed by three steam generators to cool and extract the heat from the reactor.

This nuclear reactor topology is the simplest industrial structure to build. However, recent constructions of PWR consist of 4 cooling loops.

Three water cooling pumps are required to cool the core of the reactor and remove the inner heat. A pressurizer plays an important role to maintain the pressure of the water in liquid state and avoid the boiling by sprinkling cold water inside the pressurizer or by heating the inner.

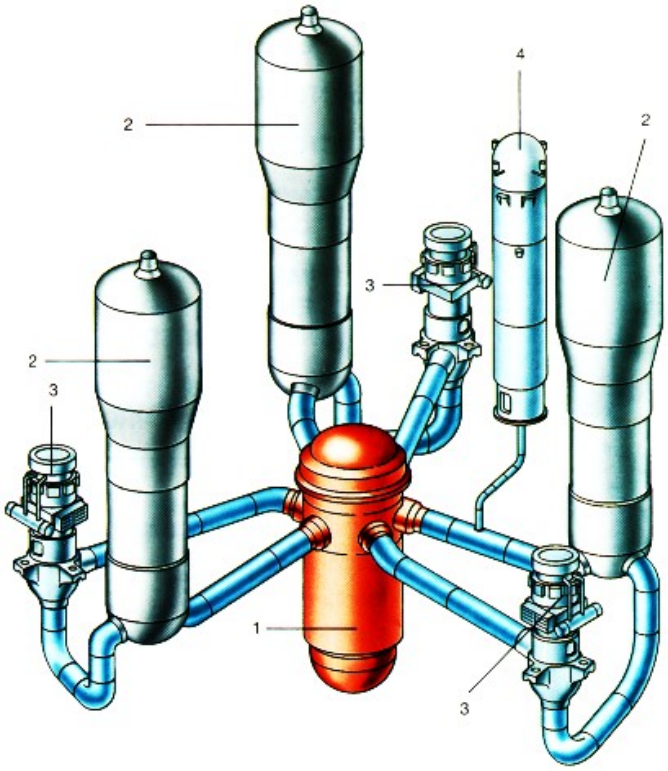

Figure 5.1: Pressurized water reactor of 3 loops. Source: Westinghouse [5].

1. Reactor vessel
2. Steam generator
3. Cooling water pumps
4. Pressurizer

5.2.1 PWR nuclear cooling topologies

The number of loops of a thermonuclear reactor depends on the thermal power generated at steady-state nominal power. In general, the thermonuclear topology requires one, two, three, or four loops connected in parallel to the reactor according to its nuclear power. In each loop, a cooling pump and a steam generator are essential components. Whereas, only one pressurizer is required for the nuclear architecture. Figure (5.2) shows normalized loops and components for several levels of electrical power.

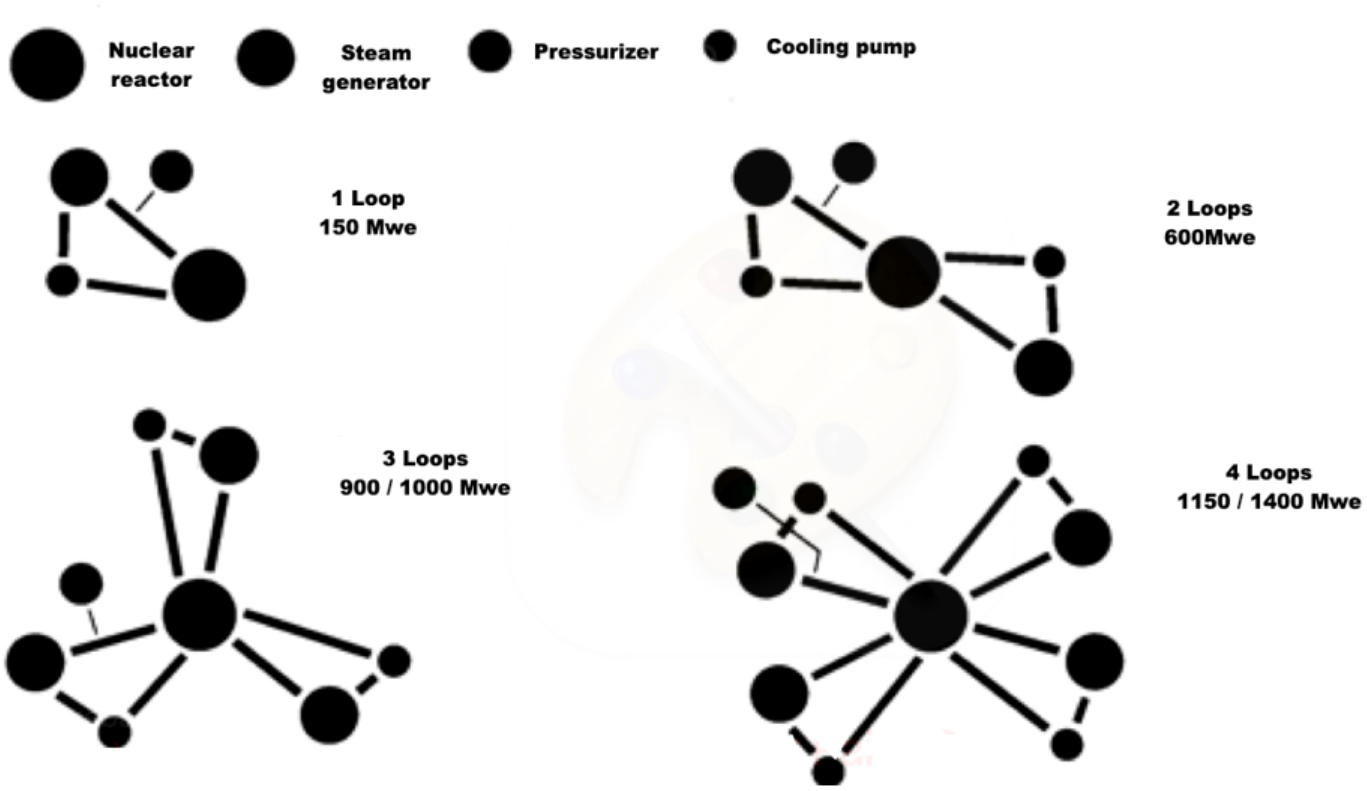

Figure 5.2: PWR for different number of loops.Source: Westinghouse [5].

The Nuclear Steam Generator System includes electrical heaters to produce steam inside the pressurizer and consequently increase the pressure of water inside the reactor and lower the level of the vessel.

On the other hand, in case of high pressure of water in the reactor then the control system activates the cold water showers inside the pressurizer to lower the pressure in the reactor (to approximately 155 bar).

The nuclear fission reaction of fuel gives off a lot of heat to be transferred to the water and therefore, the water flow inside the reactor is required to remove the heat of the core. The hot water, named hot leg, goes out from the reactor vessel by the outlet pipes towards the steam generators where the thermal energy is transferred by heat exchangers to the secondary circuit as steam (at approximately 80 bar) to thrust the steam turbine and the electrical generator. The flow of low-pressure steam outlet from the turbine (at approximately 0.05 bar) drops off in the condenser as water.

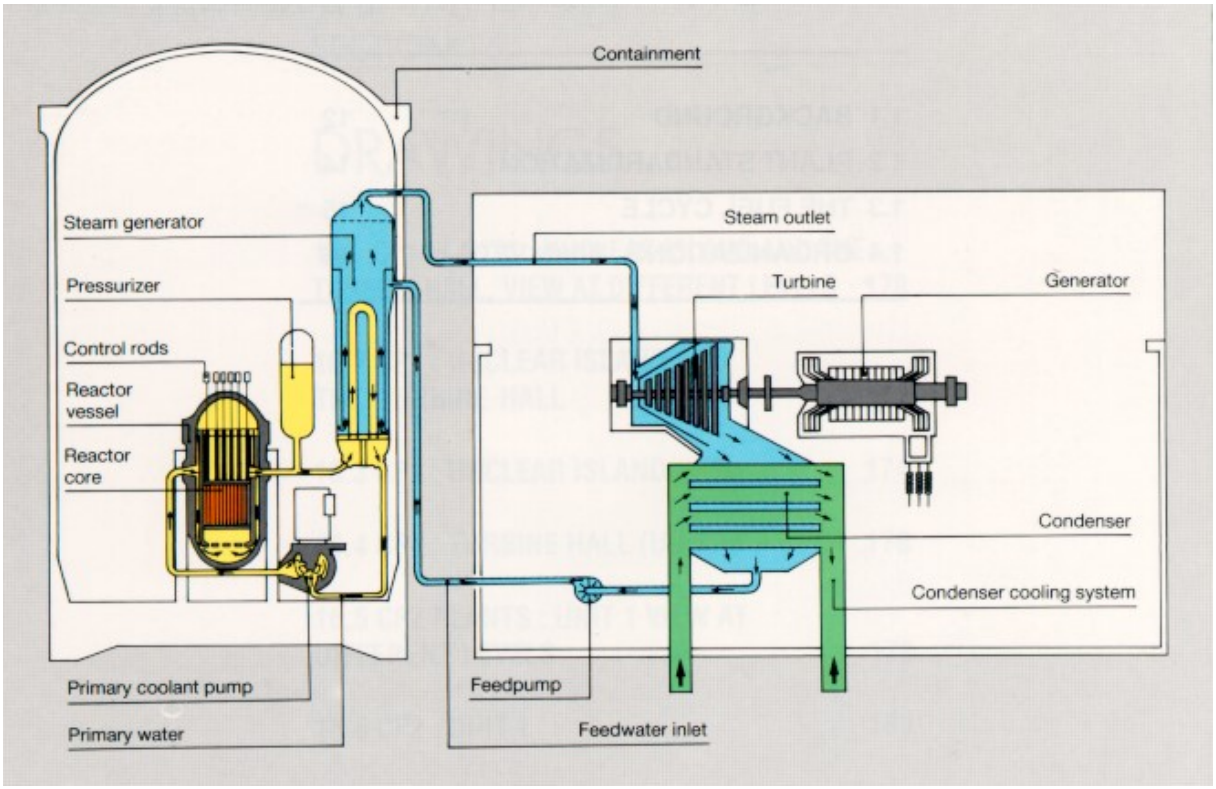

Figure 5.3: PWR diagram for one loop. Source: Westinghouse [5].

Figure (5.4) shows a brief description of the typical nuclear island of 1 loop where reactor, steam generator, cooling pump and pressurizer appear in a closed loop. Cooling pump forces cold water (563 K), cold leg, inside the core of the reactor for refrigeration and hot water (591 K) comes out from the reactor to the steam generator where heat exchangers transfer the thermal energy to the secondary circuit.

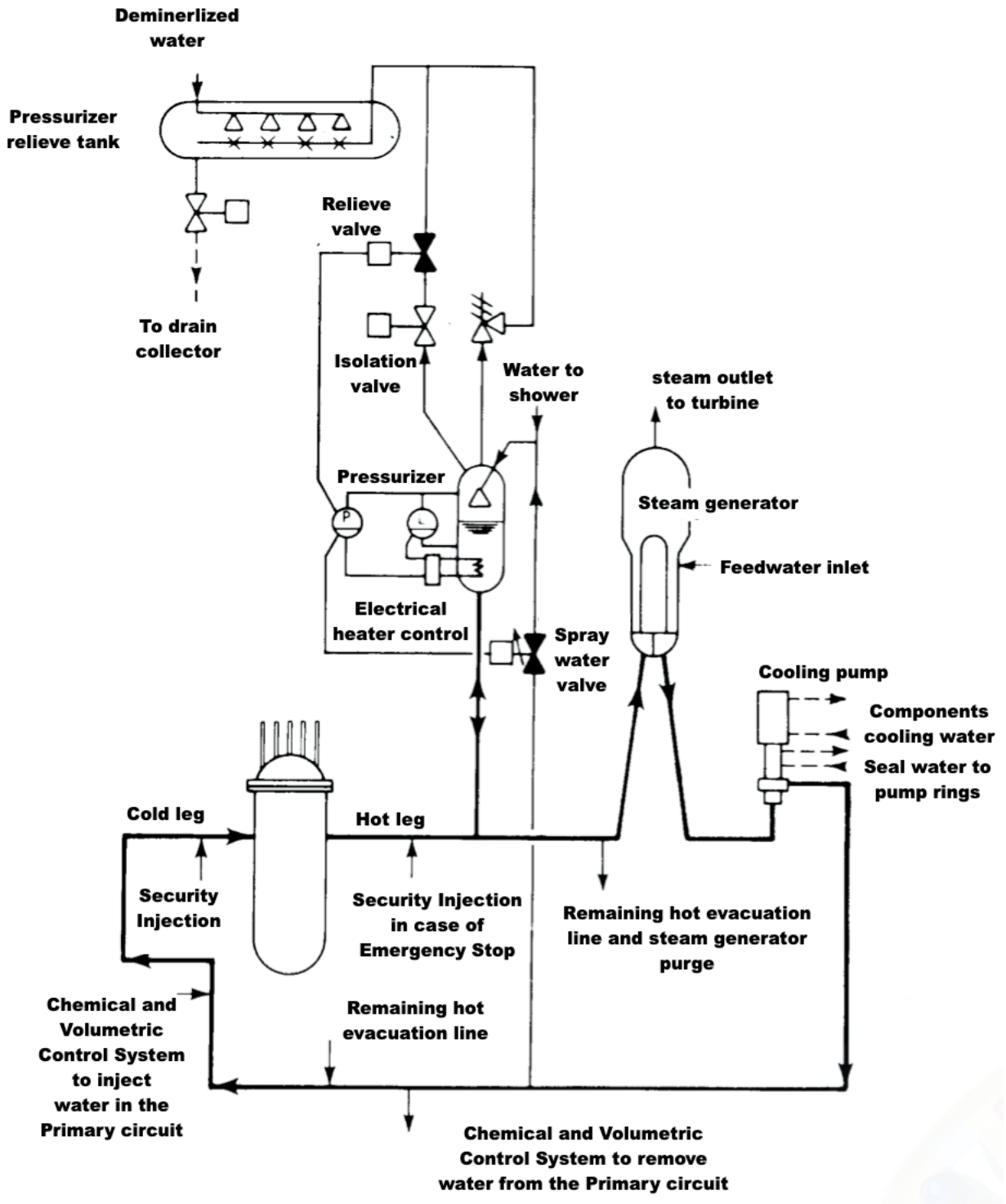

Figure 5.4: Cooling reactor system flux diagram. Source: Westinghouse [5].

The pressurizer is connected to one of the hot legs of the primary circuit and maintains and controls the pressure in the refrigeration circuit of the reactor, furthermore, it limits the variations of pressure during nuclear power transients according to design calculations.

Auxiliary components are necessary to fill up the refrigeration circuit of the reactor, addition or draining of water, purify water in the reactor, add anti corrosive chemicals and scavengers, participate in the control of power of the reactor, cool important equipment such as wirings and seals of Cooling Primary Pumps, evacuate the remaining heat in the core of the reactor during stop and stand by phases, and provide functionality to the security injections with high concentrations of acid boric to poison the water of the reactor and to scavenge neutrons and reduce the reactivity of the reactor.

5.3 Reactor internal parts

In synthesis, each pair of hot leg and cold leg, with its refrigeration pump of the reactor and its steam generator, work in parallel. The current description considers a 3 loops refrigeration system for a nuclear reactor with 1 pressurizer. The pressurizer includes: relief valves, safety valves, a relief tank, and the pipes to interconnect all the equipment to the primary circuit.

Every equipment is important in the nuclear island and a small description of many of them will be offered along this chapter to understand the essential principles of the technology it relies upon, but for the future purposes, the nuclear reactor is the main component to be considered in the aftermath analysis as the thermal generation of energy happens in this equipment.

The reactor vessel has a cylindrical geometry with a semi-spherical bottom end and a removable cover connected mechanically to the vessel by bolts, and the watertightness is assured by the installation of concentric metallic gaskets. In addition, the reactor vessel comprises its internal mechanical structure support, bundles of control rods, nuclear fuel assemblies, primary and secondary poisons, in-core nuclear instrumentation, the barrel, thermal shielding structure and other minor components. Inlet and outlet nozzles for the reactor refrigeration system are connected between the upper joint of the vessel and the core.

For North American reactors, the manufacturing and design of the vessel is according to the requirements of the Section III in the code ASME (American Society of Mechanical Engineers).

Figure (5.5) and Table (5.1) illustrate the main parameters of this kind of equipment.

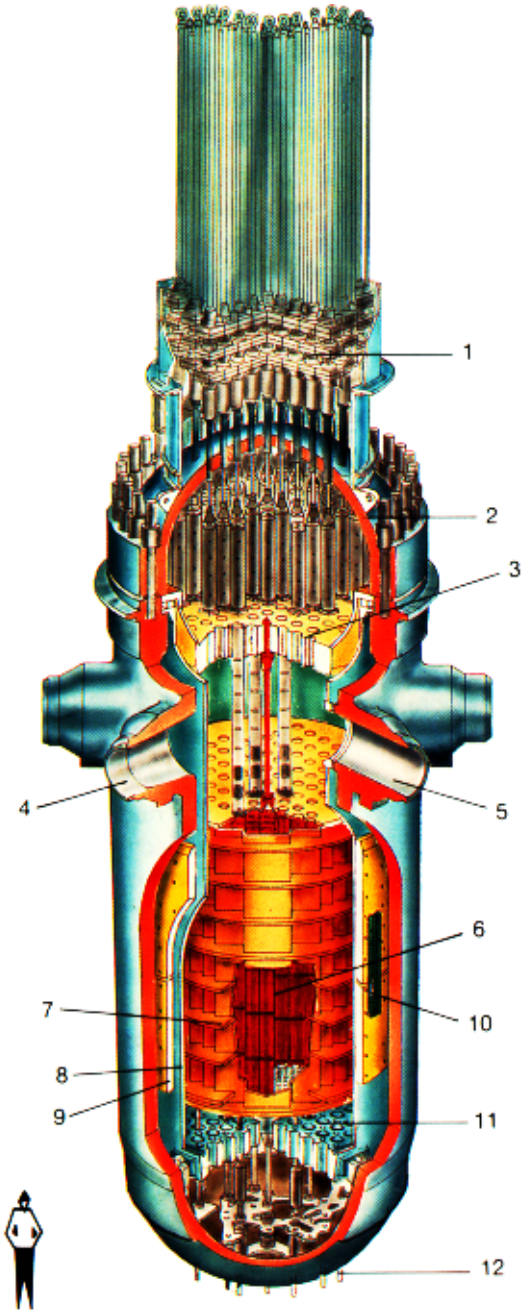

Figure 5.5: PWR vessel. Source: Westinghouse [5].

1. Control rods drive mechanism.
2. Head of the vessel (cover).
3. Plate support for guide tubes.
4. Inlet nozzle (cold water).
5. Outlet nozzle (hot water).
6. Fuel assembly.

7. Shielding.
8. Barrel.
9. Thermal covering.
10. Irradiated samples canister.
11. Core support plate.
12. Guide tubes for thimbles.

.

Thermal power (MW)	2785	3000
Length included the cover (mm)	$12,664$	$12,990$
Internal diameter	$3,990$	$3,990$
Radius from centre to inlet nozzle (mm)	3190	3190
Radius from centre to outlet nozzle (mm)	3110	3110
Nominal plated thickness (mm)	5.5	5.5
Minimum plated thickness (mm)	3.2	3.2
Volume of refrigerant with core and internal parts inserted (m^3)	104.5	112
Pressure in operation (bar)	156.569	151.961
Pressure design (bar)	167.941	168.628
Temperature design (K)	616	616
Material of the vessel	Low carbon steel alloy	
Material of the plates	Stainless-steel	

Table 5.1: Typical vessel parameters for 3 loops PWR. Source: Westinghouse [5].

Manufacturing of the reactor vessel is built upon low carbon steel alloys. Internal parts of the vessel contain a layer of austenitic stainless steel by welding deposition, which minimize the corrosion by the effect of pressure and high temperature in contact with water and chemical additives.

The vessel supports are integrated within its structure and simultaneously serve for hot legs and cold legs nozzles functionality. These support blocks lay on support plates at the upper part of the structure which is rigidly embedded to the reinforced concrete around the reactor vessel.

In general, the execution of welding activities complies with the requirements in Section III of the Code ASME, and particularly with those internal or external parts to the vessel working under pressure.

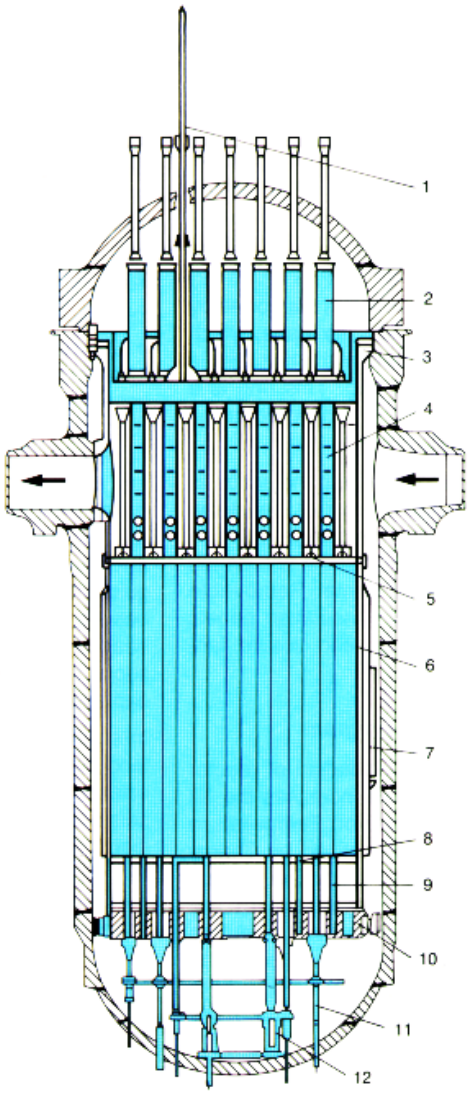

Figure 5.6: Vessel section. Source: Westinghouse [5].

- Upper internals:
  1. Thermocouples column.
  2. Guide tube.
  3. Support plate for guide tubes.
  4. Support column.
  5. Upper support plate for the core.
- Lower interns:
  1. Barrel.
  2. Thermal deflector.
  3. Lower support plate for the core.

4. Support column for the core.
5. Lower support plate.
6. Tubes for instrumentation/ thimbles.
7. Secondary support for the core.

5.3.1 Materials

Clasps, joints, and upper and lower hemispheric parts of the vessel are manufactured with low alloy steel type SA 533 grade A or B, class 1 for plates or type SA 508 class 2 or 3 in case of forged parts. The choice of this type of steels is because their mechanical properties fit with the conditions of operation, and they are available according to the requirements of sizes and thickness. The satisfactory behavior of these kinds of steel under the effects of gamma and neutronic radiation let easy welding. Every part of the reactor vessel in contact with the refrigerant, water plus chemical additives, is manufactured with a layer of stainless-steel series 300 or Inconel alloy.

On the other hand, manufacturing of bolts, nuts and washers is made with steel SA 540 class 3 (according to Std. AISI 4340), due to its mechanical properties (high strength and resiliency). Screwed surfaces and seats for surfaces with washers receive special treatments to improve resistance to the corrosion and increase their lubricants adherence properties.

5.3.2 Internal structure of the reactor

The internal structure design of the nuclear reactor has the following mechanical characteristics:

- Support and maintain in their positions the nuclear fuel assemblies and bundles of control rods.
- Compensate the dynamic efforts of the control rods.
- Transmit other mechanical loads to the joint of the reactor.
- Delimitate the water refrigeration areas in the reactor.
- Support nuclear instrumentation.

Internal screws in the core structure are manufactured with stainless-steel 316 or Inconel X750. The mission of these screws is only to fix mechanical elements.

The internal structure of the core of the reactor contains 3 main components:

- The lower support structure for the core.
- Upper support structure for the core.
- Support structure for nuclear instrumentation.

5.3.3 Internal core support structure

The lower support structure for the core is the main element for containment and global support. This structure includes the barrel of the core, deflectors, neutronic panels and lower support plate which is welded to the barrel of the core. The cover of the reactor relies on the joint at the upper end of this structure. The lower end transversal movements and vibrations of the structure are compensated by the use of radial tie-beams with the wall of the vessel. Core support relies upon the lower level of this, below the deflector plates, and functions as supports and orientation of the fuel assemblies. The lower end plate support for the core is fitted by sockets with holes and bolts to couple the fuel assemblies.

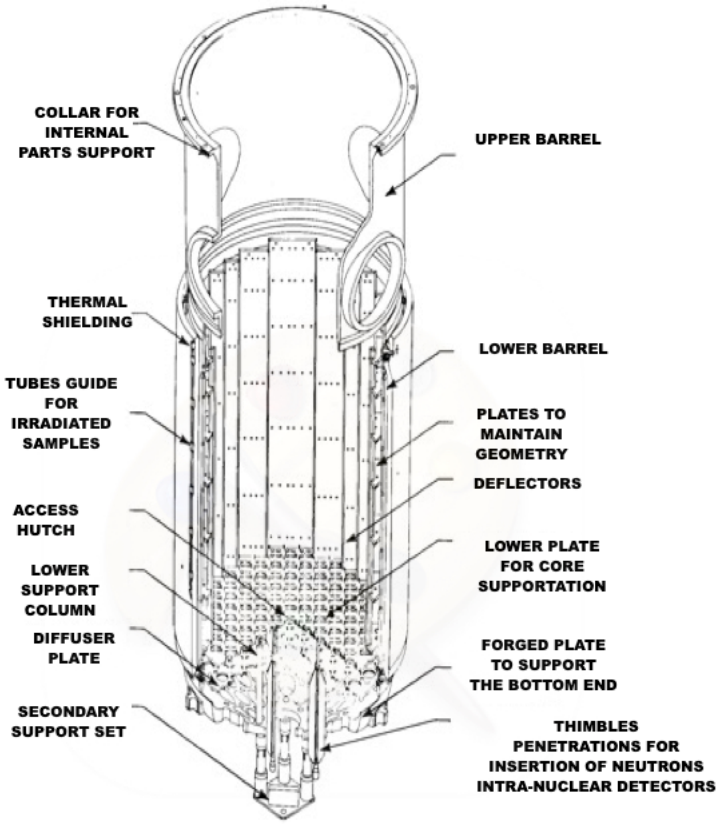

Figure 5.7: Lower support structure of the core. Source: Westinghouse [5].

The lower support structure, including the barrel, as an important thermal-hydraulic structure, it has the function to conduct, and control the flow of refrigeration water inside the core. The water flow (cold water) comes into the reactor across the inlet nozzles and comes down flowing downward in the space between the wall of the reactor vessel and the barrel of the core until the bottom end where the flow of cold water is deviated upward to refrigerate the core assemblies and the internal structure. The holes in the internal mechanical structure have been calculated according to the thermal-hydraulic requirements to optimize the refrigeration and convey the water flow upward in the core until the outlet nozzles as hot water.

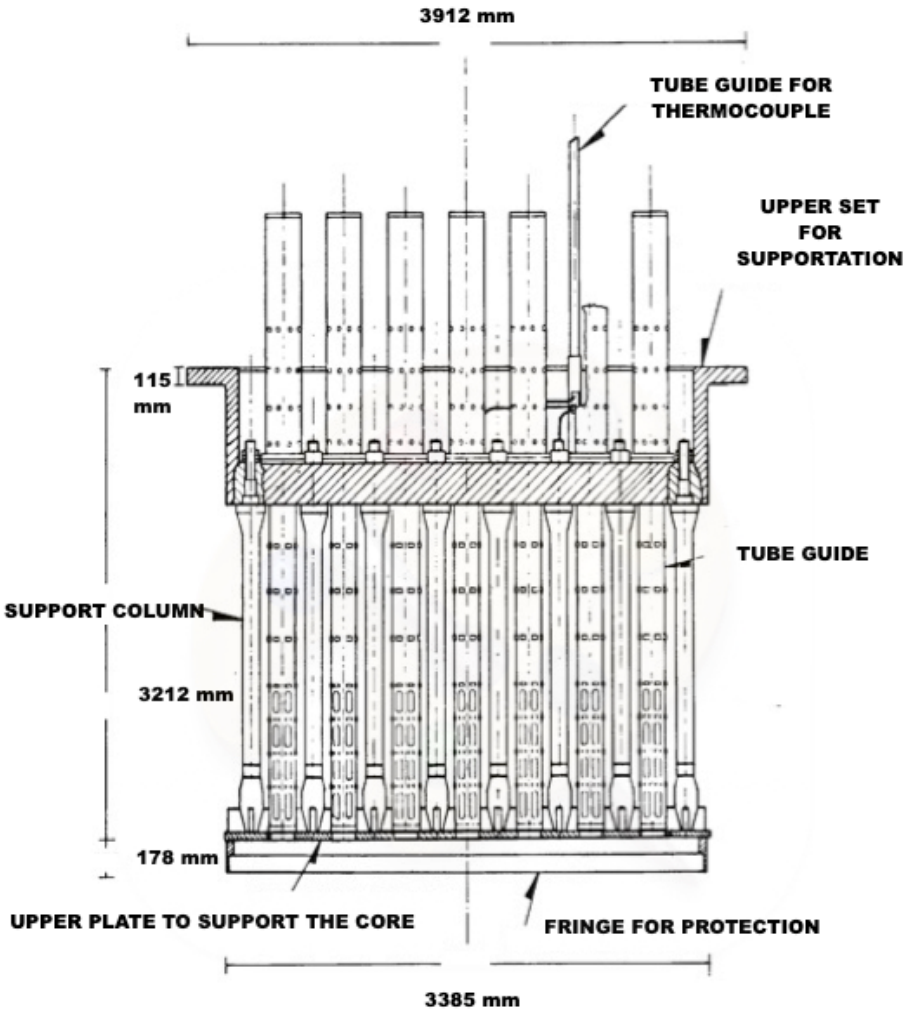

Figure 5.8: Upper support structure for the core. Source: Westinghouse [5].

5.3.4 In-core and ex-core nuclear instrumentation

Two kinds of nuclear instrumentation in the reactor are under consideration:

- In-core instrumentation.
- Ex-core instrumentation.

The support structure for in-core instrumentation is placed in two different parts of the reactor.

The scope of intra nuclear thermocouples penetrations, on the upper side of the cover of the vessel, is to place in fixed positions inside the core thermocouples to measure in-core temperatures and generate a 3D map of temperatures.

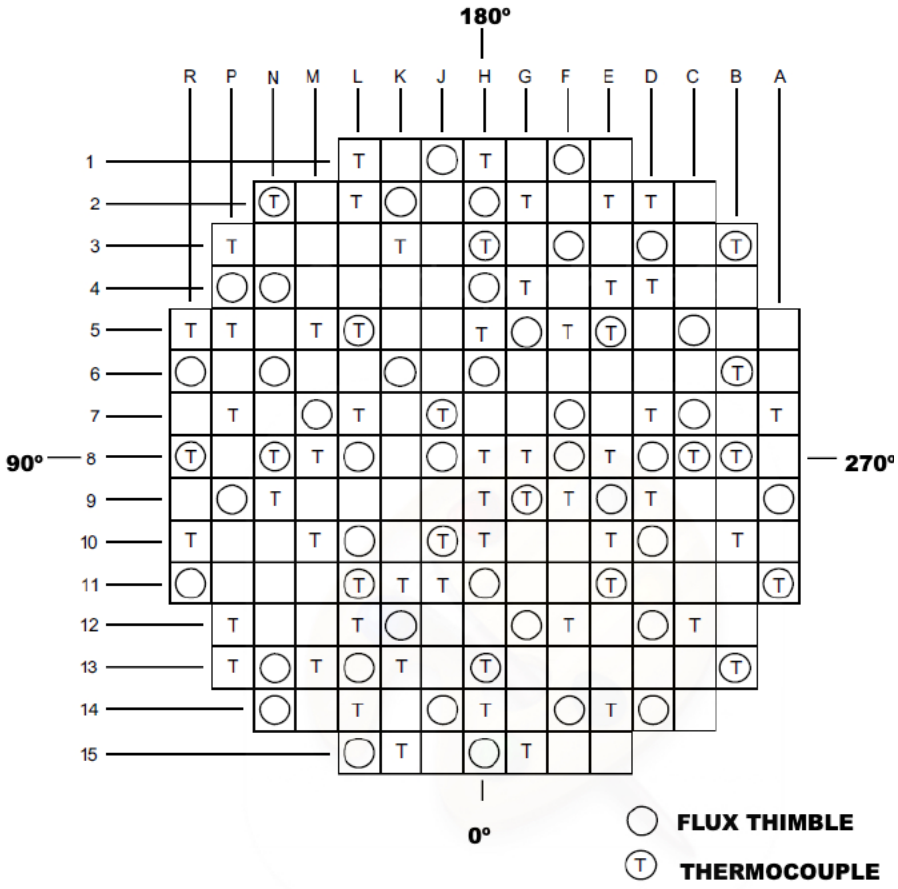

Figure 5.9: Distribution of in-core nuclear detectors and thermocouples. Source: Westinghouse [5].

The control of temperature in the core is necessary to avoid damages in the fuel rods and in the control rods by exceeding the temperature restrictions of the alloy Zircaloy-4. Fissures in the fuel rods provoke a release of nuclear fuel and other subproduct from the nuclear fission into the refrigeration water circuit what significantly increases the radioactive contamination in the water and consequently in the ambient by purges from the primary circuit of water out the building of containment.

To replace the nuclear fuel is necessary to retrieve all the thermocouples and control rods mechanisms before of removing the cover, and for this reason the thermocouples fittings are specially designed to support the pressure of 155 bars from the primary circuit and avoid any leakage of water.

At the bottom of the vessel, there are special tubes of penetrations to insert and withdraw mini nuclear detectors in different positions of the core with the purpose to generate 3D maps of the neutronic distribution. These maps are generated when the reactor is in steady state of nuclear power and the purpose is to get data for the calibration of external nuclear detectors which control the reactivity and the nuclear power of the reactor. In any case, the penetrations in the vessel are sealed to guaranty no leakages outside of the vessel.

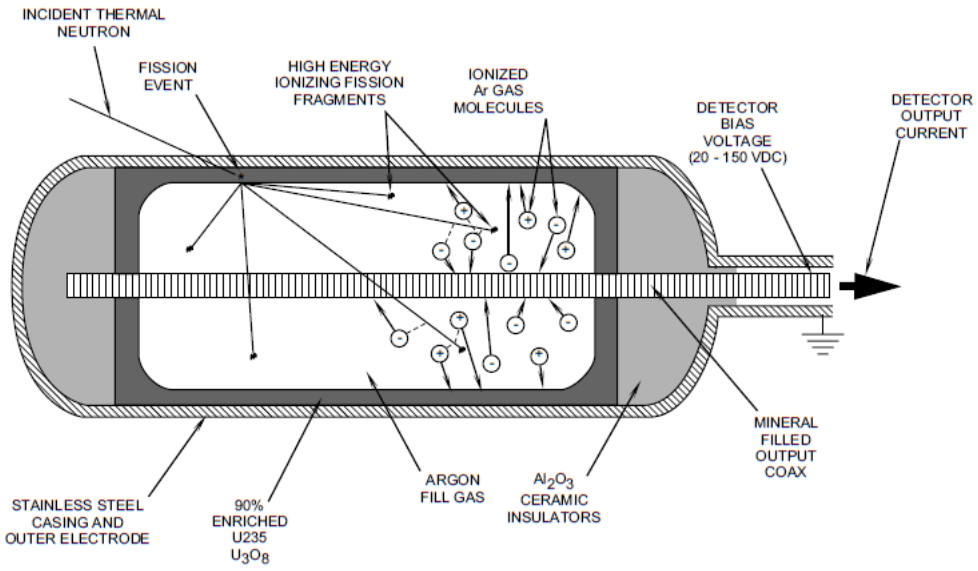

Figure 5.10: In-core neutrons detector. Source: Westinghouse [5].

The in-core nuclear detectors contain Uranium-235 highly enriched which is fissionable by the neutrons, what contributes to deliver currents about some mA when they are inserted in the core, and for this reason, following the 3D neutronic map conclusion, the in-core nuclear detectors are withdrawn from the core to avoid their destruction by the high neutronic flux in the core.

In the PWR technology, the reactor control is always performed by controlling the nuclear power of the reactor by nuclear detectors outside the vessel. The ex-core nuclear detectors are strategically placed outside the vessel and measure the percentage of neutrons fleeing from the vessel. The calibration of the ex-core nuclear detectors requires a reference from the data 3D neutronic maps generated by the in-core nuclear detectors. The ex-core nuclear detectors for the range of power are long aluminium cylindric tubes of just about 2 meters long with an inner layer of boric silicate. The atom of boron interacts very easily with neutrons and suffers an atomic transmutation which split the atom of boron and generates an alpha particle with electrical charge, (nuclei of Helium atom), and an atom of Lithium.

$$^{10}_{5}\mathrm{B} + {}^{1}_{0}\mathrm{n} \longrightarrow {}^{7}_{3}\mathrm{Li} + {}^{4}_{2(\alpha)}\mathrm{He}$$

Figure 5.11: Boron atomic transmutation.

5.4 Reactor cooling water pumps

Every refrigeration loop of the reactor requires a reactor water cooling centrifugal vertical pump to evacuate the heat from the in-core. These pumps work at extreme physical temperature and pressure, 573 K and 155 bar.

Under these work conditions, an impressive physical barrier is needed in order to isolate the primary circuit from the ambient conditions at 1 bar and 313 K inside the containment building. To

carry out the above-mentioned isolation barrier, every pump contains a sophisticated seal system with pressurized demineralized water to counteract the pressure of the primary circuit and at the same time to control the leakage of water from the primary circuit by the seals of the pumps.

5.4.1 Cooling water pumps description

Every pump boosts the water inside the reactor across its hot primary loop by a propeller in the bottom side of the axle shaft. The water, at 155 bar, runs inside the inlet nozzle of the pump and then, the propeller at the axle shaft sucks the water and communicates rotational kinetic energy which is converted into hydraulic pressure after it pass across the diffuser. Water is ejected by the outlet nozzle of the pump, at 155 bars $+\Delta P$, in the hot primary loop towards the steam generator.

Figure (5.12) illustrates a typical cooling water pump of a pressurized water reactor:

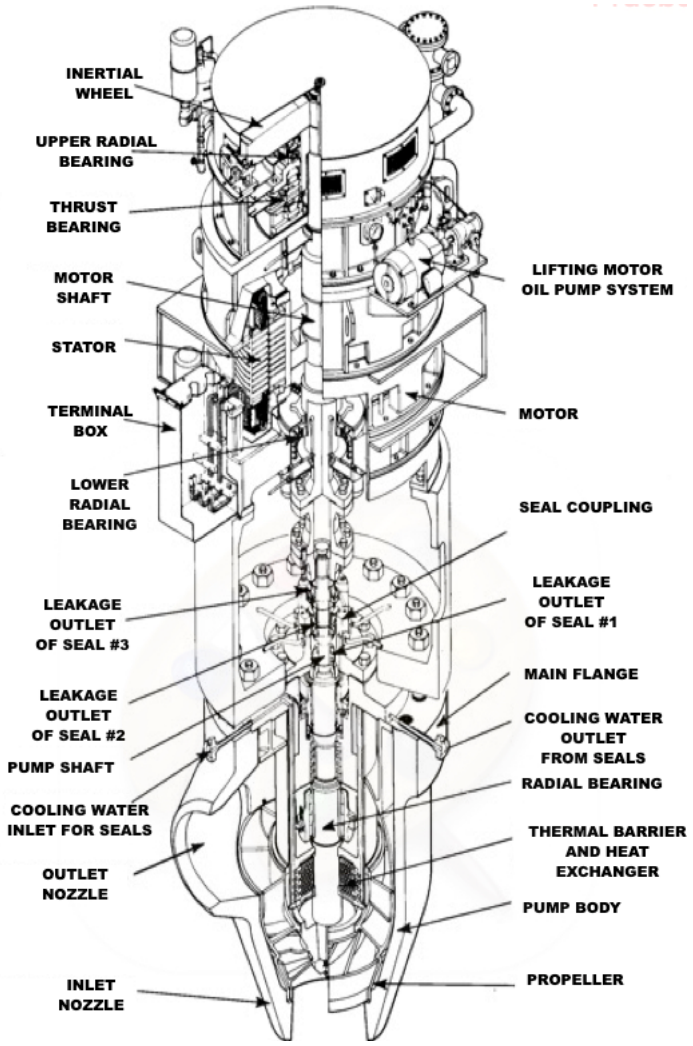

Figure 5.12: Primary cooling water pump. Source: Westinghouse [5].

Number of pumps	3
Flow of water (m^3/h)	$23,500$
Manometric height pressure (m column water)	95
Pressure design (kg/cm^2)	172
Temperature design (K)	616
Suction temperature at full load (K)	566.3
Type of motor	Induction, 3 Phases AC
Nominal voltage (V)	6.600
Body diameter (mm)	2.390
Height (mm)	8900
Rotational speed (rpm)	1485
Ambient temperature (k)	323

Table 5.2: Typical parameters of a reactor cooling water pump, 3 loops. Source: Westinghouse [5].

5.5 Steam generators

In a PWR power plant, the internal structure of each steam generator comprehends a bundle of vertical tubes in a U shape, to work as a heat exchanger.

Due to the great dimensions and heavy weight, steam generators must be manufactured in two halves to facilitate the transportation from the factory to the Power Station and at the same time each half is selected and manufactured according to specific operational requirements. In this sense, the lower half of the steam generator will operate as evaporation section, and the upper half will operate as steam and dehumidifier section. Both sections, upper and lower, will be assembled at the site. Steam generators are designed and manufactured according to the rules ASME, Sections II, III, IX y XI.

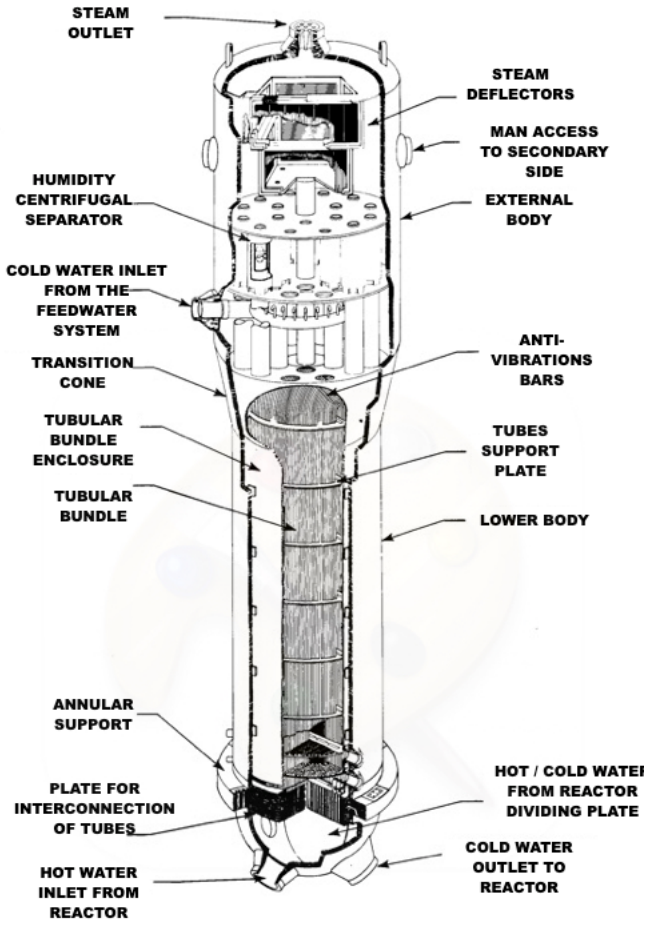

Figure 5.13: Example of a steam generator. Source: Westinghouse [5].

5.5.1 Steam generator operation

PWR power stations are based upon closed loops for refrigeration and heat extraction, what means that cooling water for refrigeration of the reactor is enclosed in the primary island or circuit completely independent to the secondary water where the steam generators produce steam, which moves the turbine rotors, producing mechanical energy.

Type	Vertical, U tubes, dehumidifier
Global height (mm)	22,000
Outer upper diameter (mm)	5,100
Outer lower diameter (mm)	3,800
Primary operation tubes pressure (kg/cm^2)	155
Primary operation tubes design (kg/cm^2)	172
Primary operation tubes temperature (K)	616
Steam pressure at full load (turbine) (kg/cm^2)	75.8
Maximum steam humidity at full load (turbine) (%)	0.25
Pressure design at secondary side (kg/cm^2)	89.5
Reactor refrigeration flow (Kg/s)	4,850
Inlet hot water from reactor (K)	605
Outlet cold water to the reactor (K)	565
Body material	Steel Mn-Mo
Bottom material	Steel, inner layer of Inconel
Tubes	Inconel 600
Outer tubes diameter (mm)	17.5
Average wall tubes thickness (mm)	1.5
Weight empty (kg)	415,000
Weight in normal operation (kg)	485,000

Table 5.3: Typical specification of a steam generator for a PWR power station. Source: Westinghouse [5].

5.6 Pressurizer

The pressurizer is the equipment responsible for maintaining the pressure of water inside the reactor during normal operation and reacts to any change of pressure in this circuit when any transient happens. Consequently, the pressurizer assures the equilibrium between the phases of water and steam at around 155 bar and 573 K.

The pressurizer is a carbon steel cylindrical structure with semi-spherical form at the top and at the bottom, but the interior is in contact with water and steam and therefore is covered with a stainless-steel plate to avoid rusting. Heating resistances are mounted at the bottom in contact with the water in such way to let their maintenance. Showers valves, relieves and safety valves are placed at the top of the pressurizer.

5.6.1 Operation

About the 60 % of volume of the pressurizer contains water during normal operation and the remaining 40 % corresponds to steam at 150 bars and around 573 K. It is extremely important to maintain the balance between water and steam, as the ratio 60% of water to 40% of steam guarantees the stability of the physical process in the primary circuit.

Electrical resistances inside the pressurizer maintain the temperature of water at the point of saturation while the pressure is constant according to the reactor requirements. At normal operation, the pressurizer must contain water under any circumstances to assure the refrigeration of the in-core of the reactor without boiling.

The showers valves open and inject "cold" water (from the cold legs of the reactor) in the pressurizer when the control system detects excess of steam beyond 60 % in the pressurizer. This action lets to low any increase of pressure, and simultaneously increasing the level of water in the pressurizer.

The thermonuclear circuit or primary island has an enormous thermal inertia when the control system demands to increase or decrease electrical power.

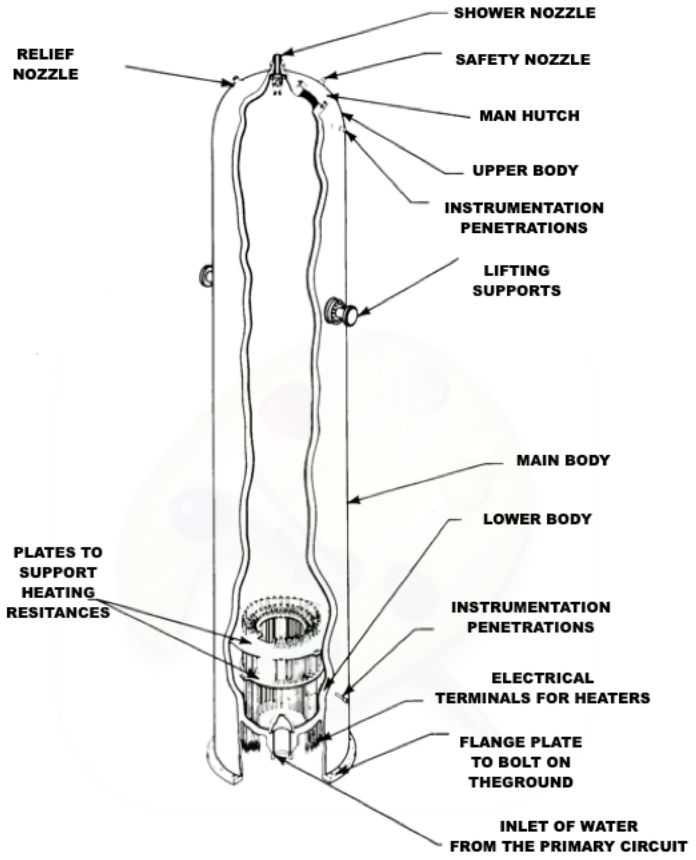

Figure 5.14: Pressurizer of a PWR power plant. Source: Westinghouse [5].

When the control system demands to reduce the electrical power generation then the average temperature of the refrigeration water in the reactor increases, and therefore, the increment of steam and pressure in the pressurizer must be compensated by the activation of shower valves.

Number and type	1 Pressurizer, 2 phases water steam
Global height (mm)	14,500
Outer diameter (mm)	2,340
Volume of water (m^3)	27.2
Volume of steam (m^3)	18.1
Pressure design (kg/cm^2)	172,4
Temperature design (K)	633
Type of heaters	Electric
Number of heating resistances	78
Heating power (Kw)	1600
Number of relieves valves	2 motorized
Number of safety valves	3
Flow of showers during a transient (l/s)	47.3
Flow of showers at steady state (l/s)	0.063
Body material	Steel Mn Mo, with inner stainless-steel plate
Weight empty (kg)	84,000
Weight during normal operation (kg)	100,000

Table 5.4: Typical specification of a pressurizer for a PWR power station. Source: Westinghouse [5].

If the control system demands to increase the electrical power generation, then the average temperature of the refrigeration water in the reactor decreases, and therefore, the saturation of steam happens in the pressurizer with a decrease in water pressure. Thus, this event must be compensated by the activation of the electrical heaters.

A high demand for electrical power from the control system provokes the extra heating of the refrigeration water of the reactor beyond the capacity to mitigate the event only with the shower valves. Under this scenario, the relieves valves automatically open to evacuate part of the steam in excess to the " relief tank of the pressurizer ". If the pressure of the steam exceeds the capability of the relief valves, then the safety valves open automatically to discharge the exceeding steam to the " relieve tank of the pressurizer ".

5.6.2 Core system of the pressurizer

As mentioned before, the control system of the pressurizer holds up the value of the pressure in the primary circuit inside the acceptable limits of operation.

A dysfunction of the control system of the pressurizer out of the working limits provokes not only a trip of the reactor, (in nuclear terminology "trip of the reactor means an emergency stop of the reactor"), but important and spontaneous changes in the reactivity of the reactor, what means instantaneous variations in the coefficient " k_{eff}" and therefore in the population of the neutron flux which affects directly to the nuclear kinetics.

In extreme situations, a transient process with a very low level in the pressurizer accompanied with high volume of steam might provoke local boiling zones in the in-core with a consequent deficiency in the refrigeration of the nuclear fuel assemblies, which could damage the fuel tubes due to high temperature beyond the thermal limits of the alloy Zircaloy-4.

5.7 Reactivity control in a reactor

The control of a fission chain reaction is carried out by the insertion of neutronic poisons or the dilution of them inside the reactor. The meaning of neutronic poisons refers to a family of chemical compounds or alloys whose atoms (at least one in the compound or in the alloy) can interact with neutrons, in such a way as to trap the neutrons in their nuclei which will suffer an atomic transmutation. The result of neutrons captures by some atoms, mainly by the poisons, provokes consequently the diminution of neutron concentration in the reactor.

As a reminder, it is necessary to consider that the fission of any atom of nuclear fuel produces more than one neutron what infers the sustainability of the reaction in chain. Thus, the neutronic population in the reactor increases or decreases according to the concentration of the poisons, and therefore, the fission reaction in chain is controllable because the coefficient of reactivity "k_{eff}" of neutronic reproduction will change from nearly "0" (sub-critical state of the reactor) to "1" or a little bit greater than "1" (critical state of the reactor).

A variety of neutronic poisons are available to control the reactivity in a nuclear reactor:

- Control rods: they are typical elements in nuclear reactor technology to control nuclear power in a reactor. This method consists in the insertion or the extraction of control rods in the core of the reactor to maintain the nuclear population in connection with the set point of nuclear power.
- Boron: as a compound of boric acid, boron atoms are great neutrons scavengers because their effective sections of nuclei are suitable to trap neutrons.

The concentration of boric acid in the refrigeration water of the reactor is extremely high (at least 2000 ppm in weight) during the state "Stop" even more when the nuclear fuel is new, "Beginning Of Life" or BOL. This high concentration assures a low neutronic population in the reactor to maintain it in sub-critic state.

Vice versa, the concentration of boric acid in the refrigeration water of the reactor is extremely low (around 100 ppm in weight) during the state "Power" even more when the nuclear fuel is

burned, “End Of Life” or EOL. This low concentration of boric acid is necessary to increase the reactivity as much as possible and maintain nuclear power according to the control set point. Burned nuclear fuel state means that the quantity of fissionable atoms has decreased considerably because of the generation of thermal power.

During normal operation the control rods are practically extracted from the reactor and the control system is in charge to insert or extract them as required to maintain the set point of thermal power. Within respect to the boric acid in normal operation, its concentration in the water of the reactor is lower than that in the Stop state to guarantee an appropriate neutron population.

The reactivity control system usually let increase nuclear power gradually by steps of 10% and steps of 5% per minute beyond the 15% of 100% of nuclear power depending on the concentration of xenon in the reactor. Otherwise, it is possible to decrease progressively and by steps the nuclear power in the range from 100% to 15% of full power.

Load fluctuations of nuclear power just to 50% of nominal power are admissible by the steam bypass of the secondary control system of turbine because the steam from the steam generators can be discharged directly to the condenser without provoking a trip of reactor.

In nuclear literature, “ reactor trip ” means emergency stop of reactor caused by any malfunction. Similarly, “ turbine trip ” means emergency stop of turbine caused by any malfunction. And “ condenser trip ” means emergency stop of condenser caused by any operational anomaly. A “ power station trip ” can be originated by a lot of different malfunctions, but here only are mentioned “ reactor, turbine and condenser trips ”.

5.8 Feedwater and steam systems

The nuclear reactor produces at secondary side of steam generators wet steam which carries the thermal energy to the turbine to be converted in mechanical energy and utterly in electrical energy by the electric generator.

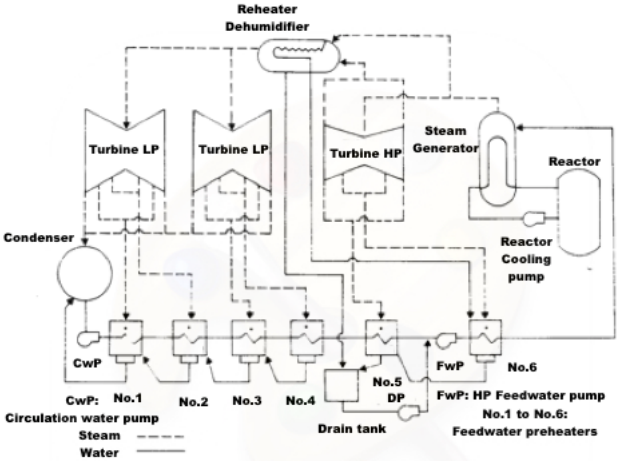

Figure 5.15: Secondary island - Steam water diagram. Source: Westinghouse [5].

Main steam passes through discharge nozzles of steam generators and main steam pipes to the

reheater dehumidifier and to the first high pressure turbine stage (approximately 80 bar at 100% of thermal power).

Steam Flow feeds low pressure turbine stages, and extractions of low quality of steam near the condensation from each turbine stage are conducted to heat the feedwater coming from the condenser pump to the steam generator by means of the pre-heaters.

Low quality steam is also profitable for auxiliary services such as mechanical seals rotors of pumps, vacuum pumps to maintain the vacuum of the condenser, auxiliary steam turbines to bust feedwater to steam generators, and much more.

Steam coming out from the last high-pressure stage of turbine contains just about 10% of humidity and therefore it is necessary to reheat it in the " reheater dehumidifier " before to be injected to medium and low-pressure stages of turbine.

In this cycle, the condenser is a cold sink and acts as a heat exchanger equipment to liquefy the steam from the low-pressure turbine stage. Usually, the temperature inside the condenser is about 298 K and the absolute pressure around 20 mm Hg. A low temperature and a great vacuum in the condenser increase the performance of the steam-water cycle. The water from the condenser is again re-injected into the steam-water circuit by the condenser pumps.

5.9 Nuclear core

The core of a Nuclear Reactor constitutes the nuclear heart where fission reactions of nuclear fuel produce thermal energy. The main function of the core is to maintain the nuclear reaction of fissionable materials, and transmit the thermal energy from neutrons and gamma photons to the water. The PWR technology uses demineralized water as a " moderator " and at the same time as a transporter of thermal energy to the Steam Generators.

The term " moderator " in nuclear technology refers to a material, in this case demineralized water, which has the property to interact with high energy neutrons released from the fission of fuel atoms.

Neutrons from fissions are released within a wide range of kinetic energies from the heart of the core to the periphery of the reactor trying to escape from the vessel. Neutrons mainly interact with hydrogen atoms of water molecules because the size of neutrons and the size of hydrogen atoms are very similar.

The interaction of high energy neutrons with hydrogen atoms provokes the vibration of hydrogen atoms and therefore it is translated to a macroscopic increase of temperature in the cooling water circuit. The process to reduce the high energy of neutrons, from 4 Mev and above 20 Mev, to very low energy by interactions with hydrogen atoms is known as "thermalization" of neutrons. Then neutrons are thermalized after multiple interactions.

Depending on the nuclear technology, the moderator is different with the purpose to get thermal energy from a particular range of energetic neutrons and simultaneously to guarantee the kinetic of the reaction for a particular nuclear fuel.

In PWR technology, the fission of Uranium-235 and in minor percentage Plutonium-239 and 241 produces thermal energy according to the process mentioned above.

The new nuclear fuel is usually delivered as fissionable Uranium-235 oxide and non-fissionable Uranium-238 oxide pellets.

The most abundant isotope of uranium in nature is Uranium-238, non-fissionable. The isotope Uranium-235 is rare in nature, less than 0,7% respect the abundance of Uranium-238. Therefore, the implementation of Uranium-235 enrichment process is necessary to get the required nuclear fuel at least with a percentage of 3% of Uranium-235.

Uranium-235+Uranium-238 compact pellets are under the form of oxide enclosed in tubes of an alloy of Zircaloy-4.
Zircaloy-4 tubes melt at a temperature of 2123 K and for this reason this alloy can not support a temperature beyond of 1873 K in the reactor to avoid mechanical degradation.

The inner pressure range of water in a PWR reactor can change from 1 bar at cold stop with " k_{eff} " near to 0, to 155 bar at hot stop or any nuclear power until 100% of power with " k_{eff} " a little bit less than 1.

Regarding to a range of pressure from 1 bar to 155 bar of the water, (as moderator), inside the reactor, Zircaloy-4 tubes containing nuclear fuel pellets must be pressurized at approximately 2 bar with Helium before being inserted in the reactor with the purpose to avoid the implosion of Zircaloy-4 tubes when their outer pressure reach 155 bar at 573 K.

Thermal power (Mw)	3000	2785
Moderator pressure (kg/cm^2)	155	155
Generation of heat by the fuel (%)	97.4	97.4
Cooling water flow (l/s)	19,000	17,500
Cooling water temperature at inlet (K)	566	564
Cooling water temperature at outlet (K)	311	300
Cooling water temperature at outlet from the vessel (K)	604	591
Core diameter (m)	3.04	3.04
Length of fuel elements (m)	4.27	3.62
Fuel weight (at first load) (kg)	84,080	72,445
Number of fuel elements	157	157

Table 5.5: Typical parameters for the design of PWR nuclear reactors. Source: Westinghouse [5].

The nuclear control of power in the reactor is carried out by a greater or lesser concentration of boric acid dissolved in the cooling water and by insertion or extraction of control rods in the core of the reactor. Both acid boric and control rods are scavengers of neutrons which usually are known as poisons and trap efficiently neutrons because of their excellent atomic properties to interact with neutrons.

Nuclear poisons have a great atomic value of crossed section offering a great target to neutrons escaping from the pellets of nuclear fuel. In case of emergency, it is necessary to stop the nuclear reaction chain by conducting the " k_{eff} " as near as possible to 0, and the nuclear control rods drop by gravity and are inserted in the core.

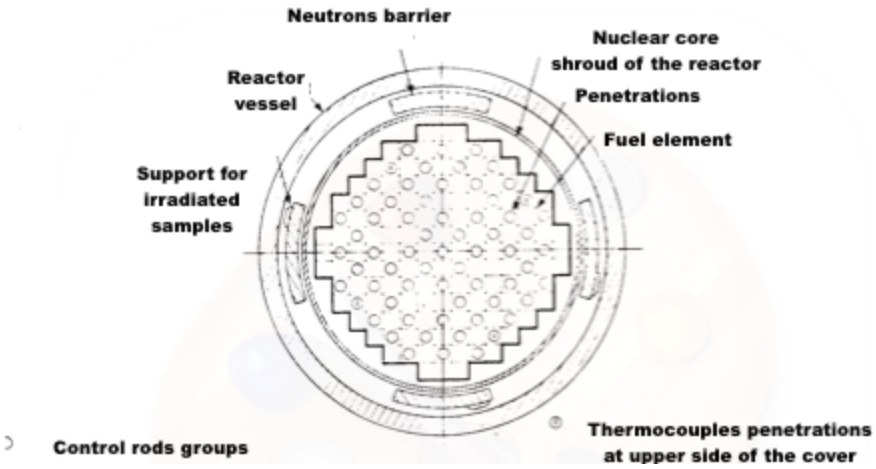

Figure 5.16: Typical transversal section of a nuclear core for a PWR (157 Elements). Source: Westinghouse [5].

5.9.1 Core description

5.9.1.1 Nuclear fuel pellets

The fuel of Uranium dioxide is slightly enriched with the isotope U-235 because its abundance in nature is less than 0.7%, and this means that the ratio of U-235 by U-238 must be increased around 3% to be used as nuclear fuel in a PWR reactor.

The initial U02 appearance is in the form of powder, which must be pressed as cold powder to be synthesized to get cylindrical pellets. Commercial UO2 pellets measure approximately 1 cm long and 1 cm width. Figure (5.17) illustrates comparative dimensions of pellets. Both ends of each pellet are concave to let axial expansion.

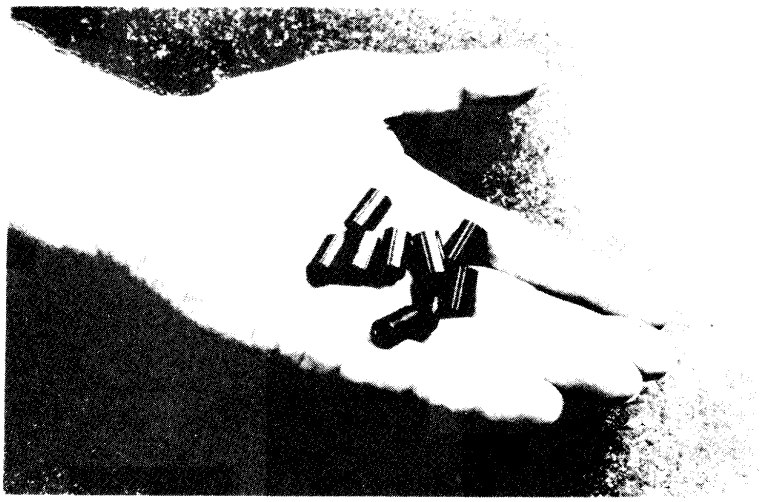

Figure 5.17: UO2 fuel pellets. Source: Westinghouse [5].

5.9.1.2 Nuclear fuel rods

Pellets are placed inside long tubes of Zircloy-4, (Alloy of Zirconium), to form fuel rods. Both ends of the rods are sealed and welded by taps. Springs inside any rod are inserted to avoid the displacement of pellets inside the fuel rods.

Outer diameter of rod (cm)	0.950
Pellet diameter (cm)	0.819
Pellet length (cm)	1.260
Rods distribution in a fuel element	17 x 17
Number of rods by a fuel element	264
Number of rods inside the core of the reactor	41,448

Table 5.6: Typical parameters for the design of PWR nuclear reactors. Source: Westinghouse [5].

Pellets diameters are slightly lesser than the internal diameter of fuel rods to let the displacement of pellets inside the rods during the manufacturing, and to avoid the compression of pellets by the implosion of rods when the reactor operates with water at 150 bar and 573 K. Each fuel rod is filled with Helium which will expanded when the temperature of the water increases, which will compensates the pressure exerted by the water against the pellets. This methodology of construction avoids damages both in the rods and the pellets.

In addition, helium has a high calorific capacity to conduct heat inside the rods what aids effectively to refrigerate the pellets of fuel and the Zircaloy-4 rods.

5.9.2 Fuel elements

The fuel element structure is a transversal square with 17 by 17 positions where the fuel rods and the control rods are placed as a bundle. See Figures (5.18) and (5.19).

To facilitate the extraction and the insertion of control rods bundles, during the operation of the reactor, each control rod is inserted in a guide tube to avoid bending or any other deformation.

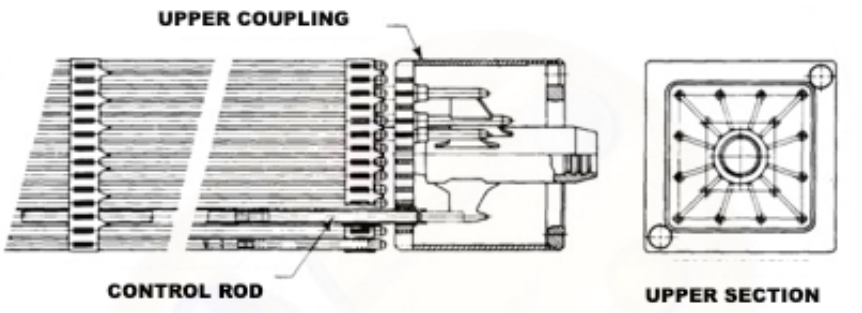

Figure 5.18: Elements in the control rod bundle, Upper section. Source:Westinghouse [5].

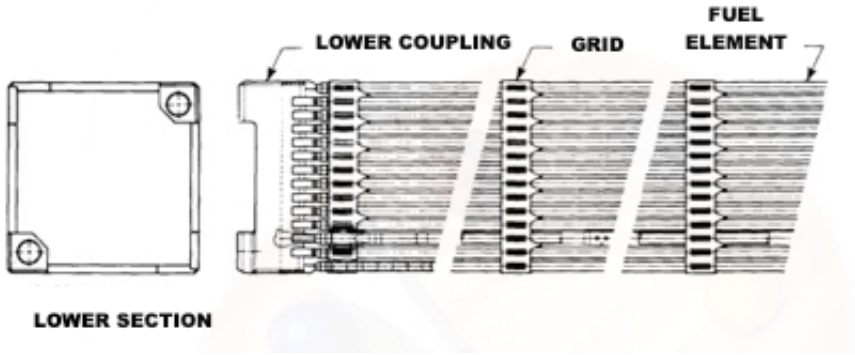

Figure 5.19: Elements in the control rod bundle, Lower section. Source:Westinghouse [5].

Guide tubes for the bundle of the control rods are supported by steel grids at several positions of the fuel element, which allows to decrease the risk of transversal vibrations along the fuel element.

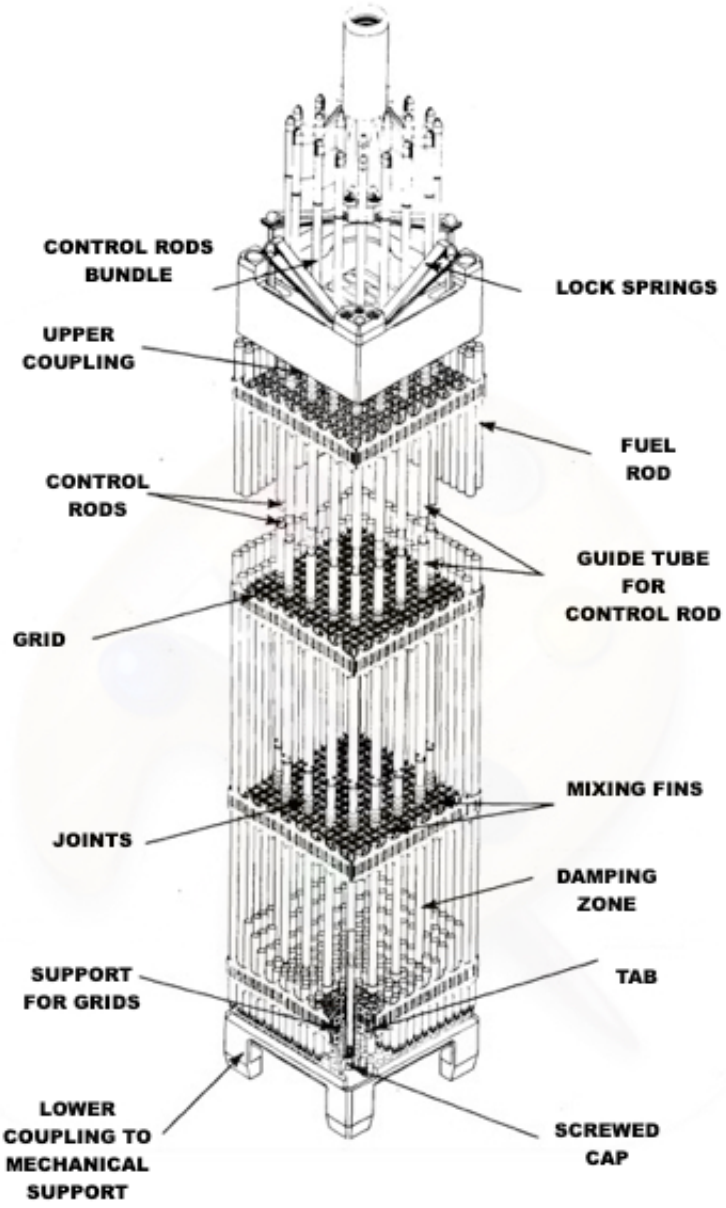

Figure 5.20: Fuel element assembly. Source:Westinghouse [5].

5.9.3 Control rods bundles

Control rods bundles operate as the quicker way to control the nuclear reaction, reducing or increasing the reactivity, "k_{eff}", of the core by the withdrawal or insertion of control rods respectively, what lets to change the nuclear power rapidly.

In case of emergency (trip of reactor), it is mandatory to stop suddenly the nuclear reaction minimizing the value of "k_{eff}" as closed as possible to "0", then, the control rods system liberates all the control rods which go down by the action of gravity.

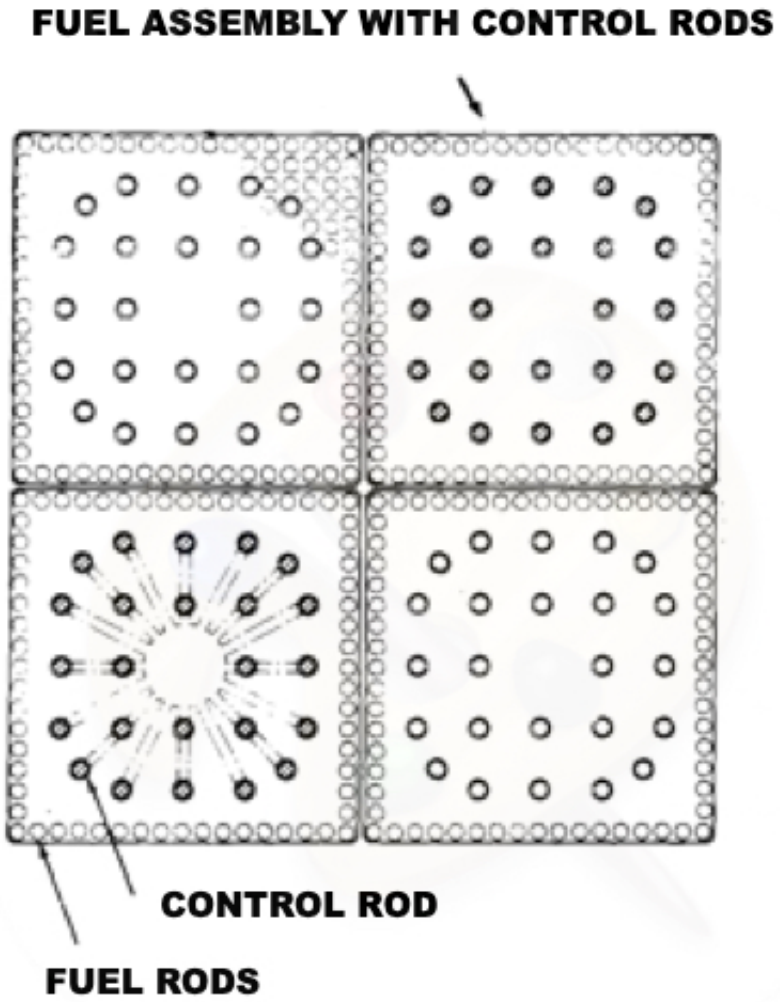

Figure 5.21: Transversal section of fuel assemblies with and without control rods. Source:Westinghouse [5].

Control rods have a cylindrical geometry and are made with an alloy composed of Silver (85%), Indium (10%), and Cadmium (5%). The Ag-In-Cd alloy of the control rods acts as a scavenger of neutrons for a large range of the neutronic spectrum of energies, from neutronic energies in the range from “ev” to “Mev”.

Each control rods bundle contains 24 control rods interconnected by an upper mechanical crow foot structure to make possible the lifting or releasing of all the control rods simultaneously. In addition, each control rod is encapsulated into a stainless-steel tube to guarantee mechanical integrity as well as to isolate the control rods from the refrigeration water.

The crow foot structure of each control rod bundle is coupled to an electro-mechanical actuator external to the vessel, over the reactor cover, to lift or introduce step by step the control rods bundle as required by the reactivity control system, except in case of trip of reactor because in such case all the control rods will be liberated to fall inside the core in a time less than 1 second.

A typical PWR of 3 loops contain 157 fuel assemblies in the core, of which 53 fuel assemblies are enriched at 2.1% with U-235 in weight, 52 have an enrichment of 2.6%, and 52 have a high enrichment of 3.1%.

The lower and medium enriched fuel assemblies are placed in the central part of the core and those with the higher enrichment are peripheral to the core.

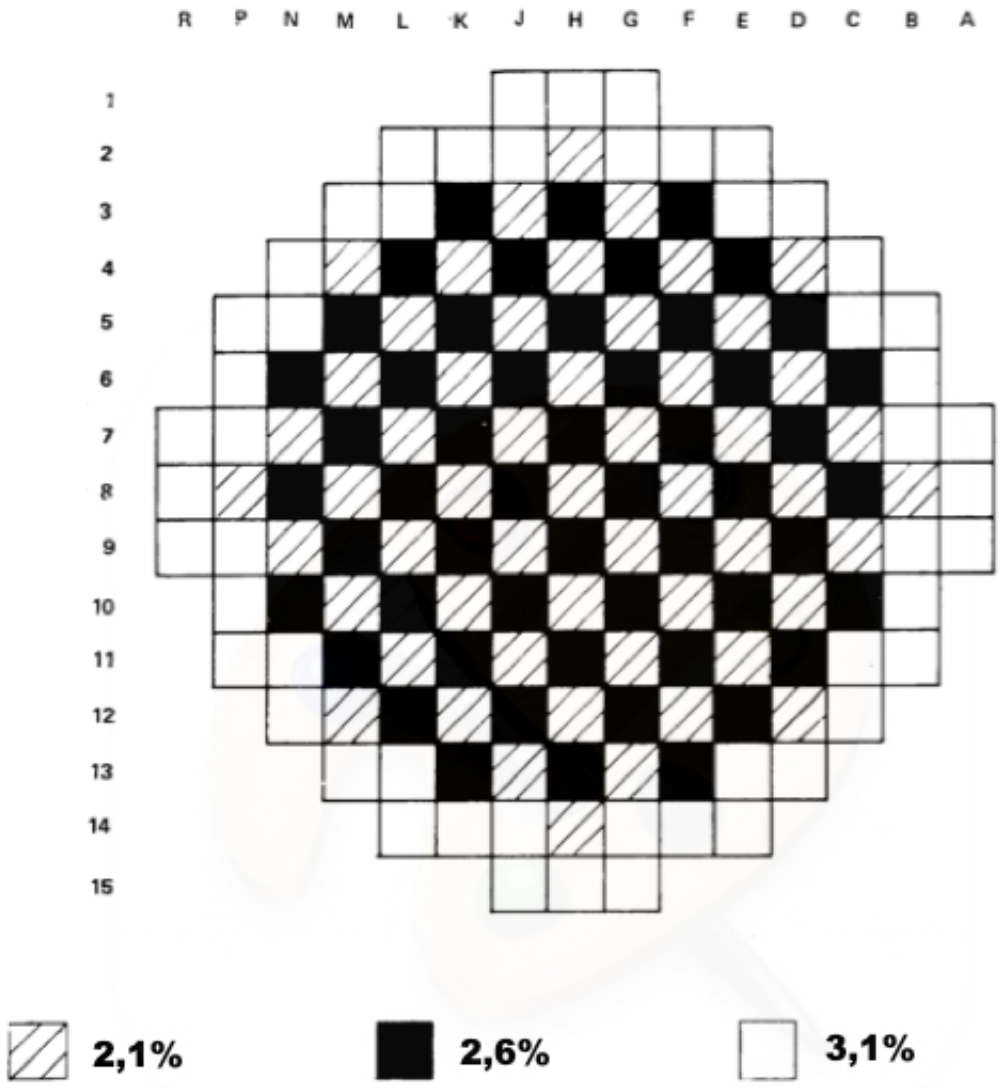

Figure 5.22: Typical distribution of fuel assemblies at the beginning of life for a 3 loops reactor with 17X17 fuel rods per fuel assembly. Source:Westinghouse [5].

The nuclear fuel reload cycle in PWR power stations can vary from 1 year to 2 or 3 years depending on the degree of fuel enrichment and ratio of fuel burn up.

At the end of a nuclear fuel cycle or “End Of Life”, the new configuration of the core requires

a redistribution of fuel assemblies. Thus, 1/3 of fuel assemblies from the center of the core is removed, the others are relocated in the direction to the center of the core, and the new nuclear fuel assemblies (with higher enrichment) occupy the periphery of the core.

5.9.4 Reactivity control

The control of reactivity is possible using control rods and boric acid diluted in the water of refrigeration, what provides the way to compensate any change of reactivity during any state of the reactor operation, and they let to shut down the reactor at the same time by keeping a reserve of negative reactivity to compensate a quick increasing of positive reactivity.

The changes of reactivity are linked to changes in the nuclear power from the core and to alterations of the refrigeration water temperature as moderator of neutrons energy. A very important concept in the PWR design is the "power negative coefficient and temperature negative coefficient", what means that any increase in the nuclear power (and in the fuel temperature) provokes a diminution of reactivity which must be compensated by a slightly lifting of control rods if the event requires an immediate action, or by a dilution of boric acid in the refrigeration water if the event requires a slow action to compensate the reactivity.

The alteration of the core during operation produces changes in the reactivity:

- The generation of thermal power comes from the consumption of the nuclear fuel in the core, or burn up of fuel, what provokes a loose of reactivity which is compensated by the extraction of consumable poisons from the core during a cycle of nuclear fuel reload.
- During operation, the generation of Xenon and Samarium by the reactor is the result of the fission of Uranium-235 atoms, and they provoke a diminution of reactivity because both elements are easily fissionable by neutrons.

When the reactor works at steady state of nuclear power generation, Xenon and Samarium concentrations reach to a constant equilibrium.

The reactor produces Xenon directly and indirectly:

- Directly from fission (0.3% yield)
- Decay of Tellurium (5.9% yield)

$$^{135}_{52}Te \rightarrow {}^{135}_{53}I + {}^{0}_{-1}\beta \rightarrow {}^{135}_{54}Xe + {}^{0}_{-1}\beta$$
$$t_{\frac{1}{2}} = 19.2\,s \qquad t_{\frac{1}{2}} = 6.7hr$$

Figure 5.23: Xenon production.

Whereas the removal of Xenon can be achieved by burn up or decay:

Burnout

$$^{135}_{54}Xe + ^{1}_{0}n \rightarrow ^{136}_{54}Xe \quad (Stable)$$

Decay

$$^{135}_{54}Xe \rightarrow ^{135}_{55}Cs + ^{0}_{-1}\beta \rightarrow ^{135}_{56}Ba + ^{0}_{-1}\beta$$

$$t_{\frac{1}{2}} = 9.2h \qquad t_{\frac{1}{2}} = 20000y$$

Figure 5.24: Xenon Removal.

Neodymium 149 is a product that comes from the fission of U-235, it has a short half life and disintegrate into Promethium 149 which decays in Samarium 149. Which is stable and is removed by burn up.

Production

$$^{149}_{60}Nd \rightarrow ^{149}_{61}Pm + ^{0}_{-1}\beta \rightarrow ^{149}_{62}Sm \quad (Stable)$$

$$t_{\frac{1}{2}} = 1.7h \qquad t_{\frac{1}{2}} = 53h$$

Removal

$$^{149}_{62}Sm + ^{1}_{0}n \rightarrow ^{150}_{62}Sm$$

Figure 5.25: Samarium production and removal.

Control rods bundles provide a quick action to palliate changes in the reactivity while boric acid diluted in the water of refrigeration is a lower control of reactivity because the operations of concentration and mainly that the dilution are slow.
Then, the control system of reactivity inserts or withdraws progressively by steps the control rods to balance quick changes of reactivity which are a direct consequence of quick changes of demand of power, quick changes of the temperature in the core, and in case of emergency reactor trip.
Boric acid diluted in the refrigeration water is ideal to balance slow variations of reactivity because of nuclear fuel burn out, fission subproducts growing, and core heating during starting up operation.

A 3 loops PWR reactor typically contain 52 control rods bundles which are distributed in the core according to its design. The control rods bundles are classified in 4 control rods bundles banks and 3 stop control rods bundles banks. The stop control rods bundles, banks BPA, BPB and BPC contain 24 control rods and they are permanently withdrawn during starting up and normal operation.

The 4 control rods bundles, banks A, B, C, and D contain 8, 8, 8 and 4 control rod bundles respectively and they are overlapped approximately 50%.

- Bank A is the first bank to be withdrawn from the core during starting up operations and as quick as it is withdrawn at 50% the control system initiates the sequence to pull out the bank B.
- When the bank A reaches the position of completely out, the bank B is at 50% and then the control system initiates the sequence to pull out the bank C
- The bank D is withdrawn following the above sequence and it stays inserted around 20% at full power during normal operation. The reason to maintain the bank D inserted around 20% is because in case of a positive demand of reactivity then this bank moves upward or downward very quickly supplying a high value of differential reactivity.

During normal operation all the control rods are synchronized by the control system, and they move permanently upward or downward according to the requirements form the control system of reactivity. The number of control rods inserted partially in the core is according to the position of each control rods bundle, and regarding the "margin of reactivity necessary to shut down the reactor".

The insertion and withdrawal of each control rod is implemented by a set of 3 electromagnetic coils which operates in co-ordination to lift or to insert the control rod step by step. In case of emergency trip of the reactor, then the control system does not supply electricity to the coils, and the control rod falls into the core by gravity.

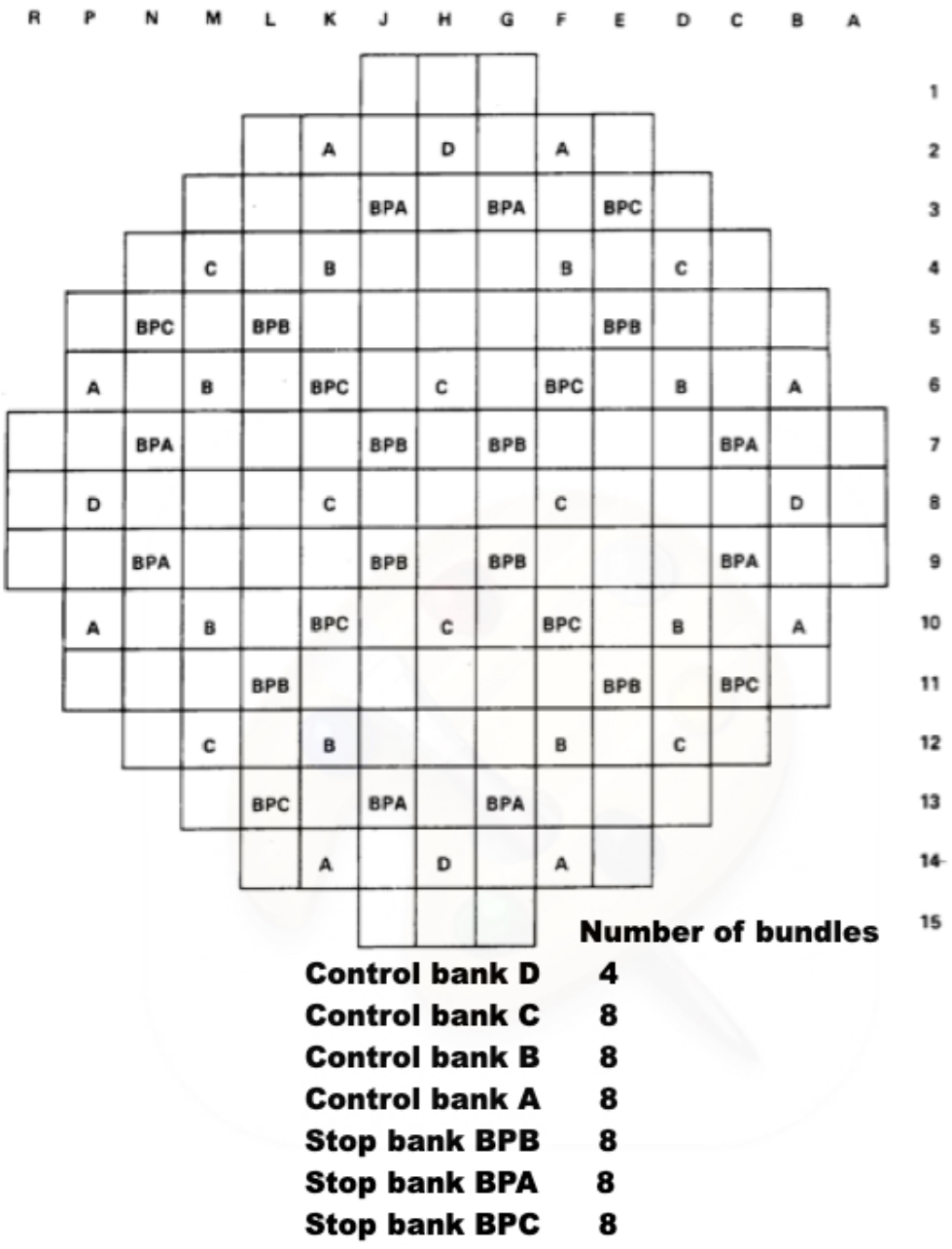

Figure 5.26: Distribution of the control rods bundles in the core. Source:Westinghouse [5].

5.9.5 Consumable poison

There is an excess of the positive reactivity for the first load of nuclear fuel because all the fuel is new, and the primary and secondary sources of neutrons are placed in the core.

To balance this excess of positive reactivity, it is necessary:

- To insert the control rods
- To increase the concentration of boric acid, but not too much beyond 2000 ppm, as for a high

concentration appears a negative effect of positive reactivity due to the high concentration of boron. So, a higher concentration of boron is not permitted because the positive reactivity increases quickly when the reactor reaches the nominal temperature around 573 K.

The consumable poisons are rods of similar size to those of control rods and they are strategically inserted in the core to generate as much as possible uniform neutronic flux. Consumable poisons reduce the reactivity by absorption of neutrons by the boron atoms, what means that the consumable poisons will reduce their negative reactivity along the burn out of the fuel.

At the end of life for the first cycle consumable poison rods will run out, and in most cases it is not necessary to insert in the core consumable poisons for successive cycles because a portion of the fuel (2/3) has a lower reactivity.

5.9.6 Thermal-hydraulic design of the core

The scope of the core design is to let an optimal heat transfer from the nuclear fuel to the moderator, in this case water which is also used for refrigeration, and the transportation of this thermal energy until the steam generators.

In addition, the design must assure the mechanical integrity of the nuclear fuel rods where extreme hot sources can appear, specially when the core is forced to work under nuclear power transients. Thus, smooth operation is very important to respect the technical specifications of the reactor and prevent the overheating of the fuel rods.

Several scenarios must be regarded with the thermohydraulic design of the reactor:

- For a regime of low nuclear power and low thermal flux, the water is completely liquid without any steam bubble, and the thermal energy from the fuel rods to the water is transmitted by convection avoiding damages in the mechanical fuel rods, as the temperature in the fuel rods is inside the limits allowed by the rod of Zircaloy-4.
- For a regime or transient when the temperature in the surface of the fuel rod is excessive and overpass the boiling point of water at 157 bar and 603 K (normal thermodynamics values for operation), then bubbles of steam appear in the refrigeration water, and consequently the temperature of the fuel increases, and the refrigeration of the fuel rods is degraded. At this point, the core is in risk to be damaged. The steam bubbles behave as a thermal insulation layer.

Thermohydraulic calculations in the design of a PWR reactor (with fuel U02) demonstrates that the linear generation of thermal power accepts safely a gradient just until 750 W/cm.

5.9.7 Sources of neutrons

The insertion of 2 primary neutrons sources in the core of the reactor is intended to give off a residual flux of neutrons during the load of nuclear fuel at any cycle, what is extremely important to measure and control the evolution of the population of neutrons and the reactivity during the load of fuel assemblies and prevent a nuclear accident by effect of spontaneous critic nuclear reaction. The measurement and control of the evolution of the neutronic population and therefore the reactivity makes possible to adjust, increasing or diluting, the concentration of boric acid in the refrigeration water of the core at any state of operation, either first fuel load, fuel reload, or

starting up the reactor.

Two kinds of sources of neutrons are implemented in PWR reactors:

- Primary
- Secondary

The main type of primary source of neutrons is by Californium-252, Cf-252, which yields neutrons by spontaneous fission. Concerning the secondary sources of neutrons, a typical and widely source used is that with a composition of Antimony - Beryllium, (approx. 50% to 50%).

The first component is antimony, which can be irradiated by fission neutrons and then emits a particle capable of knocking out a neutron from the second component. The (γ,n or gamma photon, neutron) source that uses Antimony-124 as the gamma emitter is characterized in the following endothermic reaction.

The antimony-beryllium source produces nearly monoenergetic neutrons with the dominant peak at 24 keV. The source range neutron detectors, as part of ex-core instrumentation, are placed outside the reactor and this is the reason because the sources of neutrons are in the periphery of the core, to be visible by the ex-core instrumentation.

$$^{124}\mathrm{Sb} \rightarrow {}^{124}\mathrm{Te} + \beta^- + \gamma$$

$$\gamma + {}^{9}\mathrm{Be} \rightarrow {}^{8}\mathrm{Be} + \mathrm{n} - 1.66\ \mathrm{MeV}$$

Figure 5.27: Secondary neutron source.

Using the laws of energy and momentum conservation, one can derive that the 1691 keV and 2091 keV gamma rays produce two groups of neutrons:

- 23 KeV (97%)
- 378 KeV (3%)

As stated before, sources of neutrons play an important role in the reactor safety, especially during shutdown state and reactor start up. Without source of neutrons, there would be no subcritical multiplication, and the neutron population in the subcritical system would gradually approach to zero. That means each neutron generation would have fewer neutrons than the previous one because "k_{eff}" is less than 1.0.

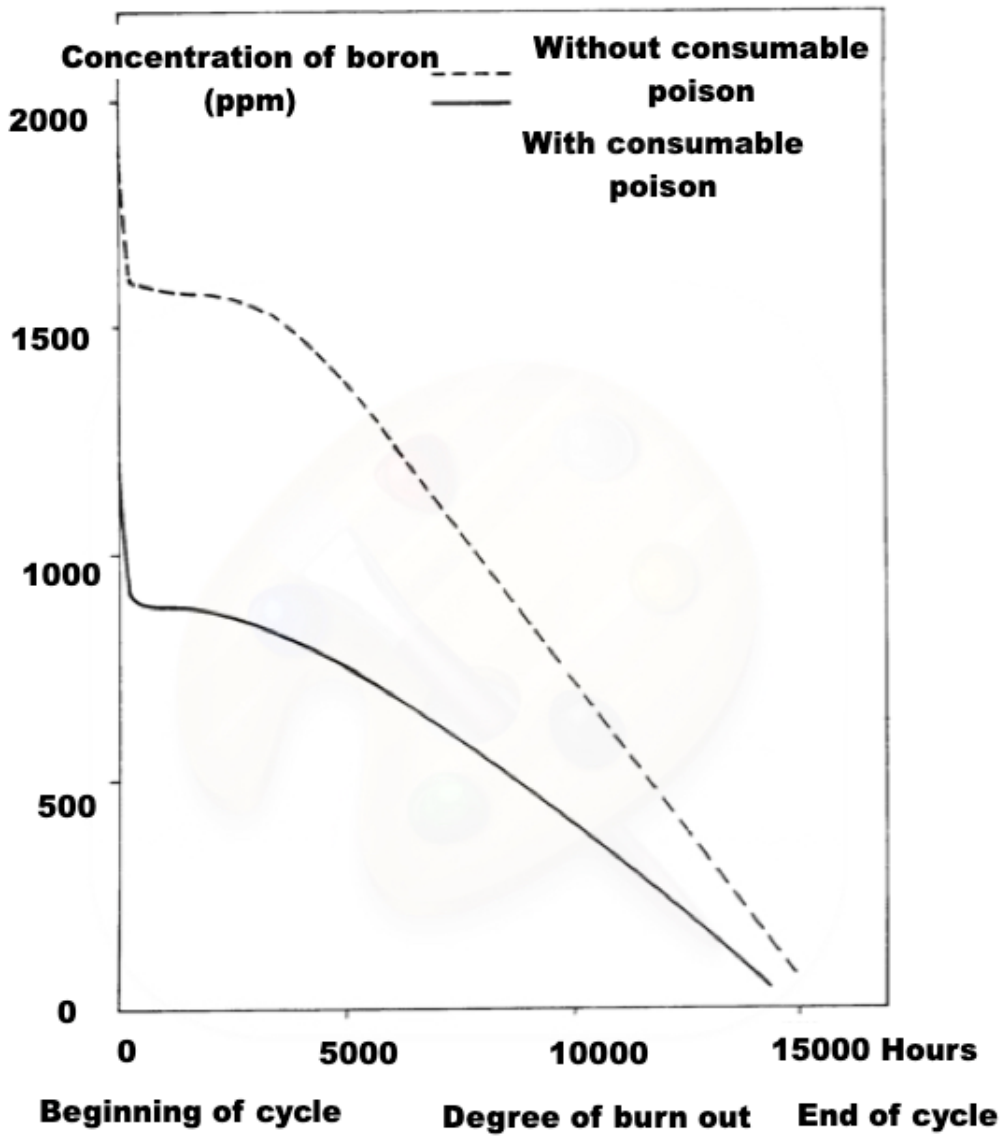

Figure 5.28: Concentration of boric acid (ppm) versus nuclear fuel burn out during the first cycle (hours). Source:Westinghouse, [5].

Chapter 6

Kinetics of nuclear reactions

6.1 Fission and the multiplication factor

Uranium-235 and others fissionable nuclei have a high probability to be split when trapping a neutron. This event is known as an atomic transmutation of the fissionable atom. Therefore, a nuclear reaction in chain occurs if any fission generates more neutrons than the precedent nuclear reaction, what means that the population of neutrons is increasing and provokes more fissions of fuel atoms.

During the fission of the nuclear fuel atom, the splitting gives off a lot of energy as the global mass of the U-235 nuclei + 1 neutron before the fission is greater than the global mass of subproducts of fission after the reaction. In other words, there is a loss of mass in this process of fuel fission.

According to the first law of thermodynamics, " energy and consequently mass cannot be created nor destroyed, it can only be converted from one form to another ". Thus, the loss of mass during the nuclear reaction is converted into energy according to the Einstein's equation:

$$E = \Delta m \cdot c^2 \tag{6.1}$$

Where c is the speed of light, equal to $3 \cdot 10^8\ m/s$, E is the energy in Joules and Δm is the loss of mass in kg.

The fission of each atom of U-235 provides a thermal energy equivalent to 200 MeV, in comparison with the energy of neutrons which is approximately around 0.025 eV to 12 MeV.
Regarding the fact that any fission of an atom U-235 produces 2 or 3 neutrons, then a nuclear reaction in chain could be happen if these neutrons are able to split other atoms of U-235.

The reactor becomes critical when the population of neutrons is sufficient to maintain an auto sustainable nuclear reaction, and in this case the reactor has enough critical mass.

Neutrons do not have electrical charge but only mass and their energy depend only on their speed, or in other words their kinetic energy.

Furthermore, neutrons can penetrate inside the nuclei of fissionable atoms to split them, but only if their cross sections are in a particular range compatible with cross sections of the fissionable

atoms.

The term cross section refers to the equivalent nuclei area or equivalent neutron area. The cross section is not a constant parameter and it depends on the thermal energy of neutrons and fissionable nuclei. The physical unit of measurement for the cross section is the " barn " :

$$1\,barn = 10^{-28}\,m^2 \tag{6.2}$$

Neutrons can also be captured by nuclear poisons, by other materials, or can escape from the reactor with any possible kinetic energy in the range of "eV" to "MeV".

Neutrons inside the reactor are being thermalized since they are generated until their absorption or escape from the reactor as they interact with water molecules which vibrate and get energy from the kinetic energy of neutrons. Nevertheless, U-238 atoms can capture easily thermalized neutrons to produce Pu-239, as U-238 atoms have a high cross section for thermalized neutrons with kinetic energy of low eV. The atomic transmutation of U-238 is the following:

$$^{238}_{92}\mathrm{U} + {}^{1}_{0}\mathrm{n} \longrightarrow {}^{239}_{92}\mathrm{U} \xrightarrow[23.5\ \mathrm{min}]{\beta^-} {}^{239}_{93}\mathrm{Np} \xrightarrow[2.3565\ \mathrm{d}]{\beta^-} {}^{239}_{94}\mathrm{Pu}$$

Figure 6.1: Transmutation of Uranium 238.

Quick neutrons are those with a high energy liberated when the nuclear fuel atoms split, so in most nuclear reactors technologies, it is necessary to slow down these neutrons by a moderator which absorbs part of the kinetic energy from neutrons and makes them more adaptable to split other fuel atoms.
In this sense, the multiplication factor, k, plays an important role as it defines the ratio of population of neutrons from a generation to the population of neutrons to the precedent generation.

Globally, to make possible an auto sustainable nuclear reaction, it is imperative that the rate of generated neutrons and the rate of fled plus absorbed neutrons would have the same value.

$$\frac{\text{Rate of born neutrons}}{\text{Rate of fled plus absorbed neutrons}} = 1 \tag{6.3}$$

In the ideal case, in order to not consider the effect of fled neutrons from the reactor, the multiplication factor, k_∞, plays a new role as a result from a set of other parameters. This is known as the four factor formula, in which the multiplication factor is defined as:

$$k_\infty = \epsilon \cdot \eta \cdot p \cdot f \tag{6.4}$$

where,

- ϵ: factor of quick fission, or the ratio between the number of quick neutrons produced by neutrons with any kinetic energy to the number of quick neutrons generated only by thermalized neutrons.
- p: capture factor, or the probability for a neutron to escape to the capture of U-238 during the thermalization phase.

- f: thermal utilization factor, or the ratio between the number of thermalized neutrons absorbed by the fuel to the number of thermalized neutrons absorbed by all the materials, included the nuclear fuel, which belong to the core of the reactor.
- η: ratio of quick neutrons generated to each thermalized neutron absorbed by the nuclear fuel.

The factor ϵ depends on the nuclear fuel kind and its enrichment, while η depends on the geometry and distribution of the fuel elements in the core.

The factor of capture, p, and the factor of thermal utilization, f, depend on the reactor geometry, materials of the structure and on the ratio moderator to fuel.

In the case of reactors based upon thermalized neutrons, such as the reactor herewith described, it is important to get a factor $p \cdot f$ as high as possible for the nuclear fuel and moderator under consideration.

The size of any nuclear reactor is finite, so the boundary restrictions imposed a new value of the multiplication factor, k_{eff}:

$$k_{eff} = \epsilon \cdot \eta \cdot p \cdot f \cdot F \tag{6.5}$$

Where F is the probability for an emitted neutron to come back, do not flee, and stays in the multiplier medium.

- If $k_{eff} > 1$, the number of neutrons between a generation and the following generation is increasing. The reactor is in a super critical state.
- If $k_{eff} = 1$, the number of neutrons is constant in the core of the reactor, and the reactor stays in the critical state.
- If $k_{eff} < 1$, the number of neutrons decreases from a generation to the following generation and the reactor is in the sub critical state.

6.1.1 Neutronic power

The fission of an atom of U-235 gives off an average thermal energy of 200 MeV, or the equivalent figure of $3.2 \cdot 10^{-11}$ Joules. Therefore, the generation of a thermal power of 1 W, requires fissions / second.

Regarding the Avogadro's number, the average thermal power generated by the fission of 1 gram of U-235 for 24 hours, amounts to 0.95 MW, and this power is usually known as the neutronic power.

In steady state, the number of neutrons in the core of the reactor is proportional to the number of nuclear fuel fissions, and the thermal power generated in the core of the reactor, or neutronic power, is proportional to such number of neutrons designated by the variable n.

6.1.2 Time of life and average life of a neutron

The average time of life of a neutron inside a reactor, in an infinite medium, is defined as the time elapsed between two consecutive generations of neutrons in such medium. It is denominated by the

Greek letter ι.

However, the average time of life of a neutron in a finite multiplier medium, θ, is the time elapsed between its generation during an event of fission and its disappearance provoking a new fission.

$$\theta \approx \frac{\iota}{k_{eff}} \tag{6.6}$$

In a multiplier medium, the average time of life of neutrons, θ, change in a finite reactor according to the core configuration.

A comparison between two thermal reactors with pressurized water of different technologies, CANDU and PWR shows a significant variation in the average time of life of a neutron:

- For a CANDU reactor which operates with heavy water, D_2O, the average time of life of a neutron is 10^{-3} seconds.
- For a PWR reactor which operates with light water,H_2O, the average time of life of a neutron is in the range from 10^{-4} seconds and 10^{-5} seconds.

6.1.3 Instantaneous neutrons and delayed neutrons

Neutrons are liberated when nuclear fissions happen, and according to their sequence of generation, neutrons are classified and instantaneous and delayed.

Most neutrons are emitted immediately after the nuclear fuel fission takes place and they are designated as quick neutrons within an interval of time of 10−14seconds.

On the other hand, delayed neutrons appear after the fission of nuclear fuel atoms with a delay from several seconds to several minutes. They appear after fissions of nuclear fuel atoms by the β disintegration and emission of neutrons, such as it happens with the radioisotopes Be-7, I-137, Br-89/91, I-139, Sb-137, As-85, Li-9, which are known as precursors of neutrons.

Nuclear fuel	Time of life (seconds)	Decay period (s^{-1})	Ratio β_i of delayed neutrons from group i to the population of neutrons
	0.33223	3.01	0.00027
	0.87719	1.1400	0.000740
U-235	3.32226	0.3010	0.002530
	9.00901	0.1110	0.001250
	32.78689	0.0305	0.001400
$\beta = 0.0064$	80.64516	0.0124	0.000210
	0.4	2.5	0.000086
	0.88496	1.1300	0.000133
U-233	3.06748	0.3260	0.000722
	7.19424	0.1390	0.000651
	29.41176	0.0340	0.000773
$\beta = 0.0026$	79.36508	0.0126	0.000224
	0.37037	2.7000	0.000093
	0.89286	1.1200	0.000179
Pu-239	3.06748	0.3260	0.000684
	8.06452	0.1240	0.000443
	33.22259	0.0301	0.000625
$\beta = 0.0021$	78.12500	0.0128	0.000072

Table 6.1: Values from precursors of delayed neutrons by fissions with thermalized neutrons.

Nuclear fuel	Time of life (seconds)	Decay period (s^{-1})	Ratio β_i of delayed neutrons from group i to the population of neutrons
	0.258	3.8800	0.000168
	0.714	1.4000	0.000824
U-235	3.215	0.3110	0.002630
	8.621	0.1160	0.001210
	31.546	0.0317	0.001370
$\beta = 0.0064$	78.740	0.0127	0.000246
	0.248	4.0300	0.001180
	0.709	1.4100	0.003540
U-238	2.778	0.3600	0.006100
	7.194	0.1390	0.002550
	31.250	0.0320	0.002150
$\beta = 0.0157$	75.758	0.0132	0.000206
	0.321	3.1200	0.000061
	0.787	1.2700	0.000194
U-233	3.300	0.3030	0.000845
	7.634	0.1310	0.000604
	29.851	0.0335	0.000730
$\beta = 0.0025$	79.365	0.0126	0.000024
	0.312	3.2100	0.000073
	0.794	1.2600	0.000216
Pu-239	3.021	0.3310	0.000687
	7.519	0.1330	0.000452
	32.154	0.0311	0.000584
$\beta = 0.002$	77.519	0.0129	0.000080
	0.304	3.2900	0.000926
	0.826	1.2100	0.003710
Th-232	3.115	0.3210	0.009620
	8.264	0.1210	0.003340
	29.851	0.0335	0.003230
$\beta = 0.022$	80.645	0.0124	0.000735

Table 6.2: Values from precursors of delayed neutrons by fissions with quick neutrons.

The above tables compile typical parameters of precursors according to the kind of nuclear fuels and with the consideration if the nuclear reaction happen with quick neutrons or with thermal neutrons.

The control of the nuclear reaction is possible because the existence of delayed neutrons. Here-

after, the parameter β refers to the percentage of delayed neutrons generated by the fission, and β_i represents the percentage of delayed neutrons from the group of precursors i when the fission happens.

6.1.4 Neutrons from sources and photodisintegration

Photodisintegration likelihood happens when high energy gamma radiation impact on Deuterium and Beryllium nuclei what conduct to the creation of neutrons, which must be computed with those delayed neutrons from nuclear fuel fissions. Neutrons sources emit neutrons within a complex way depending on the time of working of the reactor.

In general, neutrons sources in the reactor or nearby may be classified into two categories:

- Permanent or long-life neutrons sources: they are those based upon the nuclear reaction (alpha, n), from long period alpha emitters, such as Radium, Polonium or Plutonium. These category of neutrons sources use atoms of Beryllium as targets to produce neutrons.
  For example, a homogeneous mixture of Radium with an activity of 1 curie, with Beryllium constitutes a neutrons source which can emit 10^7 neutrons per second.
- Temporary neutrons sources: they relay basically on the nuclear reaction (gamma, n) with Beryllium as a target. Gamma emitters nuclei are abundant, but their targets nuclei to produce neutrons are less available, and the performances of these kind of sources are lower than the alpha particle emitters. The advantage of these neutrons sources is that they are reloaded because the gamma emitters proliferate during the reactor operation.
  Sb-124 with a period of semi disintegration of 60 days and Na-24 with a semi disintegration of 14.8 hours are commonly used to emit gamma radiation.

6.1.5 States of a reactor

Operational states of a nuclear reactor depend on the reactivity of the reactor at each scenario, in connection with a set of principles.
The main parameters to characterize the state of a reactor are the multiplication factor, k_{eff}, and the average life time of neutrons, θ.

The insertion of a neutrons source with a value S at the instant t=0 will infer after a time, $t = \theta$. A variation of the neutronic population in the multiplier medium, and the numerical value of this population will be $n_0 = S \cdot \theta$.

After an elapsed time $t = m \cdot \theta$, the neutronic population becomes:

$$n = n_0 \left(1 + k_{eff} + k_{eff}^2 + ... + k_{eff}^{m-1}\right) \tag{6.7}$$

And the summation of this geometrical series is:

$$\frac{n}{n_0} = \frac{1 - k_{eff}^m}{1 - k_{eff}} \tag{6.8}$$

If the reactor relays in super critical state, $k_{eff} > 1$, then the evolution of the neutronic population follows:

$$\frac{n}{n_0} \approx \frac{-k_{eff}^m}{1 - k_{eff}} \tag{6.9}$$

If k_{eff} is close to 1, then the following relation can be assumed:

$$k_{eff} = 1 + \delta k_{eff} \tag{6.10}$$

where, $\delta k_{eff} << 1$

After a time t, $m = \frac{t}{\theta}$ and the following relation is applied:

$$\ln\left(\frac{n}{n_0}\right) = \frac{t\,\delta k_{eff}}{\theta} - \ln\left(\delta k_{eff}\right) \tag{6.11}$$

Finally, the following equation is achieved:

$$n = n_0\,\frac{1}{\delta k_{eff}} e^{\frac{t\,\delta k_{eff}}{\theta}} \tag{6.12}$$

The neutronic population in a reactor slightly super critical, changes according to an exponential function and therefore the thermal power is also subjected to this change.

Taking the multiplication factor k_{eff} and equaling to $1 + \beta$, for delayed neutrons from the preceding tables, then the reactor reaches the critical state for instantaneous neutrons. This implies the auto sustainability of the nuclear reaction without the consideration of delayed neutrons. The evolution of power is exponential, and for this reason the design of the reactor must consider the multiplier factor at any case lower than $1 + \beta$.

6.1.6 Reactivity and period

Reactivity can be expressed as a relative increment in the population of neutrons between two successive generations. It is defined by the following equation:

$$\rho(reactivity) = \frac{n_0 k_{eff} - n_0 k_{eff}^{m-1}}{n_0 k_{eff}^{m}} = \frac{k_{eff} - 1}{k_{eff}} \tag{6.13}$$

Calling $\delta k = k_{eff} - 1$, as the excess of the multiplication factor when it is greater than 1. This is known as the excess in reactivity. Generally ,k_{eff} is close to 1, for this reason it is assumed the approach δk to ρ, without any significant error for calculations purposes.

The units to measure reactivity are commonly:

- Pcm, per cent mile, which is used by Westinghouse.
- $\%\frac{\Delta K}{K}$, commonly used in technical specifications. $1\%\frac{\Delta K}{K} = 10^5\ pcm$
- In certain countries the unit of reactivity is 1 cent $= 0.01\$ = \frac{\beta}{100}\ pcm$

If the value of reactivity in a reactor stays constant, then the number of neutrons in the reactor evolves exponentially as a function of time.

$$n = n_0 e^{\frac{t}{T}} \tag{6.14}$$

where, T is the period of the reactor.

It is commonly used the term of "doubling time", t_d, as the necessary time to get a new neutronic population multiplied by a factor of 2.

$$n = 2n_0 = n_0\, e^{\frac{t_d}{T}} \tag{6.15}$$

Which can be expressed as:

$$\frac{t_d}{T} = \ln(2) = 0.693 \tag{6.16}$$

6.2 Kinetic equations

For the following considerations, it is assumed that the reactor is at steady state, and the neutronic flux is homogeneous in the core of the reactor. This neutronic flux is composed of neutrons from:

- Instantaneous neutrons which are born directly from the fission of atoms of fuel.
- Delayed neutrons which are emitted by the precursors.
- It is accepted that sources emit S neutrons per second, and those neutrons are instantaneous because their energetic levels are very similar to the instantaneous neutrons.

The rate of neutrons generated inside the reactor is the summation of the rates of instantaneous neutrons, the rate of delayed neutrons from precursors, and the rate of neutrons from the sources:

- The rate of generation of instantaneous neutrons:

$$\frac{kn\,(1-\beta)}{\theta} \tag{6.17}$$

- The rate of delayed neutrons from precursors C_i from each group "i", which have radioactive constants of disintegration λ_i, with the consideration "m" groups of delayed neutrons:

$$\sum_{i=1}^{m} \lambda_i C_i \tag{6.18}$$

- S neutrons from the primary and secondary sources.

The rate of variation of the global number of neutrons must be equal to the summation of the 3 above rates, minus the rate of lost neutrons (by fled, and parasite absorptions), $\frac{n}{\theta}$:

$$\frac{dn}{dt} = \frac{kn\,(1-\beta)}{\theta} + \sum_{i=1}^{m} \lambda_i C_i + S - \frac{n}{\theta} \tag{6.19}$$

Reorganizing the terms in the previous equation:

$$\frac{dn}{dt} = \frac{n}{\theta}\,\left(k\,(1-\beta) - 1\right) + \sum_{i=1}^{m} \lambda_i C_i + S \tag{6.20}$$

When $k \approx 1$, then $k - 1 = \delta k$, and the rate of neutrons can be written as:

$$\frac{dn}{dt} = \frac{\delta k - \beta}{\theta} + \sum_{i=1}^{m} \lambda_i C_i + S \tag{6.21}$$

By other hand, the rate of production of delayed neutrons for a group " i ", is equal to the rate of diminution of precursors of such group " i ", being $\lambda_i \cdot C_i$.

Furthermore, the breeding rate of precursors is proportional to the rate of global generation of neutrons by the reactor is:

$$\frac{kn}{\theta} \tag{6.22}$$

Whereas, for a particular group " i ":

$$\frac{kn}{\theta}\,\beta_i \tag{6.23}$$

The rate of variations of precursors for the group " i ", or the rate of variation of these precursors C_i , is equal to the rate of breeding minus the rate of diminution:

$$\frac{dC_i}{dt} = \frac{kn}{\theta}\,\beta_i - \lambda_i C_i \tag{6.24}$$

For $k \approx 1$, the value of δk is very small and the following equation can be assumed:

$$\frac{dC_i}{dt} = \frac{n}{\theta}\,\beta_i - \lambda_i C_i \tag{6.25}$$

Finally, the set of equations which rules the kinetic behavior of the neutronic population in a nuclear reactor is the following:

$$\frac{dn}{dt} = \frac{n}{\theta}\,\left(k\,(1-\beta) - 1\right) + \sum_{i=1}^{m} \lambda_i C_i + S \tag{6.26}$$

$$\frac{dC_i}{dt} = \frac{kn}{\theta}\,\beta_i - \lambda_i C_i \tag{6.27}$$

where, $\beta = \sum_{i=1}^{m} \beta_i$.

And by assuming a multiplication factor near 1, the following system is defined:

$$\frac{dn}{dt} = \frac{\delta k - \beta}{\theta} + \sum_{i=1}^{m} \lambda_i C_i + S \tag{6.28}$$

$$\frac{dC_i}{dt} = \frac{n}{\theta}\,\beta_i - \lambda_i C_i \tag{6.29}$$

It is interesting to analyze which is the value of k, to reach the steady state corresponding to a constant power. In such situation, it is acceptable to write the following equations:

$$\frac{dn}{dt} = 0 \tag{6.30}$$

$$\frac{dC_i}{dt} = 0 \tag{6.31}$$

Applying equation (6.31) on equation (6.27) and defining it for all precursors:

$$\frac{k\,n}{\theta}\,\sum_{i=1}^{m} \beta_i = \frac{k\,n}{\theta}\,\beta = \sum_{i=1}^{m} \lambda_i C_i \tag{6.32}$$

Similarly, for equation (6.26) the same procedure is employed:

$$0 = \frac{n}{\theta}\ (k\,(1-\beta)-1) + \sum_{i=1}^{m} \lambda_i C_i + S \tag{6.33}$$

Substituting β in equation (6.33) by the expression obtained in (6.32):

$$n = \frac{S\theta}{1-k} = -\frac{S\theta}{\delta k} \tag{6.34}$$

The result stated by the last equation is only valid if $\delta k < 0$, what means that a nuclear reactor is sub critical at steady state with constant power if there is an internal source of neutrons S inside.

6.3 Decay law of radioactive materials

Whatever radioactive material suffers a modification of its nuclei. For calculations purposes, suppose an initial quantity N_0 (radioactive activity), of a radioactive material. The radioactive material suffers an atomic transmutation along the time, and the measurements of the evolution of the quantity N_0 show that this value decreases a differential quantity ΔN along the time.

Experimental measurements show that the rate $\frac{\Delta N}{N}$ decreases as a function of the time, by effect of disintegrations, according to a constant value multiplied by time increments Δt. Thus, it is accepted to write the decay of the radioactive material by the following equation:

$$\frac{\Delta N}{N} = -\lambda \Delta t \tag{6.35}$$

In a differential form, the previous equation becomes:

$$\frac{dN}{N} = -\lambda dt \tag{6.36}$$

$$N = N_0\, e^{-\lambda t} = N_0\, e^{-\frac{t}{T_s}} \tag{6.37}$$

$$T_s = \frac{1}{\lambda} \tag{6.38}$$

The constant λ is a typical value for each radioactive material. Its physical unit is s^{-1} and λ is usually known as the semi disintegration constant for a particular radioisotope. T_s is denominated the period of semi disintegration, or the needed elapsed time for a decay of the radioisotope in the quantity of " e " portions.

The quantity N does not have physical units properly, but in terms of radioactivity, it is possible to quantify it as follow:

- 1 Becquerel = 1 disintegration per second
- 1 Curie = $3.7 \cdot 10^{10}$ Becquerels

6.4 Special case of the kinetic equations

The only way to solve the general system of differential equations is by using numerical calculation algorithms. Hereafter the general equations are written considering the period, T, of the reactor.

$$\frac{1}{n}\frac{dn}{dt} = \frac{1}{T} = \frac{1}{\theta}\ \left(k\left(1-\beta\right)-1\right) + \sum_{i=1}^{m} \lambda_i y_i + z \tag{6.39}$$

$$\frac{dy_i}{dt} = \frac{k}{\theta}\,\beta_i - \lambda_i y_i \tag{6.40}$$

$$\frac{1}{T} = \frac{1}{n}\frac{dn}{dt} \tag{6.41}$$

$$y_i = \frac{C_i}{n} \tag{6.42}$$

$$z = \frac{s}{n} \tag{6.43}$$

The parameter T is known and therefore $\frac{1}{T}$, is what makes possible to determine " n ". A special and very particular case is the supposition of only one group of delayed neutrons. With this supposition, it is accepted the following equations, where all the parameters of groups "i" of delayed neutrons are summarized as follow:

$$\beta = \sum_{i=1}^{m} \beta_i \tag{6.44}$$

$$C = \sum_{i=1}^{m} C_i \tag{6.45}$$

$$\lambda C = \sum_{i=1}^{m} \lambda_i C_i \tag{6.46}$$

The above system of differential equations become to the following equations with the assumed simplifications.

$$\frac{dn}{dt} = \frac{n}{\theta}\ \left(k\left(1-\beta\right)-1\right) + \lambda C + S \tag{6.47}$$

$$\frac{dC}{dt} = \frac{kn}{\theta}\,\beta - \lambda C \tag{6.48}$$

At steady state, the following relation can be obtained:

$$\frac{dC}{dt} = 0 \tag{6.49}$$

$$C = \frac{kn}{\lambda\theta}\,\beta \tag{6.50}$$

However,

$$C = \sum_{i=1}^{m} C_i = k\ \sum_{i=1}^{m} \frac{n}{\lambda_i\theta}\,\beta_i \tag{6.51}$$

$$\lambda = \frac{\beta}{\sum_{i=1}^{m} \frac{\beta_i}{\lambda_i}} \tag{6.52}$$

6.5 Generation of poisons

Poisons are sub-products from the fission which have large effective sections and can capture thermal neutrons. In a nuclear reactor, the main nuclear poisons are Xe-135 and Sm-149. The radioisotope Xenon-135 appears either directly from the splitting of atoms of Uranium-235 or from the disintegration of Te-135 with an average life of 2 minutes to produce I-135 which decays into Xe-135.

Xenon-135 finally decays into Cs-135 by β particle emissions which is also radioactive. Xenon-135 has an effective section of $2.7 \cdot 10^{-18}\ cm^2$, it means that Xenon-135 has an effective section of $2.710 barn$, justifying its highly capability to capture neutrons.

On the other hand, some atoms of U-235 split to produce Neodymium-149 which decays into Promethium-149, and finally to Samarium-149, which is stable. In comparison with Xe-135, the effective section of Sm-149 is $5.3 \cdot 10^{-20}\ cm^2$, or $5.3 \cdot 10^{8}\ barn$.

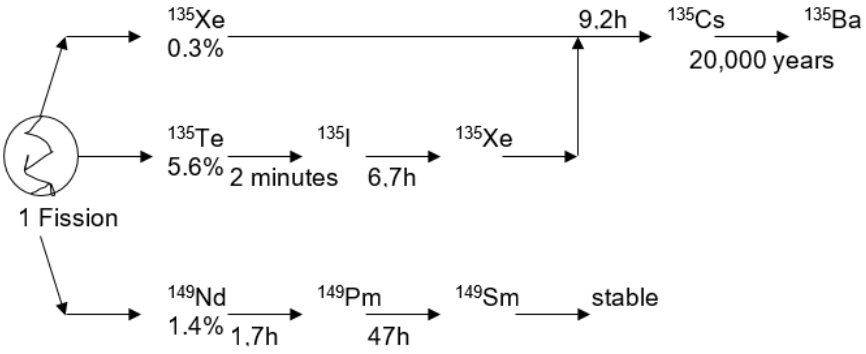

Figure 6.2: Generation of poisons.

6.6 Xe-135 equations

Assuming that the neutronic flux, Φ, stays constant inside the core of the reactor. The variation in Xenon-135 and Iodine-135 becomes a function of time and a set of constant parameters.

$$\frac{dX_e(t)}{dt} = \lambda_1 I(t) + \gamma_2 \Phi - \sigma_2 X_e(t) \Phi - \lambda_2 X_e(t) \tag{6.53}$$

$$\frac{dI(t)}{dt} = -\lambda_1 I(t) + \gamma_1 \Phi \tag{6.54}$$

where, the variation of Xenon is affected by:

- The concentration of Iodine-135, with a radioactive disintegration constant equal to $\lambda_1 = 4.145937 \cdot 10^{-5}\ s^{-1}$. Iodine generates Xenon.
- The neutronic flux, using the constant of efficiency (%) to produce Xe-135, being $\gamma_2 = 0.059$.
- The decrease of Xenon atoms, due to their burn out by the neutronic flux. It is explained by the high effective section of Xenon-134, $\sigma_2 = 2.70 \cdot 10^{-18}\ cm^2$, to capture neutrons.
- The decreasing number of Xenon atoms due to its disintegration, which is defined by the radioactive constant of disintegration, $\lambda_2 = 3.01932 \cdot 10^{-5}\ s^{-1}$.

Regarding Iodine-135, its concentration is affected by:

- The decreasing number of Iodine-135 atoms due to disintegration, its radioactive disintegration constant is $\lambda_1 = 4.145937 \cdot 10^{-5}\ s^{-1}$. Iodine-135 decays into Xenon-135.
- The neutronic flux, as the nuclear fuel fissions have an efficiency of $\gamma_1 = 0.056$ to produce I-135.

6.7 Sm-149 equations

Similarly, the above arguments for Xenon-135 are applicable for Samarium-149. The chain of Promethium decay to produce Samarium.

Similarly, the neutronic flux is assumed constant in the core of the reactor, what let to write the differential equations to balance the variations of Promethium and those of Samarium.

$$\frac{dP_m(t)}{dt} = \gamma_{P_m}\Phi - \lambda_{P_m}P_m(t) \tag{6.55}$$

$$\frac{S_m(t)}{dt} = \lambda_{P_m}P_m(t) - \sigma_{S_m}\Phi S_m(t) \tag{6.56}$$

The variation in the concentration of Samarium is affected by:

- Disintegration of Pm-149 into Sm-149, its radioactive disintegration constant is equal to $\lambda_{Pm} = 4.08 \cdot 10^{-6}\ s^{-1}$.
- The decreasing number of Sm-149 atoms, due to burn out by the neutronic flux. Due to its large effective section to capture neutrons with a value of $\sigma_{Sm} = 5.30 \cdot 10^{-20}\ cm^2$.

Whereas, the evolution in the concentration of Pm-149 is affected by:

- The decreasing number of Pm-149 atoms by disintegration, as its constant of radioactive disintegration is equal to $\lambda_{Pm} = 4.08 \cdot 10^{-6}\ s^{-1}$.
- The influence of the neutronic flux, with an efficiency of $\gamma_{Pm} = 0.014$ to split atoms of Pm-149 by their fission .

Neodymium-149 is not considered in the equation due to its short life.

Chapter 7

Thermonuclear energy in aerospace propulsion

7.1 Introduction

The Russian theoretician Konstantin Eduardovitch Tsiolkovsky advocated for the use of liquid fuel rockets for the propulsion of aerospace vehicles more than one century ago, but later Robert Hutchings Goddard launched the first liquid fuel rocket at Auburn, Massachusetts, in the United States of America. However, the creation of German rockets V-2 during the second World War was the starting point for the accelerated career in the aerospace propulsion systems.

Along the history several kinds of fuel have been used for propulsion of aerospace vehicles depending on the requirements at each mission. The following graphic from Los Alamos National Laboratory shows a comparison between different propulsion technologies.

The experience during many tests reflects that the chemical fuels are suitable for delivering powers of 60.000 kW during few minutes or several days, but beyond this period the solar panels can supply electric energy from 10 kW to 50 kW, being limited by surface area.

Alternatively, Radioisotopes sources fit the requirements for space exploration with small aerospace vehicles at long distances from Earth even beyond the Kuiper belt (which extends beyond Neptune), but they are not suitable for medium or large vehicles as their power is limited to 10 or 20 kW.

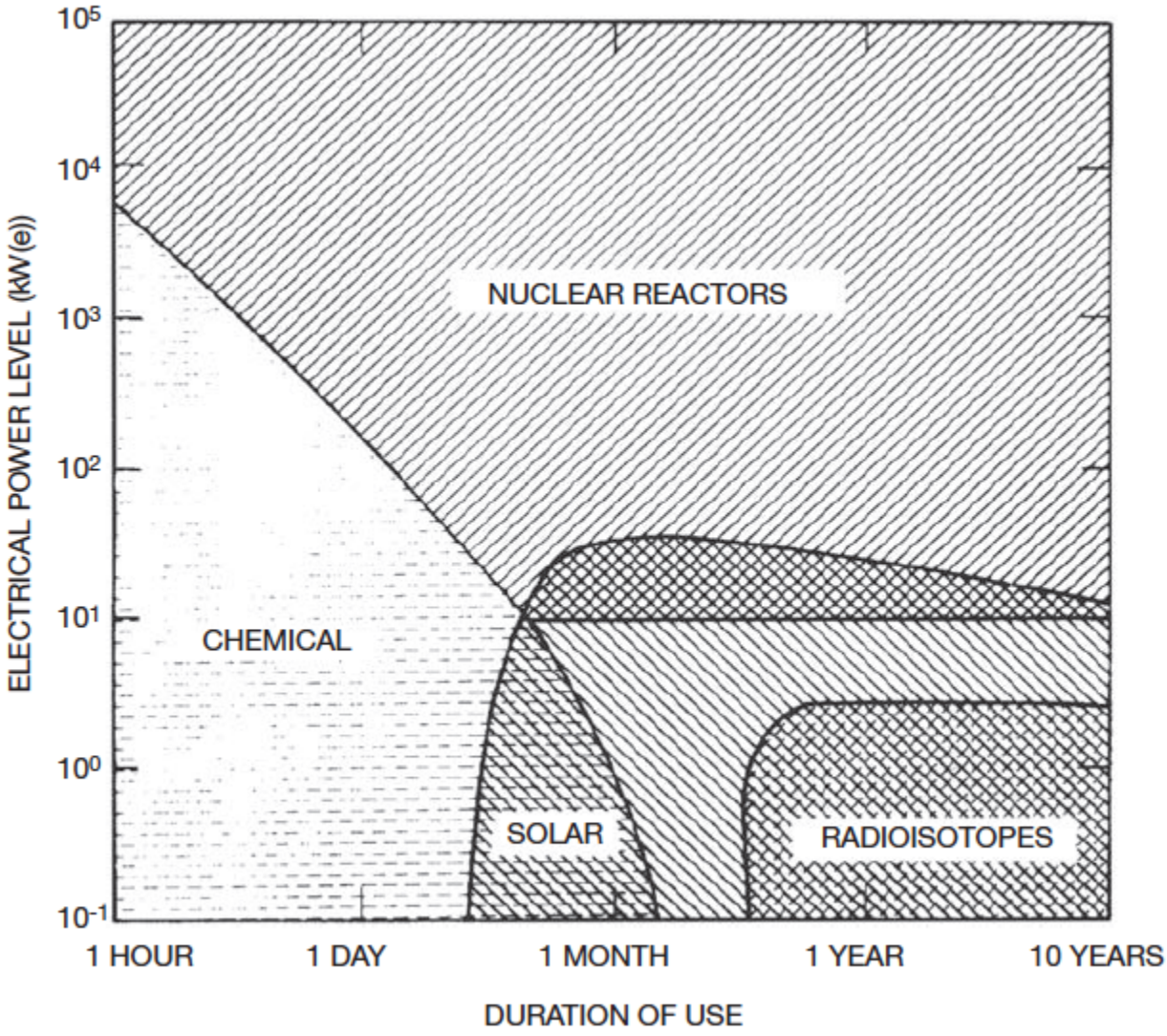

Figure 7.1: Electrical power level for different propulsion technologies as a function of time. Source: Los Alamos National Laboratory [9].

On the other hand, nuclear reactors offer the possibility to supply large quantities of electrical power for long periods of time.

The following table summarizes some of the most useful technologies according to the studies from Los Alamos National Laboratory.

(Source: Los Alamos National Laboratory)

NPS type	Electrical power range (module size)	Power conversion
RTG	Up to 500 W(e)	Static: thermoelectric
Radioisotope dynamic conversion generator	0.5–10 kW(e)	Dynamic: Brayton Organic Rankine
Reactor systems: Heat pipe Solid core Thermionics	10–1000 kW(e)	Static: Thermoelectric Thermionics Dynamic: Brayton Rankine Stirling
Reactor system: Heat pipe Solid core	1–10 MW(e)	Brayton Rankine Stirling
Reactor: Solid core Pellet bed Fluidized bed Gaseous core	10–100 MW(e)	Brayton (open loop) Stirling Magnetic hydrodynamic

Figure 7.2: Nuclear technologies for different electrical power range. Source: Los Alamos National Laboratory [9].

7.2 Nuclear propulsion using the stirling thermodynamic cycle

This chapter proposes an alternative type of nuclear propulsion for aerospace applications. It consist of a modified and compact PWR power plant, where the refrigerant and moderator is hydrogen gas instead of demineralized water. The hydrogen gas is pumped in a closed loop, where it circulates and transfer heat from the reactor core, where the fuel rods are stored, towards the stirling generator. The stirling generator produces mechanical energy by using a temperature gradient to move a piston and the alternator converts the mechanical energy into electricity.

Finally, the electric energy from the electric generators is stored in batteries and condenser banks to supply the navigation system and the propulsion system. The propulsion system uses hydrogen as a propellant, which is reheated to high temperatures inside a deposit with ferromagnetic materials, around 1500 K, by electric heaters based upon Foucault's or Eddy's currents. After heating the hydrogen, it is expanded on a convergent-divergent nozzle towards the outer space, generating thrust in the process.

There are a set of general advantages associated with this type of propulsion:

- In contrast with other nuclear technologies, the percentage of enrichment is approximately 3%, in comparison with the 70 or 90 % enrichment used in other propulsion technologies. This translate into a lower cost and a simpler control system for reactivity.
- It does not require the use of an oxidizer as there is no combustion process.
- High specific impulse in comparison with other technologies. It is limited by the temperature at which the hydrogen gas is heated. The maximum temperature is limited by the materials.
- Clean emissions without radioactive isotopes. The hydrogen gas expelled from the nozzle is independent from the hydrogen used for the refrigerant/moderator.
- Bleeding cycle is not needed, all the turbopumps can be moved by an electrical engine powered by the alternators coupled with the stirling generators.
- Relatively high energy efficiency conversion.
- Capability of high power generation in the order of 50 to 100 kW.

Hydrogen can be used as a moderator as in a conventional PWR power plant, is the hydrogen atom, from the water molecules, responsible to thermalize quick neutrons.

On the other hand, the nuclear parameters are supposedly like the PWR reactor, and the outlet temperature of hydrogen should be around 600 K.

The following graphic illustrates the classification of space nuclear power reactors and the relation between the output power kW(e) and the Specific power Kg/kW.

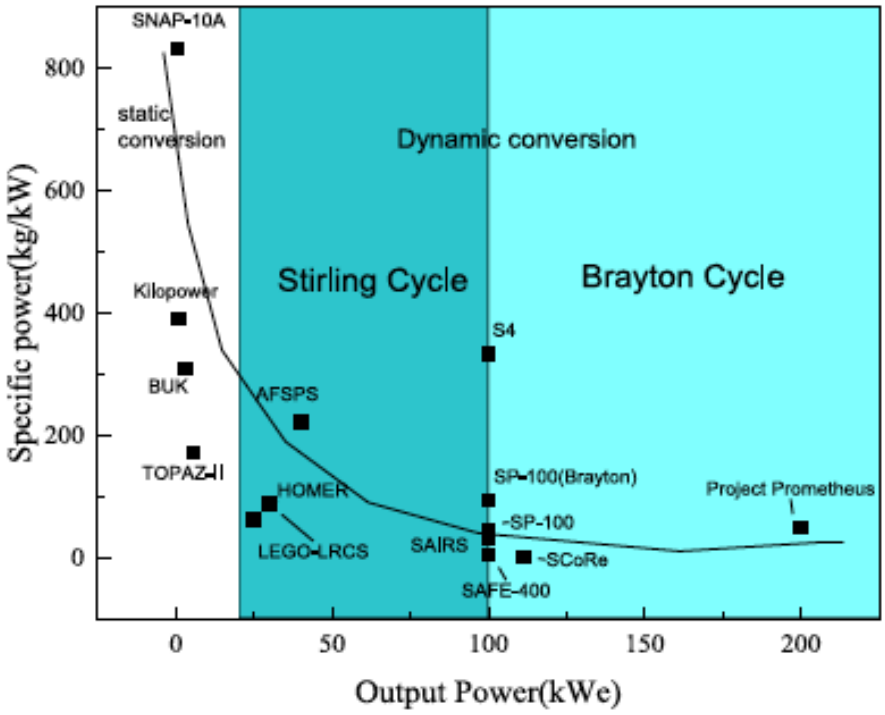

Figure 7.3: Specific power as a function of output power for different nuclear technologies. Source: [93].

The generation of electricity by the Stirling engines is in the range of 20 to 100 kW fits the criteria to supply electricity to the navigation systems and to the hydrogen propellant heaters for the propulsion system.

7.3 Nuclear technologies used in aerospace propulsion

This section describes some of the most known nuclear reactor technologies for aerospace propulsion. NASA launched the first North American engine with nuclear propulsion on 1965, the SNAP-10A, and the Soviet Union followed this technological aerospace career.

7.3.1 USA SNAP-10A engine

SNAP-10A emerges after considerable research and is launched on an Atlas vehicle. Technical details shows a power range from 3 to 35 kW.

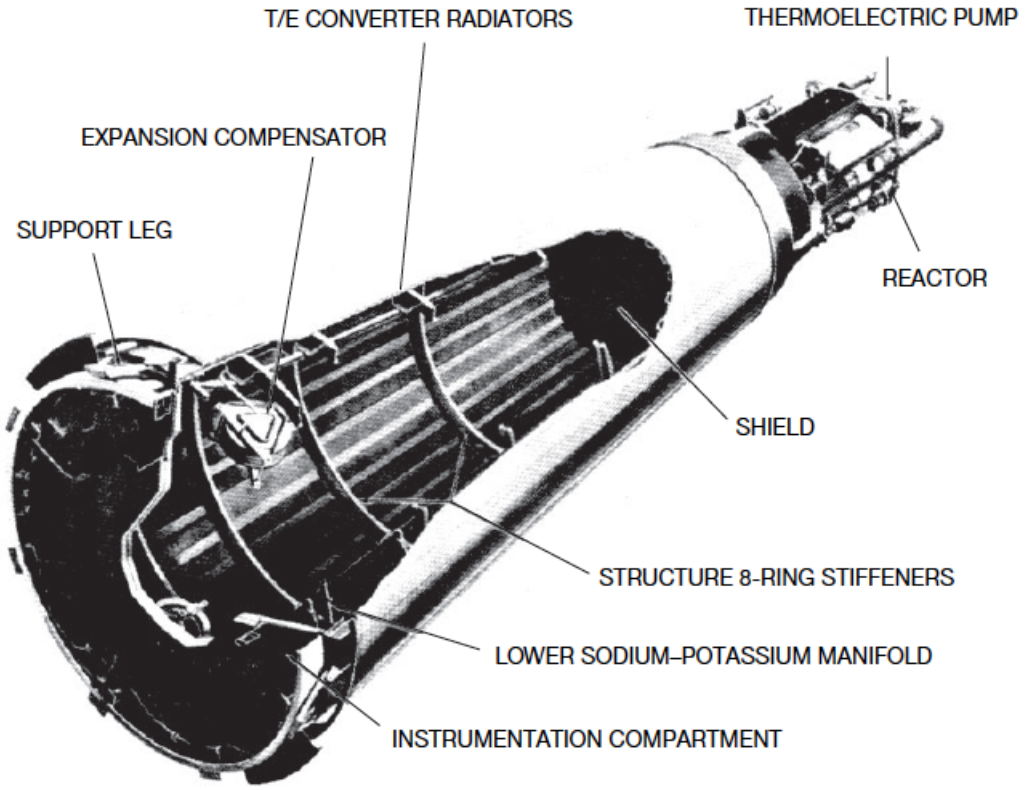

Figure 7.4: SNAP-10A nuclear rocket engine. Source: Atomics international.

Payload	SNAP-10A/Agena D
Mass	400 Kg
Type	Ion engine
Agency	USAF/AEC
Orbit Perigee altitude (km)	1270
Orbit Apogee altitude (km)	1314
Inclination (^{o})	90.3
Period (minutes)	111.4

Table 7.1: Mission parameters. Atomics international.

The spacecraft carried a SNAP-10A nuclear power source. The on-board nuclear reactor provided electrical power for an ion thruster The spacecraft telemetry failed but the reactor itself operated well. In the meanwhile, the USAF/AEC worked in two other models of SNAP and hereafter the table shows some of their main performances.

Characteristic	SNAP-2	SNAP-10A	SNAP-8
Power (kW)	3	0.58	35
Design lifetime (a)	1	1	1
Reactor power (kW)	55	43	600
Reactor outlet (K)	920	833	975
Fuel and spectrum	U–ZrH thermal	U–ZrH thermal	U–ZrH thermal
Coolant	Na–K-78	Na–K-78	Na–K-78
Power conversion	Rankine (Hg)	Thermoelectric (Si–Ge)	Rankine (Hg)
Hot junction (K)		777	
Cold junction (K)		610	
Turbine inlet temperature (K)	895		950
Condenser temperature (K)	590		645
Unshielded weight (kg)	545	295	4545

Figure 7.5: Main performance parameters of various SNAP models. Source: Atomics international.

The following diagram from Atomics international provide the energy conversion mechanism:

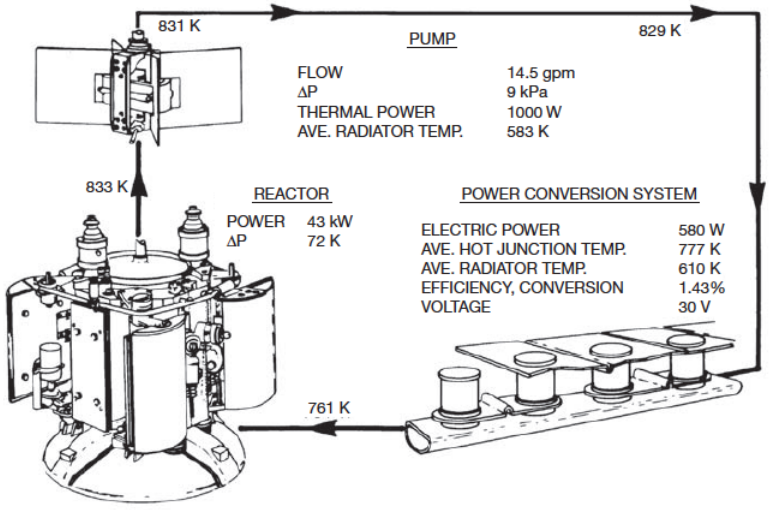

Figure 7.6: Energy conversion mechanism for SNAP propulsion system. Source: Atomics international.

The following figure shows the core of the reactor by courtesy of Los Alamos National Laboratory.

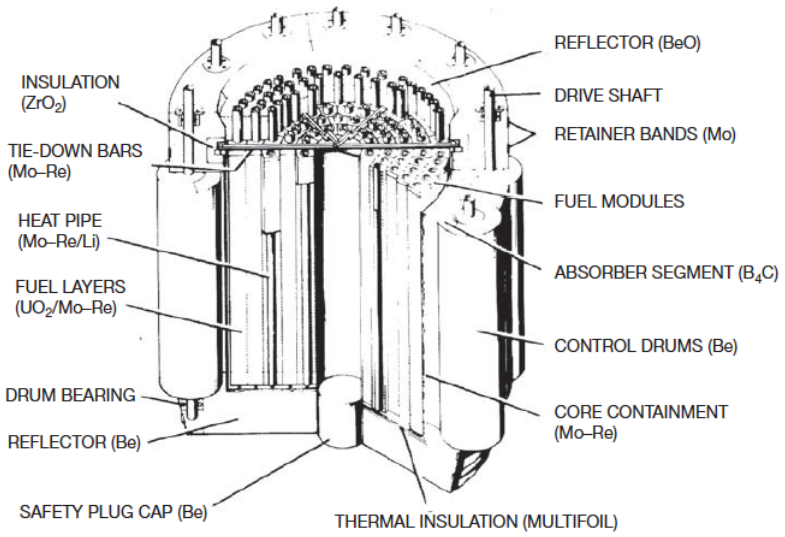

Figure 7.7: Reactor core from SNAP propulsion system. Source: Los Alamos National Laboratory.

Outlet temperature must be of the order of 1200 to 1500 K for a mass density of 30 kg/kW(e) in a small reactor what defines the type of coolant / moderator and the nuclear fuel enrichment.

In case of higher power requirements, in the 0.5 to 5.0 MW(e) range, fluid bed technologies and pellet bed reactors with gas cooling should be used.

7.3.2 Russian Romashka nuclear propulsion system

This reactor was operated in 1964 for 15,000 hours with an energy output of 6,100 kW per hour. Its nuclear reactor design is based upon a fast reactor with thermal electric generators located on the radial outer surface of the reactor. There can be found 11 nuclear fuel elements consisting on uranium carbide disks with a 99% enrichment.

Due to the high temperature inside the core of the reactor, it was required a heat insulation system made of foam graphite and multiple layers of graphite fabrics.

Characteristic	Value
Reactor core diameter/height (by package) (mm)	241/351
Radial reflector outer diameter/height (mm)	483/553
Reactor load mass by uranium-235 (kg)	49
Total mass of the TEG (with the casing and radiator) and reactor (without drives and control rods) (kg)	635
Reactor converter effective thermal power (without taking into account the end wall spread of heat) (kW)	28.2
Reactor converter electrical output (at start-of-life) (W)	460–475
Electrical power reduction over a lifetime of 15 000 h	80%
Reactor converter terminal operating voltage (four groups of thermoelectric converters connected in series) (V)	21
Number of thermoelectric converters in a TEG	3072

Figure 7.8: Several parameters of the Romashka nuclear propulsion system. Source: Kurchatov institute.

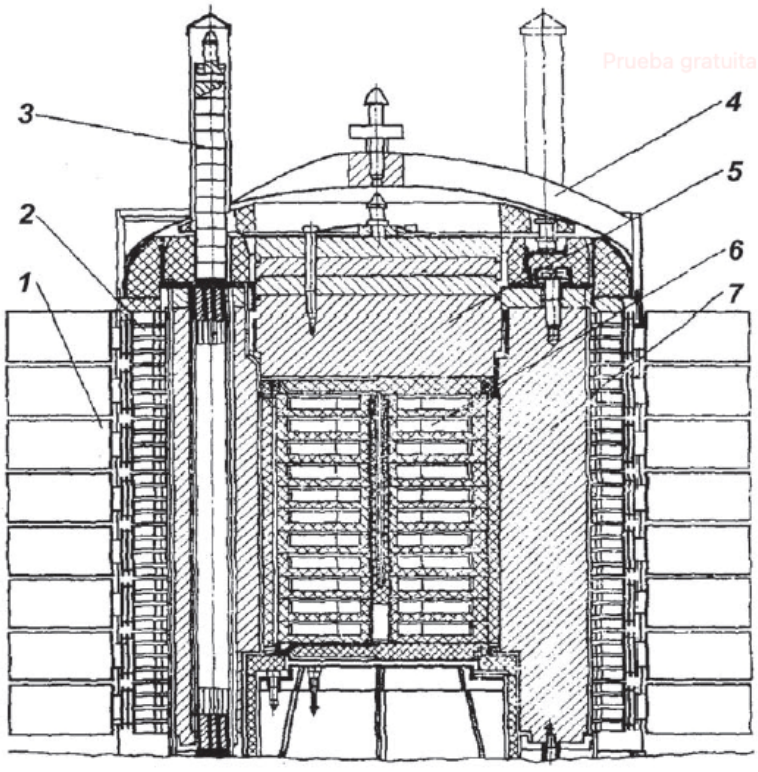

The Romashka NPS reactor converter layout: (1) radiator ribs, (2) thermoelectric elements, (3) control rod, (4) reactor vessel, (5) upper reflector, (6) reactor core, (7) radial reflector. Source: Kurchatov Institute.

Figure 7.9: Internal components of the Romashka nuclear reactor. Source: Kurchatov institute.

The Romashka nuclear reactor used for the thermal electric generators, a grade silicon-germanium semiconductor (85% Si and 15% Ge).

7.3.3 Russian BUK nuclear propulsion system

The BUK nuclear propulsion system is based upon a small and fast reactor which contains a total of 37 fuel rods. The fuel weights around 30 Kg and is a highly enriched uranium–molybdenum alloy. This reactor contains two-loops of liquid metal as heat removal system and uses a eutectic alloy of sodium and potassium as the coolant. The first loop of the cooling system reaches a temperature around 973 K.

The maximum power of this reactor is limited to 100 kW and the maximum electric power conversion reaches 3 kW. Therefore, the efficiency is about 3%.

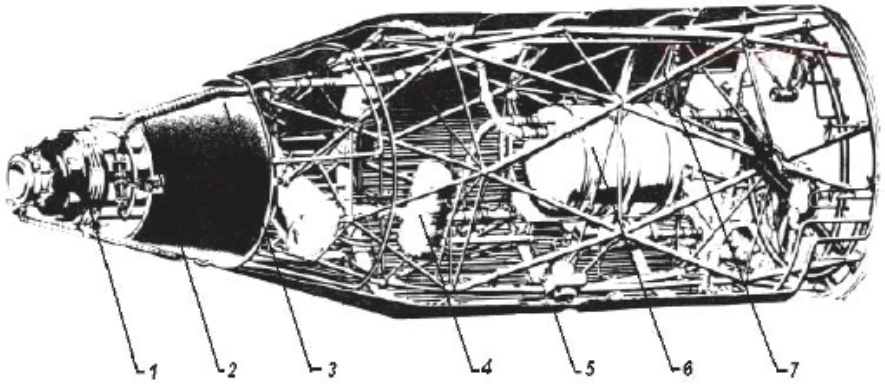

The BUK NPS layout: (1) nuclear reactor, (2) liquid metal circuit pipeline, (3) reactor shielding, (4) liquid metal circuit expansion tanks, (5) radiator, (6) TEG, (7) load bearing frame structure. Source: Kurchatov Institute.

Figure 7.10: BUK nuclear propulsion system layout. Source: Kurchatov institute.

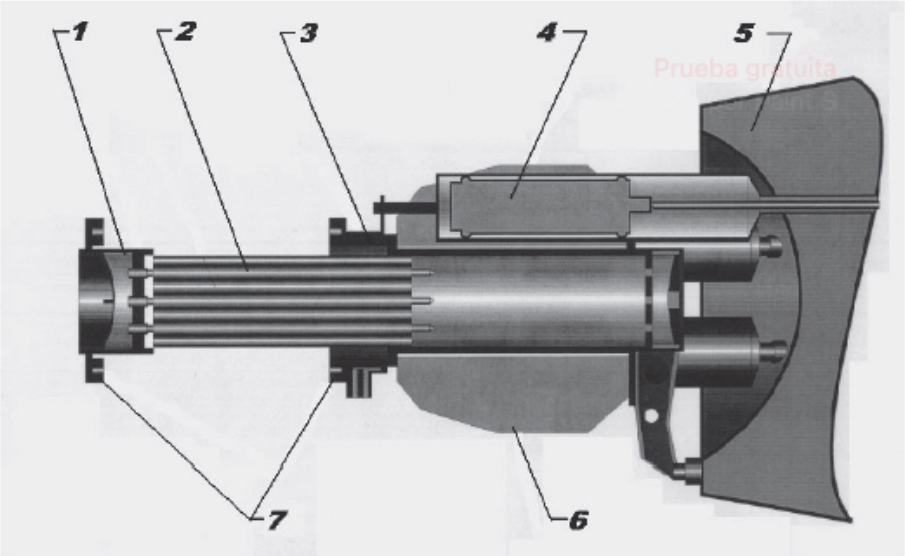

Diagram of the fuel element assembly ejection system for the BUK NPS: (1) tube plate, (2) fuel element assembly, (3) reactor vessel, (4) control rod, (5) reactor shielding, (6) side reflector, (7) actuating mechanism. Source: Kurchatov Institute.

Figure 7.11: Fuel rod diagram of the BUK NPS. Source: Kurchatov institute.

Characteristic	Value
Power (kW(e))	<3
Design lifetime (a)	1
Reactor power (kW)	<100
Reactor outlet temperature (K)	973
Fuel and spectrum	U–(90% enriched)–Mo, fast
Coolant	Na–K eutectic
Power conversion	Two cascade thermoelectric converter (Si–Ge)
Hot junction temperature (K)	623
Unshielded weight (kg)	900

Figure 7.12: Some important parameters of the BUK NPS. Source: Kurchatov institute.

7.3.4 Russian TOPAZ nuclear propulsion system

The TOPAZ NPS implements a thermionic reactor converter with a caesium vapor supply system. The core of the reactor consists of 79 TFEs and four zirconium hydride moderator discs

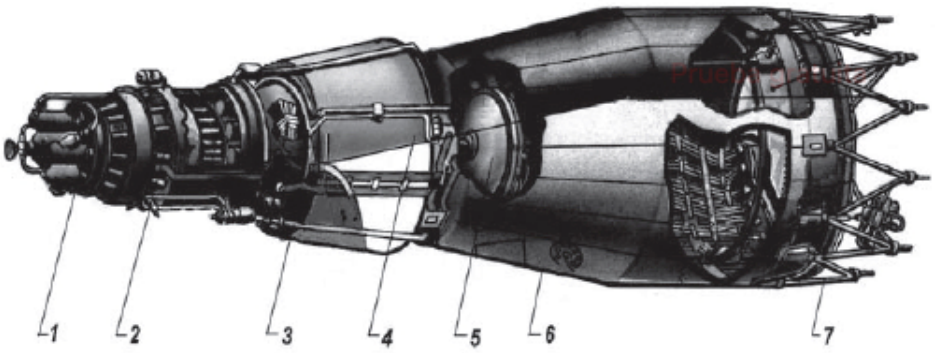

The TOPAZ NPS layout: (1) caesium vapour supply system and control drum drive unit, (2) thermionic reactor converter, (3) liquid metal circuit pipeline, (4) reactor shielding, (5) liquid metal circuit expansion tank, (6) radiator, (7) frame structure. Source: Kurchatov Institute.

Figure 7.13: TOPAZ NPS layout. Source: Kurchatov institute.

Twelve rotating cylinders or drums are placed in the side reflector to provide neutronic and thermal power control, and when necessary, reactivity compensation and emergency shutdown.

A single circuit of sodium–potassium acts as moderator and is responsible for the heat extraction of 170 kW from the core at around 880 K. TOPAZ NPS nuclear reactor generates approximately 6 kW, at a voltage of 32, during the start-of-life with an efficiency of just about 5.5%. The global mass of the reactor is about 1200 kg, with a lifetime design of 4400 h. The dimensions of the nuclear power unit are 4.7 m long and 1.3 m of diameter.

7.3.5 Russian yenisey (TOPAZ-2) nuclear propulsion system

Yenisey (TOPAZ-2) reactor is the evolution of TOPAZ. TOPAZ and Yenisey NPSs reactors have similar structures and design implementations, but the Yenisey thermionic reactor converter contains a single unit TFE.

Figure 7.14: TOPAZ-2 general view. Source: Kurchatov institute.

Description	Value
Maximum electrical power at the reactor unit terminals supplied to consumer (kW)	5.5
Current type	Direct
Voltage (V)	27
Reactor thermal power (kW(th))	135
Maximum coolant temperature at the reactor outlet (°C)	550
Maximum emitter temperature (°C)	1650
Lifetime corroborated by nuclear tests (a)	1.5
Reactor unit mass (kg)	1000
Dimensions of the reactor unit:	
Length (mm)	3900
Maximum diameter (mm)	1400
Radiation situation over a plane of diameter 1.5 m at 6.5 m from the core centre:	
Fluence of neutrons with energy >0.1 MeV (n/cm^2)	5×10^{12}
Gamma radiation exposure dose (R)	5×10^5
Core diameter (mm)	260
Core height (mm)	375
Number of TFEs in the core	37
Number of rotational control elements in the side reflector	12
Loading of uranium-235 in the core (kg)	25
Effective neutron multiplication factor (control elements out, cold state) (k_{eff})	1.005
Total reactivity temperature effect ($\Delta k/k$)	0.012
Worth of 12 control elements ($\Delta k/k$)	0.055
Peak to average power density:	
Along to the core radius	1.1
Along to the core height	1.26
Lifetime ensured by the reactivity margin	3

Figure 7.15: Table containing main parameters of the TOPAZ-2 NPS. Source: Kurchatov institute.

Similarly to the PWR reactors, the clearance between the TFEs and their container tubes are filled with helium to compensate the effects of pressure excursion versus evolution of temperature.

The efficiency of the Yenisey nuclear thermionic reactor converter is about 4.5% when the electrical power system provides 4.5 kW.

7.3.6 USA Directions - Gas propellant for nuclear reactor propulsion systems

At first glance, it seems advantageous to heat a gas by the used of thermal energy from the nuclear reactor to produce thrust instead of the conventional combustion process in chemical rocket engines.

Nuclear reactors usually work with the limitation of temperature as the moderator and coolant fluid do not exceed temperatures beyond 900 K in the best cases. The specific impulse provided by the rocket engine is a function of the temperature, the higher the temperature at the exit of the nozzle, the higher the specific impulse. Therefore, several methods have been proposed to increase the temperature of the gas propellant from cryogenic state to temperatures as high as 1500 K or even greater. Nevertheless, the maximum temperature will be always limited by materials.

- Recovering thermal energy from the coolant fluid of the reactor to boost a thermal engine based upon a thermodynamic **Rankine cycle**. This engine converts thermal energy into mechanical energy and an electric generator transforms mechanical energy into electricity which can be used to heat the gas propellant as much as suitable.
- Recovering thermal energy from the coolant fluid of the reactor boosts a thermal engine based upon a thermodynamic **Brayton cycle**. This engine converts thermal energy into mechanical energy and an electric generator transforms mechanical energy into electricity which can be used to heat the gas propellant as much as suitable.
- The proposal in this work is recovering of thermal energy from the coolant fluid of the reactor boosts a thermal engine based upon a thermodynamic **Stirling cycle**. This engine converts thermal energy into mechanical energy and an electric generator transforms mechanical energy into electricity which can be used to heat the gas propellant as much as suitable.

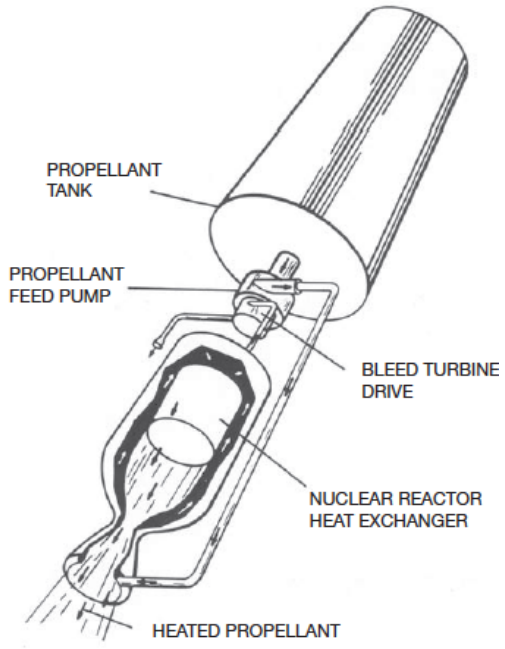

Typical nuclear rocket propulsion module. Source: NASA/US

Figure 7.16: Typical nuclear rocket design. Source:NASA/US

7.3.7 USA SAFE-400 fission engine

The project SAFE, is a propulsive heat pipe power system developed at the Los Alamos National Laboratory. The nuclear reactor NTP SAFE-400 is designed to provide 400 kW of thermal power for more than ten years through two independent Brayton power systems, the reactor heat is transferred to the gas (He 72%, Xe 28%) flow via two independent heat pipes towards gas heat exchangers. This engine provides 100 kW(e) for a 25% of efficiency.

The SAFE-400 nuclear reactor contains 127 modules made with niobium– zirconium (1 % in weight) alloy. Each module contains a Nb1Zr–Na heat pipe at its center, surrounded by three niobium–zirconium tubes each of which contains a rhenium clad uranium nitride fuel sleeve. The thermal energy from the nuclear fission is transferred to the heat pipes at a vapor temperature of 1200 K and, and from here, to the Brayton cycle heat exchangers.

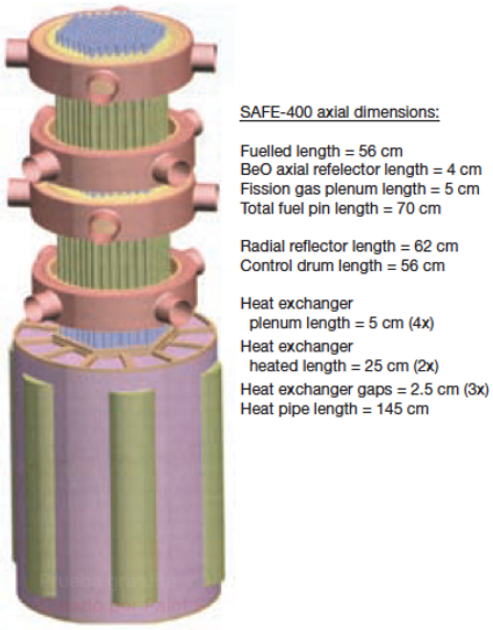

Figure 7.17: SAFE400 NPS design. Source: Nuclear News.

This nuclear reactor can be adapted with Stirling or Brayton cycles. The neutronic flux and therefore the reactivity of this reactor is controlled by Nb1Zr clad beryllium control drums which have a boron carbide absorber layer. The mass of the reactor is 512 kg.

7.3.8 Usa HOMER nuclear reactor - Mars exploration

The nuclear reactor HOMER is a heat pipe operated engine of small power capability generation for surviving purpose on the surface of Mars.
The nuclear reactor HOMER-15 generates 15 kW of thermal power and is designed to be adapted with a Stirling engine via heat pipes to provide 3 kW of electrical power.

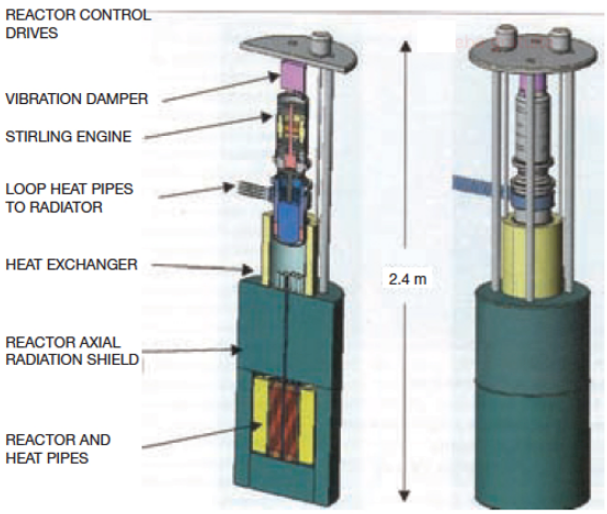

Figure 7.18: SAFE400 NPS design. Source: Nuclear News.

The reactor uses a total of 102 uranium nitride fuel pins, each pin is 44 cm long and they are inside stainless steel clads. The moderator in this reactor is sodium which works as coolant fluid of the core. The heat pipes length is 40 cm beyond the core axial shield to a heat exchanger. The function of the heat exchanger is to remove the thermal energy from the coolant fluid and transmit the energy to a Stirling engine for the generation of electric power.

7.4 Russian orientation

Russian technology focus most of it efforts into the manufacture of engines which can provide a specific impulse between 2 and 2.5 times greater than chemical rocket engines. To achieve such specific impulse is necessary to work with low atomic mass propellants and high temperatures. Hydrogen is a perfect candidate as propellant due to its low atomic mass. However, in order to surpass the specific impulse obtained with chemical rocket engines, for example 450s could be obtained with the combustion of LOX and LH2, it is necessary that the reactor produce enough power to heat the hydrogen gas to temperatures beyond 1500 K. The specific power flux in the reactor core would be around 30 kW/cm^3 to reach the suitable temperature.

Russia chose an architecture of a heterogeneous reactor layout with the neutron moderator location separately from the uranium fuel elements.

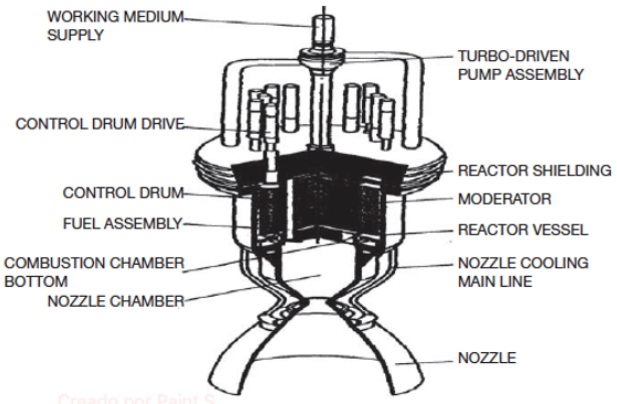

Figure 7.19: Nuclear thermal propulsion system, concept design. Source: Kurchatov institute.

The fuel elements are surrounded by a heat insulation layer and enclosed in the metal casing forming the complete independent reactor unit what is considered as the fuel assembly. This preference for a heterogeneous reactor and element-by-element testing is the main difference between the Russian and USA Nuclear Thermal Propulsion programs.

This concept of NTP nuclear reactor with a heterogeneous core comprises individual fuel assemblies (including fuel elements based on uranium, zirconium and niobium carbides) which are situated in the zirconium hydride moderator body. The beryllium reflector acts as a shadow radiation shielding. Finally, the hydrogen loop surrounds the core to capture a maximum of thermal energy.

The nuclear fuel and other performances for this architecture of NTP impose special requirements:

- High density of the enriched uranium per unit of volume fuel.
- High resistance to radiation swelling.
- High corrosion resistance to the working coolant fluid.
- A maximum allowable temperature of the working coolant fluid.
- A maximum number of the heating and cooling cycles.
- The reactor properties must provide passive safety.

The nuclear fuel must give off enough thermal power with the scope to heat the hydrogen propellant until a temperature of about 3300 K. The nuclear fuel compounds must comply with mechanical, nuclear and thermal requirements to fulfil the extreme working conditions such as carbides (UC–ZrC, UC–NbC, UC–TaC) with an enriched uranium density of approximately 2 g/cm^3.

7.4.1 Russian IGR reactor

The experimental IGR nuclear reactor let research on 1961 to select nuclear fuel and to find out assembly materials under full-scale operational conditions.

The purpose of IGR nuclear reactor during the tests is summarized as follows:

- Check the reliability of selected materials and protective coatings of fuel elements in hydrogen at temperatures between 3000 and 3300 K in a high neutron and γ irradiation environment.
- Substantiate the optimum steady state for the operational temperatures of the nuclear fuel elements.
- Check the fuel assembly structural elements and architecture, the methodology of construction and assembly of heat insulation materials.
- Get data on specific fuel assembly parameters, and particularly about the specific impulse thrust.
- Log data on the dynamic characteristics of nuclear fuel assemblies and about the optimal modes of neutronic flux control.
- Examine the nuclear fuel assembly operating peculiarities, particularly to determine the amount of the uranium and fission byproducts released into the hydrogen.

7.4.2 Russian IVG-1 experimental bench reactor

The nuclear reactor IVG-1 NTP worked as an experimental bench prototype unit delivering intermediate power to provide thrust between 200 kN and 400 kN. The IVG-1 nuclear reactor design delivers a power of thermal 720 MW.

Each fuel assembly can be tested at different rated gas outlet temperatures by the individual injection of gaseous hydrogen by assembly what let to make tests at a range of thrust from 40 T to 200 T.

The IVG-1 experimental reactor is a heterogeneous gas cooled reactor where light water acts as nuclear and an internal coating of beryllium operates as neutrons reflector.

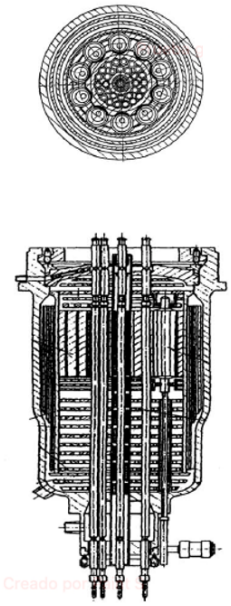

Figure 7.20: IVG-1 reactor sectional view. Source: Kurchatov Institute.

This nuclear reactor was tested in a bench and the reactor generated a thrust of 36 kN.

Figure 7.21: IVG-1: Startup, at 225 MW and outlet temperature of 3000 K. Source: Kurchatov Institute.

7.4.3 Russian IRGIT reactor

The IRGIT nuclear reactor is a NTP prototype design to make tests at several stages:

- Reactor physical startup.

- Cold gas dynamics test.
- Physical startup check.
- Cold hydrodynamics tests.
- Power startup.
- Fuel fired test and post-tech research.

The IRGIT NTP nuclear reactor went through two series of fuel fired tests in July and August 1978. Following the results of the tests it was confirmed that the nuclear fuel characteristics achieved the requirements and that it was possible to design a compact reactor core with varying power output to provide a specific impulse greater than 900 s.

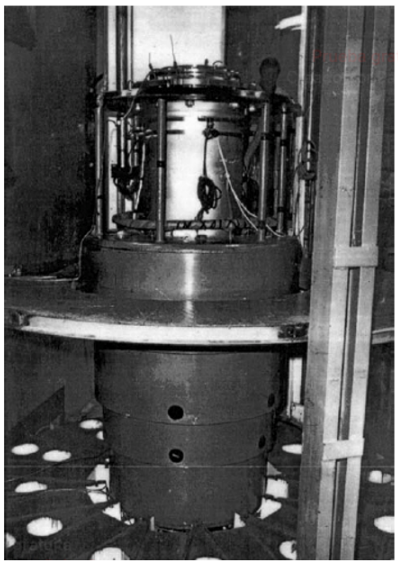

Figure 7.22: IRGIT reactor. Source: Kurchatov Institute.

Parameter	Powered startup	Fuel fired test 1	Fuel fired test 2
Power (MW)	24	33	42
Rated duty duration (s)	70	93	90
Flow rate of working medium (kg/s) through:			
Vessel–reflector–moderator	1.72	3.23	3.51
Fuel assemblies	1.18	1.46	2.01
Working medium average temperature at the fuel assembly outlet (K)	1670	2630	2600
Working medium pressure (MPa) at:			
Reactor vessel inlet	6.04	9.46	10.65
Fuel assembly inlet	1.9	2.2	2.4
Fuel assembly outlet	1.1	1.2	1.3
Material average temperature (K):			
Moderator units	405	397	398
Reflector units	356	381	371
Reactor vessel (from the outside)	315	320	325
Flow rate of water for cooling of device process arm (kg/s)	8	8.3	8.3

Figure 7.23: IRGIT reactor, main parameters. Source: Kurchatov institute.

7.5 Cooperation for missions to Mars

From 1994 to 1995 the Agencies Russian RKK and the American NASA Jet Propulsion Laboratory analysed the project "Mars Together". This evaluation studied the use of spacecraft equipped with solar arrays or nuclear reactors to supply power of up to 30–40 kW needed for insertion into Martian orbit and the operation of a sideways radar to map the surface digitally. As a preliminary step, a demonstration launch was proposed of a spacecraft with a mass of 120–150 kg, a solar panel area of 30 m^2 and engines with a thrust of 3 kN.

Chapter 8

Thermodynamic principles of the nuclear propulsion system

8.1 Internal energy of an ideal gas

The content of this section is intended to explain the main equations regarding the thermodynamic Stirling cycle that the nuclear propulsion system employs.

Firstly, the expression that relates the internal energy of the system with the gas temperature is going to be obtained. After that, a set of different thermodynamic processes involving an ideal Stirling cycle will be studied and finally the eddy current will be briefly presented.

Considering a cube as a thermodynamic boundary, where rigid molecules of a gas with a given mass, m, are moving with in the axial directions (X, Y, Z). The molecules are moving with a velocity, v_i and their linear momentum is equal to $p_i = m \cdot v_i$. When the molecules collide with the walls of the container, assuming no energy loss in the process, they bounce back with the same velocity but in the opposite direction.

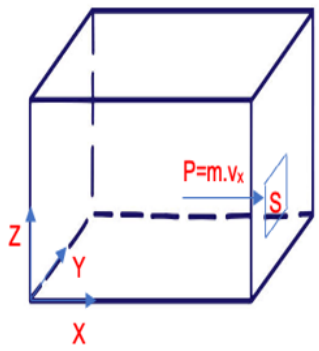

Figure 8.1: Thermodynamic boundaries.

The variation in linear momentum in the X direction for a given molecule before and after the collision with the walls, can be expressed as: $\Delta p = -2mv_{x_i}$

It can be admitted that half of the particles moving in the x direction, are moving in the positive direction and the other half are those bouncing from the walls and moving towards the negative

direction. The same can be considered for the particles in the Y and Z axis.

At a certain time interval, t, it is assumed that the concentration of particles $N_{x_i}/2$ with a velocity v_{x_i} which bond against the section S of the wall is:

$$\frac{N_{x_1}}{2} \cdot S \cdot v_{x_1} \cdot t \tag{8.1}$$

Consequently, the global variation of linear momentum in the x direction for a given particle i and for a given time interval t and considering absolute values is:

$$\left|\frac{\Delta p_i}{\Delta t}\right| = \left|\frac{\frac{N_{x_i}}{2} S v_{x_i} t\,(-2 m v_{x_i})}{t}\right| = N_{x_i} S m v_{x_i}^2 \tag{8.2}$$

Defining the second law of Newton, it can be seen the relation between the force exerted by the particles and their linear momentum, assuming no external forces:

$$F = m\ a = m\frac{\Delta V}{\Delta t} \tag{8.3}$$

$$F = \frac{\Delta p}{\Delta t} = \frac{\Delta p}{t} \tag{8.4}$$

Therefore, by defining the pressure as a force divided by the surface, the following expression is obtained:

$$P_{x_i} = N_{x_i} m v_{x_i}^2 \tag{8.5}$$

where, pressure is denoted by P and linear momentum by p.

The total pressure in the X axis is defined as:

$$P_{total_x} = m\left(N_{x_1} v_{x_1}^2 + N_{x_2} v_{x_2}^2 + ... + N_{x_n} v_{x_n}^2\right) \tag{8.6}$$

Considering the following parameters:

$$\overline{v_x}^2 = \frac{N_{x_1} v_{x_1}^2 + N_{x_2} v_{x_2}^2 + ... + N_{x_n} v_{x_n}^2}{N_{x_v}} \tag{8.7}$$

$$N_{x_v} = \sum_{i=1}^{n} N_{x_i} \tag{8.8}$$

The total pressure in the x axis becomes:

$$P_{total_x} = N_{x_v} m \overline{v_x}^2 \tag{8.9}$$

N_{x_v} is the number of molecules per unit of volume in the x axis.

Considering that the total number of molecules inside the boundaries is evenly distributed in each axis, then:

$$N_{x_v} = N_{y_v} = N_{z_v} = \frac{N_v}{3} \tag{8.10}$$

In addition, it is assumed that the average velocity in each axis is equal and therefore:

$$\overline{v_{global}} = \overline{v_x} = \overline{v_y} = \overline{v_z} \tag{8.11}$$

Finally, the average pressure exerted in a wall is defined as:

$$P_{Wall} = \overline{P_{Wall}} = \frac{2}{3}\frac{N_m}{V}\frac{m\overline{v_{global}}^2}{2} \tag{8.12}$$

where V is the volume inside the boundaries, N_m is the number of molecules and the right term of the equation containing a velocity square is the kinetic energy of the molecules.

$$P \cdot V = \frac{2}{3} \cdot N_m \cdot \frac{m \cdot v^2}{2} \tag{8.13}$$

where v is the average global velocity of the molecules inside the thermodynamic boundaries, $\overline{v_{global}}$.

With the previous equation the total internal energy of the system can be defined as a function of temperature:

$$U = \frac{3}{2} \cdot P \cdot V \tag{8.14}$$

By using the ideal gas law:

$$U = \frac{3}{2} \cdot n \cdot R \cdot T \tag{8.15}$$

where n is the number of moles, R is the perfect gas constant ($8.31 \cdot 10^3 J/(mol\ K)$) and T is the temperature in Kelvin.

Another definition for the interval energy, involving the previous equation, it is by the used of the Boltzmann constant, k, and the number of molecules,$N_{molecules}$, instead of the previously used number of mols, n.

$$U = \frac{3}{2} \cdot N_{molecules} \cdot k \cdot T \tag{8.16}$$

8.2 First principle of thermodynamics

The first principle of thermodynamics states that any positive contribution of heat to a gas provokes an increment of the internal energy in the gas and the generation of work, according to the following differential equation:

$$dQ = dU + P \cdot dV \tag{8.17}$$

8.2.1 Isobaric process

During an isobaric process the pressure of the gas stays constant, and by applying the first law of thermodynamics:

$$\int dQ = \int dU + \int P \cdot dV \tag{8.18}$$

$$n \cdot c_p dT = dU + PdV \tag{8.19}$$

where c_p is the heat coefficient at constant pressure.

8.2.2 Isochoric process

The volume of the gas remain constant and therefore the first law becomes:

$$\int dQ = \int dU \tag{8.20}$$

$$n \cdot c_v dT = dU \tag{8.21}$$

where c_v is the heat coefficient at constant volume.

8.2.3 Adiabatic process

If there is no heat exchange, then it is an adiabatic process. The first law becomes:

$$0 = dU + p \cdot dV \tag{8.22}$$

The internal energy can be defined as:

$$dU = n \cdot c_v dT \tag{8.23}$$

Therefore,

$$0 = n \cdot c_v dT + \frac{nRT}{V} dV \tag{8.24}$$

Reorganizing the previous equation,

$$\frac{dT}{T} + \frac{R}{c_v} \cdot \frac{dV}{V} = 0 \tag{8.25}$$

With the heat coefficients a set of expressions can be defined:

$$\gamma = \frac{c_p}{c_v} \tag{8.26}$$

$$R = c_p - c_v \tag{8.27}$$

Solving the differential equation and applying the previous expressions yields:

$$ln(T) = (\gamma - 1) \cdot ln(V) \tag{8.28}$$

$$T \cdot V^{\gamma - 1} = P \cdot V^{\gamma} = cte \tag{8.29}$$

8.3 Stirling thermodynamic cycle

The ideal thermodynamic Stirling cycle is a reversible regenerative closed cycle, in which the regenerator, in the Phase 2-3 recovers part of the heat used, to use it back in the phase 1-4. Additionally, this ideal cycle have two isothermal stages and two isochoric stages.

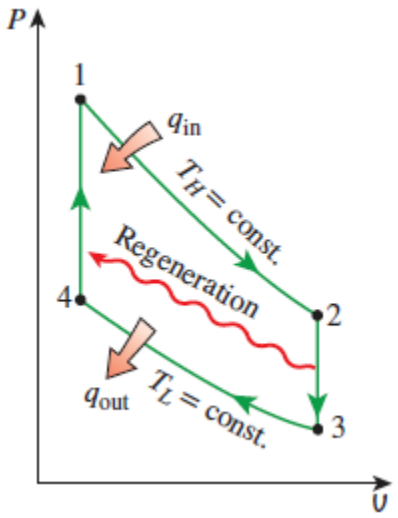

Figure 8.2: Pressure - Volume diagram. Source: [53].

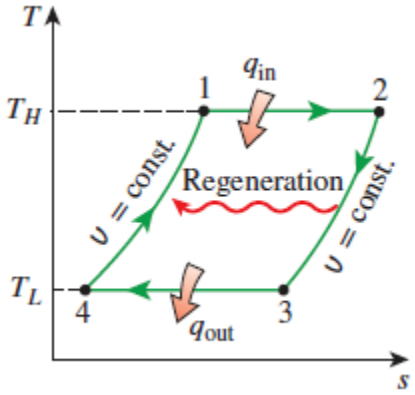

Figure 8.3: Temperature - Entropy diagram. Source: [53].

The stages of the thermodynamic cycle are:

- Phase 1-2: Isothermal expansion.
- Phase 2-3: Isochoric cooling process, where it is possible to use the rejected heat in a regenerator to heat the stages 4-1 and therefore increasing the efficiency of the system.
- Phase 3-4: Isothermal compression.
- Phase 4-1: isochoric heating where the heat comes from a heat exchange that is fed by the hot hydrogen of the nuclear reactor. Additionally, if a regenerator is used part of the heat comes from the previous stirling cycle.

By using figure (8.4), the previous phases can be explained by the movement of the two pistons:

- Phase 1-2: the right piston stays in a fix position after the compression, and the left piston starts to expand until it reaches the state 2.

- Phase 2-3: Both pistons move to the right until state 3, to maintain constant volume.
- Phase 3-4: The right piston moves to the left while the left piston is fixed, increasing the pressure and decreasing the volume.
- Phase 4-1: the left piston is fixed and the right piston moves to the left while heat is being added.

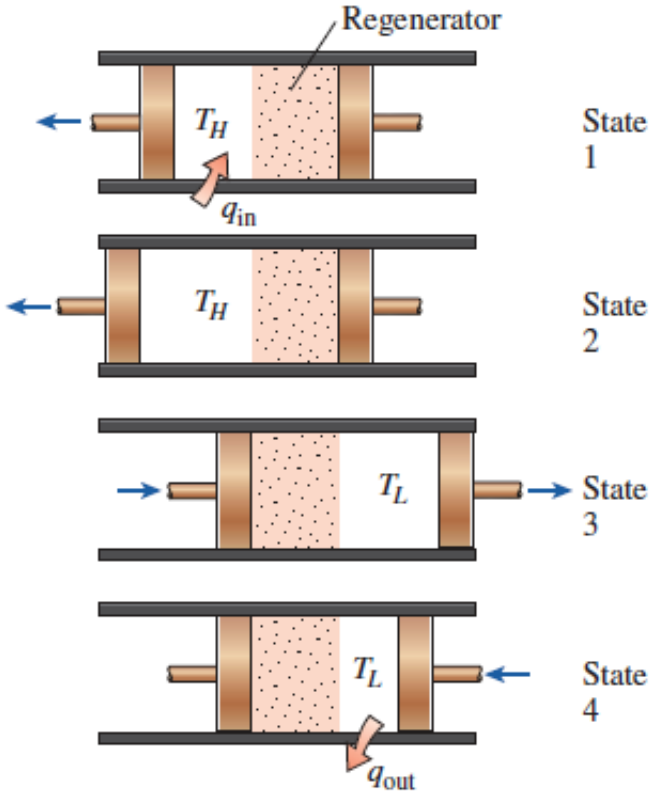

Figure 8.4: Stirling engine, pistons movement. Source: [53].

This engine contains an internal porous regenerator which separates the left side from the right side and lets the transit of the fluid in both directions according to the thermal phase. At the left of the regenerator, the temperature TH corresponds to that of the heat source, and at the right of the regenerator, the temperature TL corresponds to the heat sink.

8.3.1 The stirling cycle efficiency

8.3.2 Phase 1-2

This phase is characterized by an isothermal expansion at temperature T_H. During this phase is when the thermal energy supplied by the hot gas is converted into mechanical work by the piston.

By using the first law of thermodynamics:

$$dQ = dU + p \cdot dV \tag{8.30}$$

Using the definition of the internal energy as a function of temperature:

$$U = \frac{3}{2} \cdot N_{molecules} \cdot k \cdot T \tag{8.31}$$

$$dU = \frac{3}{2} \cdot N_{molecules} \cdot k \cdot (T_H - T_H) = 0 \tag{8.32}$$

Therefore, as the temperature is constant there is no variation in the internal energy of the system. However, the variation in heat and work is not zero:

$$dQ = p \cdot dV = \frac{nRT}{V} dV \tag{8.33}$$

$$\int_{state_1}^{state_2} dQ = \int_{V_1}^{V_2} \frac{nRT}{V} dV \tag{8.34}$$

Solving the integral, yields:

$$Q_{1-2} = n \cdot R \cdot T_H \cdot ln\left(\frac{V_2}{V_1}\right) \tag{8.35}$$

8.3.2.1 Phase 2-3

This phase is characterized by an isochoric heat rejection process from the hot source to the cold sink. Both pistons move simultaneously toward the right to maintain the volume of the gas constant. Similarly to the previous process, the first law of thermodynamics and the equation that relates the internal energy with temperature are applied:

$$\Delta U = \frac{3}{2} \cdot n \cdot R \cdot (T_L - T_H) \tag{8.36}$$

$$dQ = dU + 0 \tag{8.37}$$

$$W_{2-3} = 0 \tag{8.38}$$

Therefore, the work performed in this phase is zero, whereas the internal energy variation is equal to the heat variation.

$$Q_{2-3} = \frac{3}{2} \cdot n \cdot R \cdot (T_L - T_H) \tag{8.39}$$

The previous equation can also be expressed as:

$$Q_{2-3} = n \cdot c_v \cdot (T_L - T_H) \tag{8.40}$$

8.3.2.2 Phase 3-4

This phase is characterized by an isothermal compression at temperature T_L. Therefore, as the temperature is constant, the variation in the internal energy of the system is zero and the work variation is equal to the heat variation.

$$U_{3-4} = 0 \tag{8.41}$$

$$W_{3-4} = Q_{3-4} < 0 \tag{8.42}$$

$$Q_{3-4} = n \cdot R \cdot T_L \cdot ln\left(\frac{V_3}{V_4}\right) \tag{8.43}$$

8.3.2.3 Phase 4-1

Similarly to the phase 2-3, this phase is isochoric and happens at constant volume with gas from the cold sink to the hot source. Both pistons move toward the left to maintain the volume of gas constant, while the temperature and the pressure increases.

$$W_{4-1} = 0 \tag{8.44}$$

$$dQ = dU + 0 \tag{8.45}$$

$$Q_{4-1} = \frac{3}{2} \cdot n \cdot R \cdot (T_H - T_L) \tag{8.46}$$

$$\tag{8.47}$$

The previous equation can also be expressed as:

$$Q_{4-1} = n \cdot c_v \cdot (T_H - T_L) \tag{8.48}$$

8.3.2.4 Stirling cycle efficiency

The efficiency of the stirling cycle, considering 100% efficiency for the regenerator, is equal to the between the total work done by the system divided by the heat supplied to the system.

$$\eta = \frac{W_{1-2} + W_{3-4}}{W_{1-2}} = \frac{Q_{1-2} + Q_{3-4}}{Q_{1-2}} = \frac{n \cdot R \cdot T_H \cdot ln\left(\frac{V_2}{V_1}\right) + n \cdot R \cdot T_L \cdot ln\left(\frac{V_3}{V_4}\right)}{n \cdot R \cdot T_H \cdot ln\left(\frac{V_2}{V_1}\right)} \tag{8.49}$$

$$\eta = 1 - \frac{T_L}{T_H} \tag{8.50}$$

$$\frac{V_3}{V_4} = \frac{V_2}{V_1} \tag{8.51}$$

If the regenerator efficiency is not 100%, then the efficiency of the cycle is equal to:

$$\eta = \frac{n \cdot R \cdot T_H \cdot ln\left(\frac{V_2}{V_1}\right) + n \cdot R \cdot T_L \cdot ln\left(\frac{V_3}{V_4}\right)}{n \cdot R \cdot T_H \cdot ln\left(\frac{V_2}{V_1}\right) + (1-\epsilon) \cdot \frac{3}{2} \cdot n \cdot R \cdot (T_H - T_L)} \tag{8.52}$$

$$\eta = \frac{(T_H - T_L) \cdot ln\left(\frac{V_2}{V_1}\right)}{T_H \cdot ln\left(\frac{V_2}{V_1}\right) + (1-\epsilon) \cdot \frac{3}{2} \cdot (T_H - T_L)} \tag{8.53}$$

where ϵ is the regenerator efficiency and η is the efficiency of the stirling cycle.

Therefore, for an ideal stirling engine with $\epsilon = 1$, the efficiency is equal to the Carnot cycle.

8.3.2.5 Practical example

Considering that the temperature of the hot source from the stirling engine is around 600 K and the cold source is 150 K and the regenerator efficiency is 100 %, the stirling engine efficiency would be given by:

$$\eta = 1 - \frac{150\ K}{600\ K} = 0.75 \tag{8.54}$$

8.4 Electric heater based on Eddy currents

8.4.1 Introduction to Eddy currents

The heating occurs without physical contact between the inductors and the induced parts. The induced parts are ferromagnetic elements that are being heated. Additionally, the main characteristic of this electric heating process is the high efficiency transfer without loss of heat from the inductor to the induced element.

The depth of penetration of the generated currents in the induced ferrous metallic elements is directly correlated to the working frequency of the generator used, the higher the frequency, the greater the induced currents concentration on the surface will be. In this case, the heating homogeneity on a relevant mass, can be obtained by thermal conduction which allows the heating of the ferrous metallic elements.

The magnetic induction is based upon the following physical principles:

- Firstly, the energy transfer from the inductor's coils to the ferromagnetic element occurs by means of electromagnetic fields.
- Secondly, the conversion of the electric energy into heat in the ferromagnetic elements happens by the Joule effect, according to the equation:

$$P = I^2 \cdot R \tag{8.55}$$

  where, R is the equivalent electric resistance of the induced metallic part and I the equivalent electric current on the induced metallic part.
- Thirdly, the transmission of the heat inside the induced metallic part is carried out by thermal convection to the working gas, which after reaching the adequate temperature is expanded in the nozzle.

8.4.2 Generation of an electromagnetic field by an electric current along a coil

The electromagnetic field created by a current moving along an electric single loop conductor responds to the physical principle described by the Biot and Savart's Law.

The magnetic field, dB, created by a current, I, in a closed loop coil is defined by the next equation:

$$d\boldsymbol{B} = \frac{\mu_0 I}{4\pi} \cdot \frac{\boldsymbol{u_t} \times \boldsymbol{u_r}}{r^2} dl \tag{8.56}$$

where, $\mu_0 = 4\pi \cdot 10^{-7}\ Tm/A$, $\boldsymbol{u_t}$ and $\boldsymbol{u_r}$ are orthogonal vectors.

$d\boldsymbol{B}$ can be decomposed into:

- Along the closed loop coil, z axis:

$$dB \cdot cos(90 - \theta) \tag{8.57}$$

- Perpendicular to the z axis:

$$dB \cdot sin(90 - \theta) \tag{8.58}$$

By symmetry, the perpendicular components to the z axis are opposite elements and consequently they cancel each other. The final resulting vector is that along the z axis and it corresponds to the summation or contributions of each element: $dB \cdot cos(90 - \theta)$

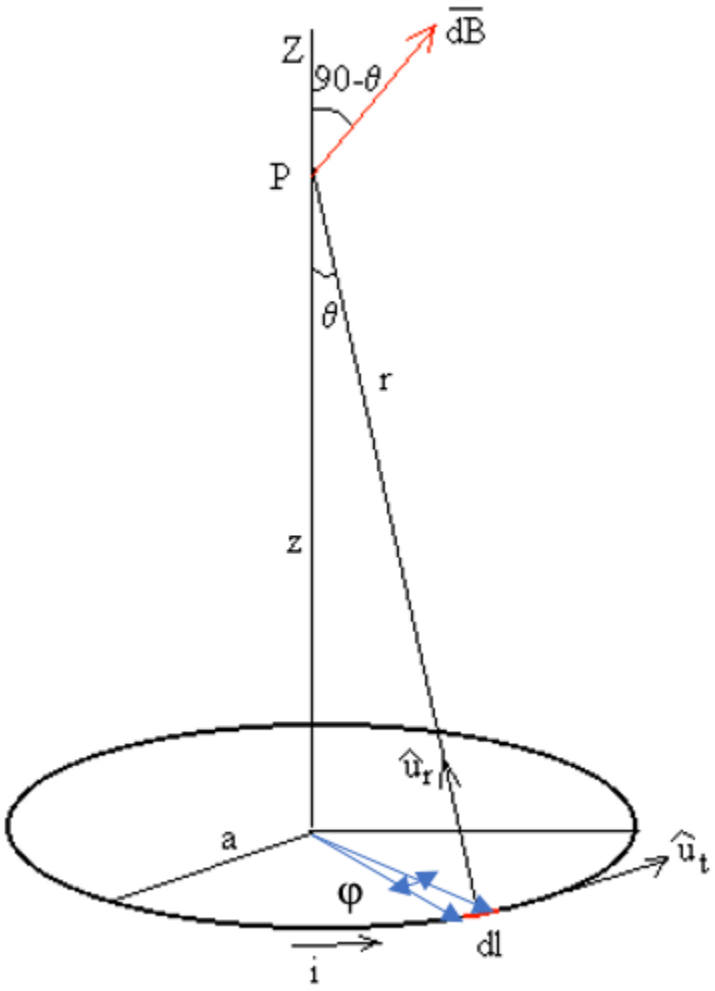

Figure 8.5: Magnetic field representation. Source: [2].

Considering a point, p, where r is constant and θ is also constant. Thus, by the Laplace Law:

$$B = \int dB \cdot cos(90 - \theta) = \frac{\mu_0 I}{4\pi r^2} \oint \sin(\theta) dl = \frac{\mu_0 I}{4\pi r^2} \int_0^{2\pi} \sin(\theta) a d\phi \tag{8.59}$$

$$\sin(\theta) = \frac{a}{\sqrt{a^2 + z^2}} \tag{8.60}$$

$$B = \frac{\mu_0 I a^2}{2\left(a^2 + z^2\right)^{\frac{3}{2}}} \tag{8.61}$$

This means that at the origin, with z=0 (centre of the coil), the value of the magnetic field is:

$$B = \frac{\mu_0 I}{2a} \tag{8.62}$$

An example of the evolution of the magnetic field with the distance to centre of the loop is graphically by Figure (8.7).

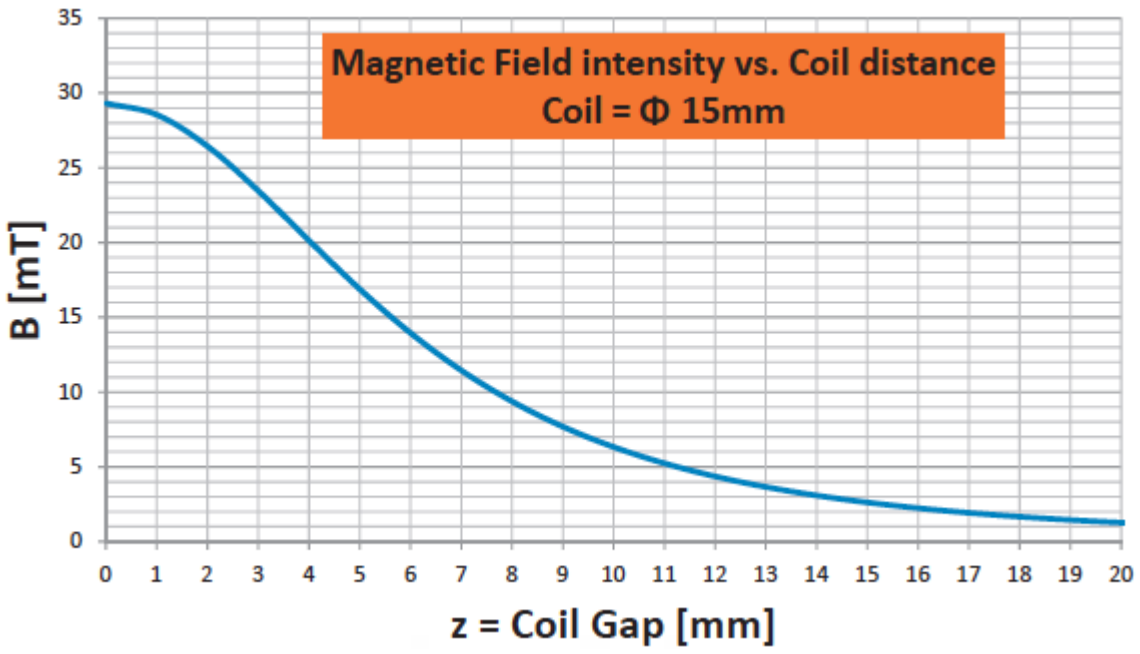

Figure 8.6: Magnetic field as a function of the distance to the centre of the loop. Source: [3]

Hence, it is important to apply the coil as near as possible to the metallic part, in order to be heated. In general, it is assumed that the magnetic field created by a solenoid with "N" loops and length "l" is:

$$B = \mu_0 \frac{NI}{l} \tag{8.63}$$

An alternating electric current, I, along the coil means a movement of electric charges with the frequency of the generator, they are typically electrons who interact with the free electrons in the metallic part to be induced.

In fact, each electron along the coil, moving forward and backward to the frequency of the generator, generates an electric field which interact with the free electrons in the metallic part to be induced, what provokes the movement of those electrons in the metallic part.

Therefore, the combination of this alternating field electric with the above magnetic field constitutes the known electromagnetic field. Under this hypothesis, the magnetic field is alternating and fluctuates according to the frequency of the generator.

8.4.2.1 Induced electromotive force generated on the heating element

According to the Faraday – Lenz's Law, the induced electromotive force generated on a solenoid, or a closed loop coil, metallic part to be heated, is negatively proportional to the rate of variation of the electromagnetic flux across the section of the coil.

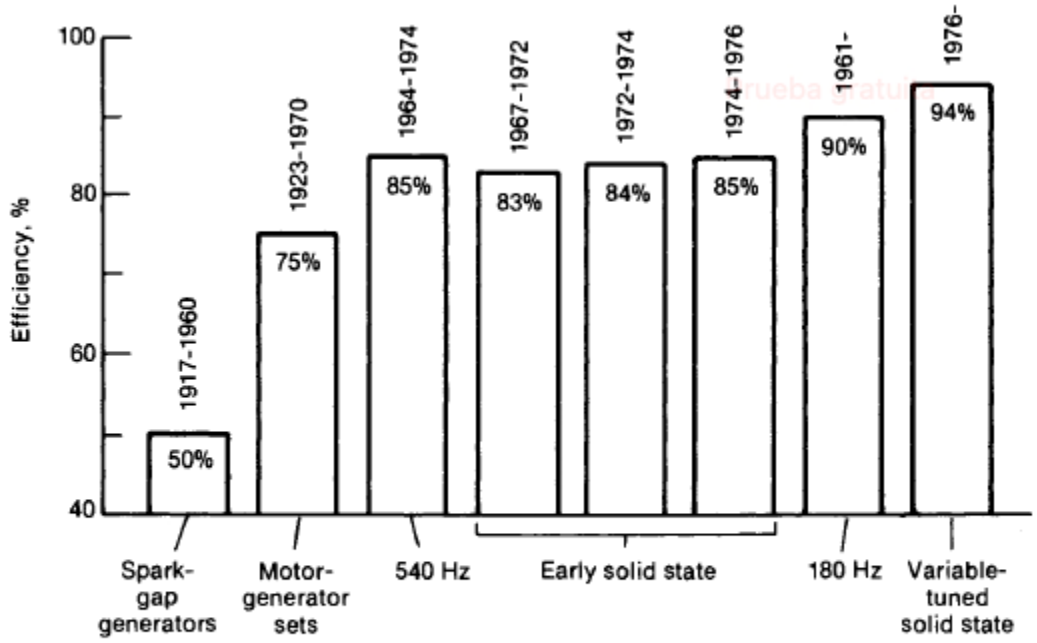

Conversion efficiency of induction heating power supplies (from R. W. Sundeen, *Proceedings, 39th Electric Furnace Conference*, Houston, TX, AIME, New York, 1982, p. 8)

Figure 8.7: Evolution of the efficiency as a function of the frequency of the current for different technologies. Source: R.W. Sundeen.

Eddy currents or Foucault currents are currents induced in conductors, opposing the change in flux that generated them. It is caused when a conductor is exposed to a changing magnetic field. The induced voltage is the following in a case of one loop or planar metallic part.

$$\epsilon(V) = -\frac{d\phi}{dt} \tag{8.64}$$

These circulating eddy currents create induced magnetic fields that oppose to the change of the original magnetic field due to Lenz' laws, causing repulsive or drag forces between the conductor and the magnet.

The stronger the applied magnetic field, or the greater the electrical conductivity of the conductor, or the faster, frequency, the field that the conductor is exposed to changes, then the greater the currents that are developed.

The magnetic permeability of a material is the capability of this material to channel magnetic induction.

In addition, the magnetic field H and the magnetic induction field B are linked, for a given material, by the equation :

$$B = \mu \cdot H \tag{8.65}$$

where μ is the magnetic permeability of the material (in Henry/meter or Tesla), $\mu = \mu_0 \cdot \mu_r$. μ_r depends on the material to be heated:

- For diamagnetic materials (copper, gold, silver, aluminium oxide) : $\mu_r \leq 1$
- For paramagnetic materials (aluminium, titanium, molybdenum, stainless steel): $\mu_r \geq 1$
- For ferromagnetic materials (carbon steel): $\mu_r \gg 1$

8.4.2.2 Skin effect on parts to be heated

The AC current on a workpiece decreases exponentially from the surface of the material to the inner because the Foucault currents on the workpiece oppose to the magnetic field from the currents on the inductor coil. This can be expressed by the following equations:

$$I = I_0 \cdot e^{-\frac{d}{\delta}} \tag{8.66}$$

where, δ is the skin depth, which can be calculated by:

$$\delta = \sqrt{\frac{2\rho}{\omega \cdot \mu}} \tag{8.67}$$

With,

- ρ is the resistivity of the workpiece.
- $\omega = 2\pi f$
- μ is the magnetic permeability of the material.

Therefore,

$$\delta = \sqrt{\frac{\rho}{\pi f \mu}} = \frac{1}{\sqrt{\pi f \mu \sigma}} \tag{8.68}$$

where, σ is the conductivity of the workpiece.

The skin depth and the distribution of the magnetic field depends on the electromagnetic characteristics of each material. The following figure compares the effects of the electromagnetic field distribution in the material between high values of electromagnetic parameters and low value of electromagnetic parameters.

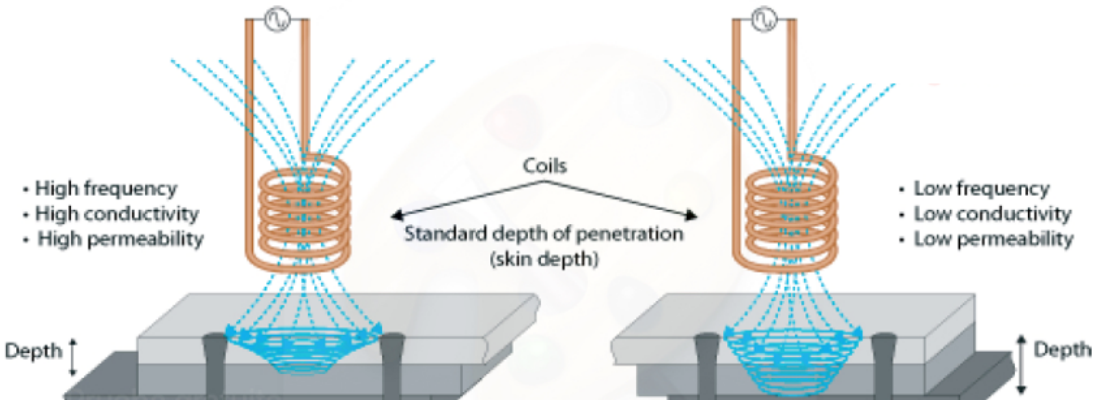

Figure 8.8: Electromagnetic field distribution for two different scenarios. Source: [3].

Skin Depth [mm]

Frequecy [Hz]	Steel AISI 316 (μ_r=1)	Copper Cu (μ_r~1)	Steel AISI 420 (μ_r=2000)
100	43,32	6,68	0,83
1.000	13,70	2,11	0,26
10.000	4,33	0,67	0,08
100.000	1,37	0,21	0,026
200.000	0,97	0,15	0,019
1.000.000	0,43	0,067	0,008

Figure 8.9: Skin depth values for different materials. Source: [3].

The better the electric conductivity and the high magnetic permeability properties of a given material, the lower is the skin depth. In these cases, the electric current will flow nearest to the surface of the material.

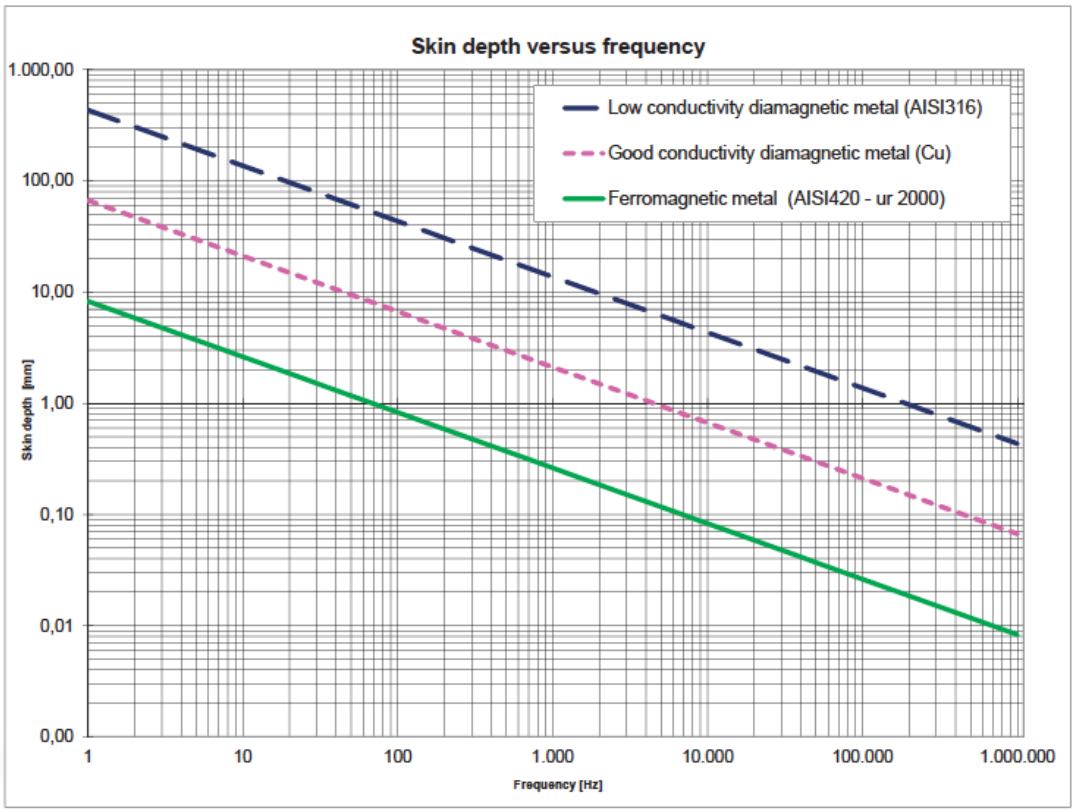

Figure 8.10: Skin depth as a function of frequency for diamagnetic, paramagnetic and ferromagnetic materials. Source: [3].

8.4.2.3 Example of inductive power calculated by using graphics

It is important to consider the energy absorption rates for several materials to evaluate as a first approach the electric power necessary for heating a workpiece.

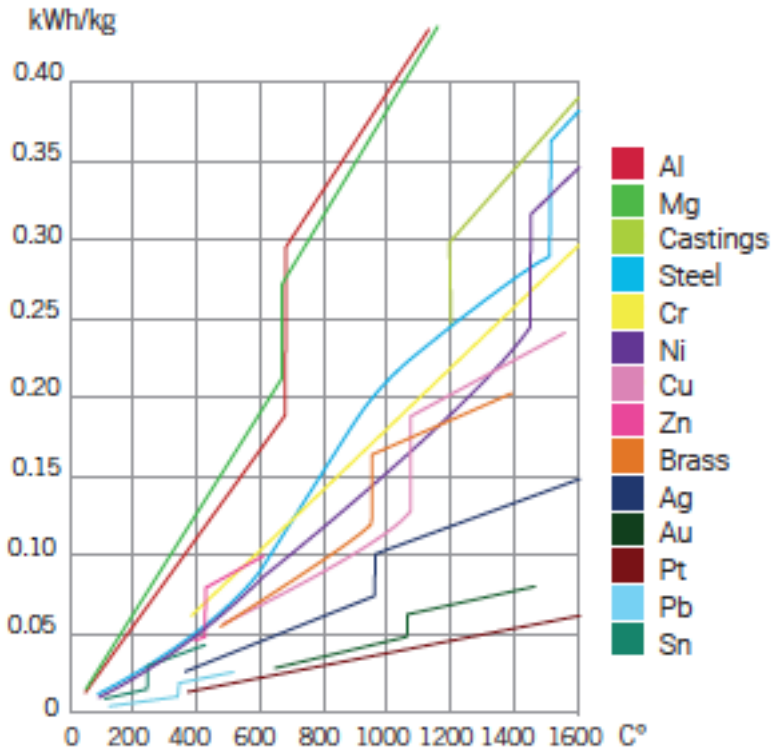

Figure 8.11: Energy absorption rate for different materials as a function of temperature. Source: ENRX, Induction Heating Applications.

The following Table (8.12) shows typical induction heater efficiency levels for a set of materials. The values assume the use of enveloping multi-turn coils.

Material	Final temp.°C	Efficiency
Carbon steel	1250	0.65
Carbon steel	700	0.80
Stainless steel	1250	0.60
Brass	800	0.50
Copper	900	0.40
Aluminum	500	0.40

Figure 8.12: Table containing efficiency by Eddy heating for different materials. Source: ENRX, Induction Heating Applications.

Considering a steel component to be heated to 1473 K from 293 K and it has a mass of 0.5 kg and the time to heat the piece is 60 seconds, then by looking at the tables:

- Energy absorption rate: 0.25 kWh/kg.
- Electric heating efficiency: approximately 0.7.

Therefore,

$$P_{absorption} = \frac{0.25 \cdot 0.5 \cdot 3600}{60} = 7.5kW \tag{8.69}$$

$$P_{generator} = \frac{7.5}{0.7} = 10.7kW \tag{8.70}$$

8.4.2.4 Conclusions about Foucault current heaters for aerospace propulsion

An essential requirement is to heat the hydrogen to temperatures greater than 1500 K, in order to achieve an adequate specific impulse and high exit velocity at the nozzle.

Nevertheless, electromagnetic constraints and other thermal and mechanical properties, set limitations to heat the hydrogen gas at temperatures beyond 1500 K.

Nevertheless, the use of special alloys would let to reach temperature as high as 2500 K what offers a vast study in the field of materials technology.

Heating the hydrogen gas to temperatures as high as 2500 K depends essentially on the metallic materials to construct the hydrogen chambers, as currently many heaters by Foucault currents can be cooled with a refrigerant to avoid damages in the inductors.

Chapter 9

Main propulsion elements

The objective of this chapter is to provide an introduction to several important parameters necessary to define the main rocket propulsion systems and relate these new parameters with the Delta-V obtained in the chapters related with orbital mechanics. At the end, an approximation of the amount of fuel needed, based on the transfer time from Earth to Mars, will be provided.

In order to simplify the calculations, a set of hypothesis regarding the ideal rocket engine will be employed:

- The rocket engine is in a fix test bench at sea level, therefore the variation in velocity is assumed constant.
- Constant mass flow through the nozzle.
- The convergent-divergent nozzle is adapted, therefore the pressure at the exit is equal to the atmospheric pressure at sea level.
- The working fluid, hydrogen, is assumed as an ideal gas. The state equation is employed.
- No heat losses, the walls are considered adiabatic.
- Shock waves are not considered as well as any other effect associated with viscosity is neglected (no friction with the walls).
- The working fluid is irrotational, adiabati, reversible (isentropic) and steady.
- Unidimensional flow.

9.1 Thrust generation

As seen before, the hydrogen gas is stored in an intermediate tank where it is heated by using eddy currents. This temporal storage tank must contain a set of ferromagnetic plates in order to heat the hydrogen by using magnetic fields. Once the hydrogen reaches the adequate temperature, the valve opens and the working fluid expands through the nozzle to the outer space.

As it can be seen, this propulsion system is similar to a pulse-jet, in the sense that both are not continuous thrust generation systems. However, the difference with a pulse-jet is that with orbital

mechanics it is possible to have an estimate of the exact amount of fuel needed to perform a certain maneuver. Therefore, the amount of hydrogen gas in this intermediate tank can be the exact quantity needed to perform the desired maneuver. For example, during the departure from Earth sphere of influence the tank contains the necessary amount of hydrogen for departure and once the vehicle reaches the Mars orbit, the tank is filled with the hydrogen needed for the arrival hyperbola.

The thrust generation can be explained as a reaction force produced due to a change in momentum as a result of the expelled gas through the nozzle to the exterior. In other words, this leads to the following equation:

$$Thrust = \frac{d(m \cdot V_{exit}}{dt}) = V_{exit} \cdot \dot{m} \tag{9.1}$$

As the exit velocity is assumed constant and the mass flow is also constant, the thrust generation for an ideal rocket engine is constant. However, thrust generation is also affected by the pressure at the exit of the nozzle and the outer pressure. The previous equation is considered for an adapted nozzle, where both pressures are equal.

To properly define the value of thrust, it is necessary to use the momentum conservation equation with the continuity equation.

9.1.1 The continuity equation

The first step to obtain the mass conservation equation, it is to apply the Reynolds transport theorem. This theorem relates the variation in any flow property inside a Lagrangian control volume with the variation of the same property in a Eulerian control volume at a given instant that coincides with the Lagrangian control volume. This statement can be summarized with the following equation:

$$\frac{d}{dt}\int_{V_f} \phi(x,t)\ dV = \frac{d}{dt}\int_{V_c} \phi(x,t)\ dV + \int_{S_c} \phi(x,t) \cdot (\boldsymbol{U} - \boldsymbol{U_c}) \cdot \boldsymbol{n}\ dS \tag{9.2}$$

where, the volume integrals are denoted by V and the surface integral is denoted by an S. Additionally, the left hand side of the equation refers to the Lagrangian framework whereas the right term to the Eulerian frame.

The next step is to substitute the undefined variable ϕ with the density ρ, which is an intensive variable.

$$\frac{d}{dt}\int_{V_f} \rho(x,t)\ dV = \frac{d}{dt}\int_{V_c} \rho(x,t)\ dV + \int_{S_c} \rho(x,t) \cdot (\boldsymbol{U} - \boldsymbol{U_c}) \cdot \boldsymbol{n}\ dS \tag{9.3}$$

For any Lagrarian control volume, mass is always conserved:

$$\frac{d}{dt}\int_{V_f} \rho(x,t)\ dV = 0 \tag{9.4}$$

Therefore, with the use of the Reynolds theorem and considering that a given time instant the Eulerian control volume is equal to the Lagrange control volume, it is possible to state that:

$$\frac{d}{dt}\int_{V_c} \rho(x,t)\ dV + \int_{S_c} \rho(x,t) \cdot (\boldsymbol{U} - \boldsymbol{U_c}) \cdot \boldsymbol{n}\ dS = 0 \tag{9.5}$$

Equation (9.5) is known as the mass conservation or continuity equation. Applying it to the following control volume, Figure (9.1) and assuming uni-dimensional flow:

$$\frac{d}{dt}\int_{V_f} \rho \, dV + \frac{d}{dt}\int_{V_p} \rho \, dV + \int_{S_{exit}} \rho \cdot U_{exit} \, dV = 0 \tag{9.6}$$

where, U is referred to the velocity, V_p is the volume of propellant that moves through the nozzle (hydrogen) and V_f is the fixed volume. The previous equation can be developed into:

$$\frac{dM_f}{dt} + \frac{dM_p}{dt} + \int_{S_{exit}} \rho \cdot U_{exit} \, dV = 0 \tag{9.7}$$

where, M_f is the fixed mass and M_p is the propellant mass.

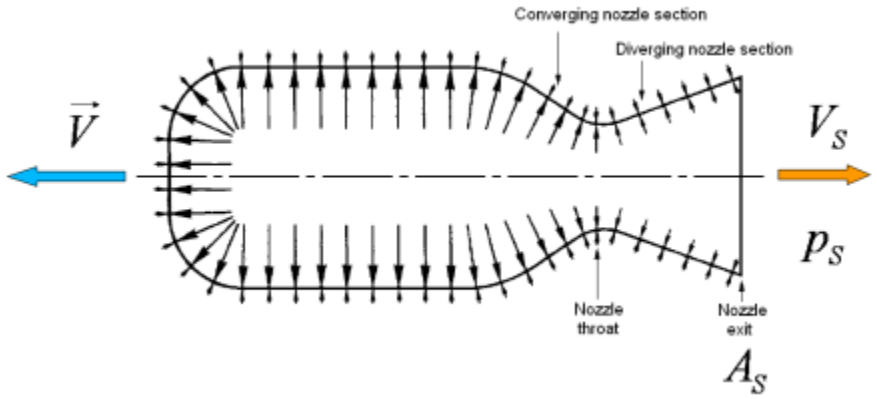

Figure 9.1: Eulerian control volume of a convergent-divergent nozzle. Source: Rocket propulsion elements, Sutton.

9.1.2 Conservation equation

Similarly to the mass conservation equation, the Reynolds transport theorem is employed but now ϕ is substituted by $\rho \cdot U$. Additionally, the second Newton law is employed and unidimensional flow is assumed:

$$\frac{d}{dt}\int_{V} \rho \cdot U \, dV + \int_{S} \rho \cdot U_{exit}(U + U_{exit}) \, dS = \sum F_v \tag{9.8}$$

where, F_v are the forces acting over the Eulerian control volume.

Expanding the surface and volume integrals:

$$\frac{d}{dt}\int_{V_f} \rho \cdot U \, dV + \frac{d}{dt}\int_{V_p} \rho \cdot (U + U_R) \, dV + U\int_{S_{exit}} \rho \cdot U_{exit} \, dS + \int_{S_{exit}} \rho \cdot U_{exit}^2 \, dS = \sum F_v \tag{9.9}$$

where, U_R is the relative velocity of the propellant with respect to the vehicle.

In the initial hypothesis of the ideal rocket engine, it is assumed that U is constant. Therefore, the previous equation can be expressed as:

$$\begin{aligned} &U\frac{d}{dt}\int_{V_f} \rho \, dV + \frac{dU}{dt}\int_{V_f} \rho \, dV + \frac{d}{dt}\int_{V_p} \rho \cdot U_R \, dV + U\frac{d}{dt}\int_{V_p} \rho \, dV + \frac{dU}{dt}\int_{V_p} \rho \, dV \\ &+ U\int_{S_{exit}} \rho \cdot U_{exit} \, dS + \int_{S_{exit}} \rho \cdot U_{exit}^2 \, dS = \sum F_v \end{aligned} \tag{9.10}$$

This equation can be further simplified, by considering that $U_R << 1$ and by using the fixed and propellant masses and the continuity equation:

$$U\left(\frac{dM_f}{dt}+\frac{dM_p}{dt}+\int_{S_{exit}}\rho\cdot U_{exit}\ dS\right)+\frac{dU}{dt}\cdot M+\int_{S_{exit}}\rho\cdot U_{exit}^2\ dS=\sum F_v \tag{9.11}$$

$$\frac{dU}{dt}\cdot M+\int_{S_{exit}}\rho\cdot U_{exit}^2\ dS=\sum F_v=F_a+F_g+F-\int_{S_{exit}}(P_S-P_{amb})\,dS \tag{9.12}$$

where,

- $M=M_f+M_p$
- F_a, is the aerodynamic force.
- F_g, gravitational force.
- P_S is the pressure at the exit of the nozzle and P_{amb} is the ambient pressure.

As the engine is assumed to be in a test bench at seal level, the previous equation can be simplified by:

- $\frac{dU}{dt}=0$
- $F_a=0$
- $F_g=0$

Finally, thrust can be defined as:

$$Thrust=T=F=\int_{S_{exit}}\rho\cdot U_{exit}^2\ dS+\int_{S_{exit}}(P_S-P_{amb})\,dS \tag{9.13}$$

It can also be expressed as a function of the mass flow, the exit velocity, the exit area of the nozzle and the variation in pressures:

$$T=\dot{m}\cdot U_{exit}+(P_S-P_{amb})\cdot A_{exit} \tag{9.14}$$

For an adapted nozzle, the previous equation becomes:

$$T=\dot{m}\cdot U_{exit} \tag{9.15}$$

9.2 Specific impulse

The specific impulse, I_{sp}, is a performance parameter that is directly related with the specific fuel consumption. It is defined as the thrust force per mass flow of propellant for a time interval and it is commonly expressed in seconds by dividing it with the Earth's gravitational force, $g_0=9.8m/s^2$.

$$I_{sp}=\frac{\int_0^t\ T\ dt}{g_0\cdot\int_0^t\ \dot{m}\ dt} \tag{9.16}$$

As seen before, the thrust generation and the mass flow rate for an ideal rocket engine are constant. Therefore, the previous equation becomes:

$$I_{sp} = \frac{T}{g_0 \cdot \dot{m}} \tag{9.17}$$

The specific fuel consumption or TSFC (thrust specific fuel consumption) is defined as the fuel mass flow rate, in this case the hydrogen mass flow rate, divided by the net thrust. Introducing this definition into the previous definition of specific impulse:

$$I_{sp} = \frac{1}{g_0 \cdot TSFC} \tag{9.18}$$

Therefore, the specific impulse is inversely proportional to the specific fuel consumption. This explains why it is desired to achieve large specific impulses in rocket engines. However, a high specific impulse, such as in ionic propulsion engines, does not always means a large thrust output from the engine. This statement can be visualized in Figure (9.2).

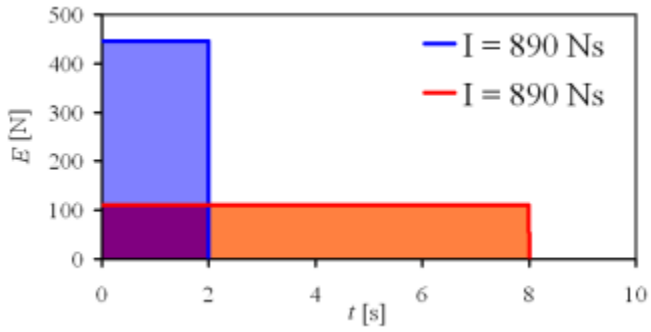

Figure 9.2: Example of two rocket engines with the same specific impulse but different values of thrust. Source: UPV, Motores cohete.

9.2.1 Exhaust velocity

Neither equation (9.17) nor equation (9.18) include directly the effect that temperature, pressure and molecular weight have on the specific impulse. Specifically, it is the effect of the molecular weight of the working propellant that sets one of the main advantages of thermonuclear propulsion with respect to the conventional chemical rocket engines and explains why hydrogen is chosen as the propellant.

In order to obtain the specific impulse as a function of the aforementioned variables, it is needed to find the relation between specific impulse and exhaust velocity. By using equation (9.17) and substituting the thrust force, T, by its definition for an adapted nozzle:

$$I_{sp} = \frac{V_{exit}}{g_0} \tag{9.19}$$

The next step is to find the isentropic flow equations, for which the second law of thermodynamics and a set of expressions defined in chapter 8 are going to be employed.

$$dS = \frac{dQ}{T} \tag{9.20}$$

$$\gamma = \frac{C_p}{C_v} \tag{9.21}$$

$$R = C_p - C_v \tag{9.22}$$

Defining the internal energy of a system and its enthalpy:

$$dE = dQ - dW = TdS - dW \tag{9.23}$$

$$dH = dE + d(PV) = dE + PdV + VdP \tag{9.24}$$

where, H is the enthalpy and E the internal energy of the system.

Expressing the heat of the system as a function of the enthalpy:

$$dQ = dH - VdP \tag{9.25}$$

Now, defining the heat of the system for two scenarios:

$$dQ = dH = C_p \cdot dT \quad \text{For constant pressure} \tag{9.26}$$

$$dQ = dE = C_v \cdot dT \quad \text{For constant volume} \tag{9.27}$$

Applying equation (9.26) in equation (9.25) and applying equation (9.27) in (9.25):

$$dQ = C_v dT + RT\frac{dV}{V} \tag{9.28}$$

$$dQ = C_p dT - RT\frac{dP}{P} \tag{9.29}$$

Using the definition of entropy in the previous equations:

$$dS = C_v\frac{dT}{T} + R\frac{dV}{V} \tag{9.30}$$

$$dS = C_p\frac{dT}{T} + R\frac{dP}{P} \tag{9.31}$$

Considering an isentropic process and using equation (9.31):

$$0 = C_p\frac{dT}{T} + R\frac{dP}{P} \tag{9.32}$$

Applying the equation of state:

$$\frac{C_p}{R}d\left(\frac{P}{\rho}\right) = \frac{dP}{\rho} \tag{9.33}$$

$$\frac{C_p}{R}\left[\frac{dP}{\rho} - \frac{P}{\rho^2}d\rho\right] = \frac{dP}{\rho} \tag{9.34}$$

$$\frac{dP}{P} = \gamma\frac{d\rho}{\rho} \tag{9.35}$$

Integrating the last equation, where the total conditions of pressure and density are used as the constants of integration.

$$\frac{P}{P_t} = \left(\frac{\rho}{\rho_t}\right)^{\gamma} \tag{9.36}$$

where, P_t is the total pressure and ρ_t is the total density. The term total means that the thermodynamic variable is taking into account both the static and the dynamic terms. For instance, the total pressure is equal to the sum of the dynamic pressure (associated with the movement of flow particles) and the static pressure.

By using the equation of state, the previous equation can also be expressed as:

$$\frac{P}{P_t} = \left(\frac{T}{T_t}\right)^{\frac{\gamma}{\gamma-1}} \tag{9.37}$$

where, T_t is the total temperature.

From this point on, it is convenient to move from this definition of enthalpy: H, to this other definition: h. The difference is that h is the specific enthalpy. The advantage of working with specific variables is that some important parameters can be obtained in their dimensionless form which later can be used to perform a parametric study. As the specific form of enthalpy is used, the heat capacities, C_p and C_v, must also be used in their specific form: c_p and c_v.

Defining the specific total enthalpy, h_t, and making use of the previously obtained equations:

$$h_t = h + \frac{U^2}{2} \tag{9.38}$$

$$U = M \cdot a \tag{9.39}$$

$$c_p T_t = c_p T + \frac{M^2 \cdot (\gamma \cdot R \cdot T)}{2} \tag{9.40}$$

where, M is the mach number and a is the speed of sound, $a = \sqrt{\gamma \cdot R \cdot T}$.

Dividing the last equation by c_p and using the definition of R and γ:

$$T_t = T\left(1 + \frac{\gamma - 1}{2} M^2\right) \tag{9.41}$$

The previous equation relates the total and static temperatures by using the Mach number and the specific heat capacity ratio. This equation can also be used for other variables such as the pressure:

$$P_t = P\left(1 + \frac{\gamma - 1}{2} M^2\right)^{\frac{\gamma}{\gamma-1}} \tag{9.42}$$

Going back to the hypothesis of the ideal rocket engine, it is assumed isentropic flow and therefore, the previous equation can be used. Additionally, the mass flow is constant, which means that:

$$\dot{m} = \rho \cdot U \cdot A = cte \tag{9.43}$$

where, A is the area.

Defining again the total enthalpy and substituting:

$$c_p T_t = c_p T + \frac{V^2}{2} \tag{9.44}$$

$$1 = \frac{T}{T_t} + \frac{V^2}{2c_p T_t} \tag{9.45}$$

$$V^2 = \left(1 - \frac{T}{T_t}\right) 2\frac{\gamma}{\gamma - 1} R T_t \tag{9.46}$$

Using equation (9.37) and particularizing for the nozzle outlet:

$$V_{exhaust} = \sqrt{\left(1 - \left(\frac{P_{amb}}{P_{i_t}}\right)^{\frac{\gamma-1}{\gamma}}\right) \frac{2\gamma}{\gamma - 1} R T_{i_t}} \tag{9.47}$$

where, T_{i_t} and P_{i_t} are the total temperature and pressure respectively at the nozzle inlet.

Including the molecular weight in the previous equation:

$$V_{exhaust} = \sqrt{\left(1 - \left(\frac{P_{amb}}{P_{i_t}}\right)^{\frac{\gamma-1}{\gamma}}\right) \frac{2\gamma}{\gamma - 1} \frac{R_u}{PM} T_{i_t}} \tag{9.48}$$

where, $R_u = 8.314\ J/(mol \cdot K)$ is the ideal gas constant and PM is the molecular weight.

Therefore, the specific impulse for an adapted nozzle is inversely proportional to the square root of the molecular weight and directly proportional to the square root of the temperature at nozzle inlet. This explains why a low molecular weight for the working fluid is desired.

$$I_{sp} \propto \frac{\sqrt{T_{i_t}}}{\sqrt{PM}} \tag{9.49}$$

9.3 Delta-V

The relation between the required Delta-V to perform any maneuver and the specific impulse is given by the Tsiolkowsky equation:

$$\Delta V = I_{sp} ln\left(\frac{M_0}{M_f}\right) \tag{9.50}$$

where, M_0 is the initial mass of the vehicle and M_f is the final mass.

The previous equation can be also expressed as:

$$\Delta V = -I_{sp} ln\left(\frac{M_0 + \Delta M}{M_0}\right) \tag{9.51}$$

$$\frac{\Delta M}{M_0} = \Delta m = 1 - e^{-\frac{\Delta V}{I_{sp}}} \tag{9.52}$$

where, $\Delta M = M_0 - M_f$ and $\Delta m = \frac{\Delta M}{M_0}$.

9.4 Conclusions

For this final section, a set of conclusions will be presented, ranging from the main parameters and their evolution as a function of different variables that affect propulsive systems, the environmental effects associated with thermonuclear propulsion based on a stirling cycle, the costs associated with this propulsion system, and lastly a practical case where the results obtained in the orbital mechanics sections are employed.

9.4.1 Propulsive parameters

It can be concluded that an ideal propulsion system would be the one that produces both large thrust output and high specific impulse. Ionic propulsion systems are capable of achieving large specific impulses but at the cost of low thrust output. Due to this reason, it is not possible to use these systems for launch vehicles as the thrust-weight ratio is very small. However, they can be used once in a parking orbit for minor corrections or in deep space exploration.

Another alternative are the chemical propulsion engines, they are characterized by a large thrust output but a low specific impulse. The highest specific impulse with chemical propulsion has been achieved with a LOX-LH2 combustion engine, and it was approximately 450 seconds. These propulsion systems can be used for launch vehicles due to their large thrust-weight ratio, but for deep space exploration they are limited by their specific impulse and could only be used for low Delta-V maneuvers.

Therefore, there is the need of an alternative propulsion system capable of achieving both high specific impulse and large thrust output. Nuclear propulsion systems are capable of achieving this feat, specifically thermonuclear propulsion. Similarly to a combustion engine, the working fluid is heated to high temperatures and then it exists through the nozzle. The main difference is in the chemical composition of the working fluid, the oxidizer is not needed, so the propellant could just be diatomic hydrogen, which has a molecular weight of $2 \cdot 10^{-3} Kg/mol$.

As seen before the specific impulse is inversely proportional to the square root of molecular weight, so by using hydrogen gas as the working fluid the specific impulse can be greatly improved in contrast with chemical rocket engines, which have a larger molecular weight.

Additionally, from figure (9.3) it can be seen that for a temperature as low as 1000 K it is already possible to surpass the specific impulse in chemical engines. Whereas for the thrust generated, Figure (9.4), is in the order of magnitude of around 10^5 N.

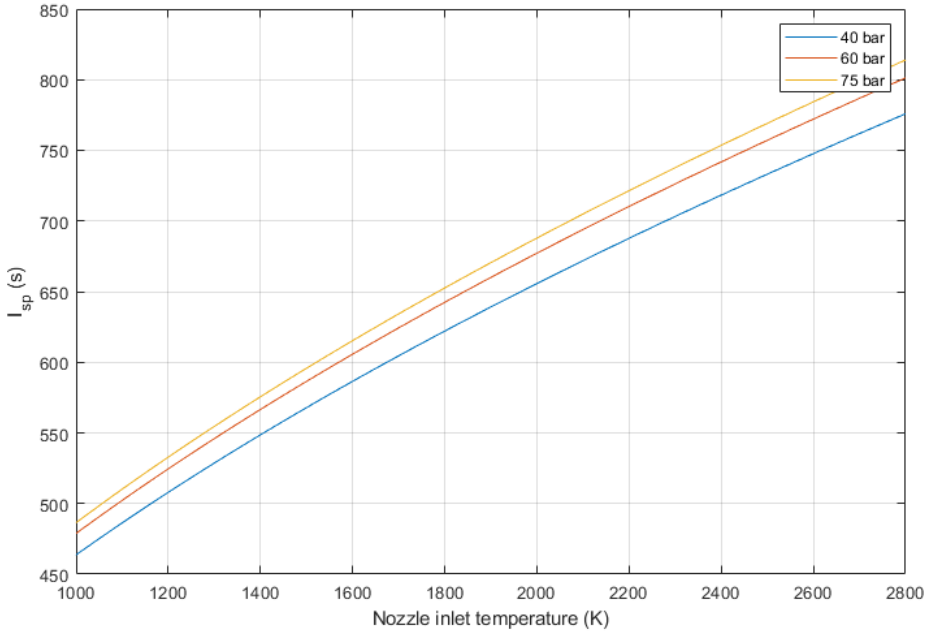

Figure 9.3: Specific impulse as a function of the total temperature at the nozzle inlet for different total pressures.

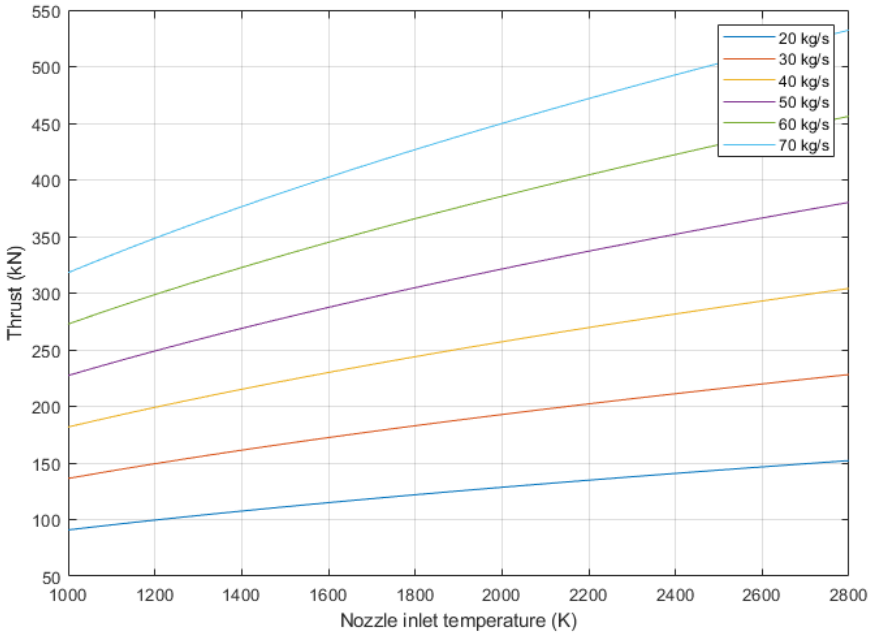

Figure 9.4: Thrust in kN as a function of the total temperature at the nozzle inlet for different mass flows and for a total pressure of 40 bar.

In conclusion, there exit different ways of increasing the specific impulse:

- Increasing the temperature of the working fluid. However, the maximum temperature it is going to be limited by materials and cooling technologies.
- Working with low molecular weight fluids. In this case, hydrogen is an alternative.
- Increasing the total pressure at the nozzle inlet. However, the increase in specific impulse becomes asymptotic as pressure increases. Additionally, there could be large pressure gradients that lead to the appearance of shock waves inside the nozzle.

9.4.2 Practical case

In chapters 3 and 4 an estimation for the required delta-v was obtained, specifically in chapter 4. By using equation (9.52) and the required delta-v with the specific impulse, it is possible to obtain an approximation of the required propellant mass needed for the departure and the arrival.

For the next calculations, it is going to be considered three different scenarios:

- Scenario 1: inlet nozzle total temperature of 1500 K and total pressure of 60 bars. It corresponds to a specific impulse of 586 seconds.
- Scenario 2: inlet nozzle total temperature of 2500 K and total pressure of 75 bars. It corresponds to a specific impulse of 769 seconds.
- Scenario 3: inlet nozzle total temperature of 2800 K and total pressure of 75 bars. It corresponds to a specific impulse of 814 seconds.

9.4.2.1 Hohmann transfer

For the Hohmann transfer the delta-V for departure is 3.617 km/s and for arrival is 1.264 km/s, using equation (9.52) and the specific impulse for the different scenarios proposed, the percentage of propellant mass can be obtained:

Departure hyperbola	
Scenarios	Propellant mass percentage
Scenario 1	0.467
Scenario 2	0.381
Scenario 3	0.3645

Table 9.1: Hohmann transfer: Departure, propellant mass percentage needed for different specific impulses.

Arrival hyperbola	
Scenarios	Propellant mass percentage
Scenario 1	0.198
Scenario 2	0.154
Scenario 3	0.147

Table 9.2: Hohmann transfer: Arrival, propellant mass percentage needed for different specific impulses.

9.4.2.2 Lambert transfers

Regarding the Lambert transfers, from the 200 by 200 matrix containing all the studied transfer, it has been selected the optimum transfer as well as other transfer with flight times ranging from 100 days to 80 days.

Departure hyperbola	
Scenarios	Propellant mass percentage
Optimum transfer (210 days)	
Scenario 1	0.490
Scenario 2	0.400
Scenario 3	0.383
100 days transfer	
Scenario 1	0.710
Scenario 2	0.611
Scenario 3	0.590
90 days transfer	
Scenario 1	0.777
Scenario 2	0.682
Scenario 3	0.661

Table 9.3: Lambert transfers: Departure, propellant mass percentage needed for different specific impulses.

80 days transfer	
Scenario 1	0.842
Scenario 2	0.755
Scenario 3	0.736
45 days transfer	
Scenario 1	0.986
Scenario 2	0.962
Scenario 3	0.955

Table 9.4: Lambert transfers: Departure, propellant mass percentage needed for different specific impulses.

Arrival hyperbola	
Scenarios	Propellant mass percentage
Optimum transfer (210 days)	
Scenario 1	0.383
Scenario 2	0.308
Scenario 3	0.294
100 days transfer	
Scenario 1	0.653
Scenario 2	0.554
Scenario 3	0.533
90 days transfer	
Scenario 1	0.692
Scenario 2	0.592
Scenario 3	0.571

Table 9.5: Lambert transfers: Arrival, propellant mass percentage needed for different specific impulses.

80 days transfer	
Scenario 1	0.745
Scenario 2	0.647
Scenario 3	0.626
45 days transfer	
Scenario 1	0.965
Scenario 2	0.922
Scenario 3	0.910

Table 9.6: Lambert transfers: Arrival, propellant mass percentage needed for different specific impulses.

9.4.2.3 Application of the practical case and conclusions

Considering the optimum case for scenario 1, the spacecraft would depart from Earth the 21/02/2031 and arrive to Mars the 19/09/2031.

The mass of propellant needed for this mission can be calculated by the following equation:

$$M_{propellant} = M_0 \cdot \delta m_{departure} + M_0 \cdot (1 - \delta m_{departure}) \cdot \delta m_{arrival} \tag{9.53}$$

where, $\delta m_{departure}$ and $\delta m_{arrival}$ is the propellant mass percentage needed for the departure and arrival, respectively.

Assuming that the initial mass before departure, M_0, is 40 tons:

$$M_{propellant} = 40 \cdot 0.49 + 40 \cdot 0.51 \cdot 0.383 = 27.41 \text{ tons of propellant} \tag{9.54}$$

Therefore, for the entire trip to Mars, it is needed that 68.5 % of the total mass of the vehicle is propellant. This percentage can be decreased by achieving larger specific impulse or in other words, a greater total temperature at the nozzle inlet. However, this is limited by materials and cooling technologies.

Furthermore, the other percentage corresponds to 12.6 tons for which it must be considered the payload, the nuclear fuel (approximately 60 kg of 3% U-235), the weight of the reactor and its components, all on-board equipment, pipes and valves, the tanks in which the propellant is stored, the propulsion system components, auxiliary power systems (solar panels), the electrical panel, batteries, pumps, supplies for the crew, etc.

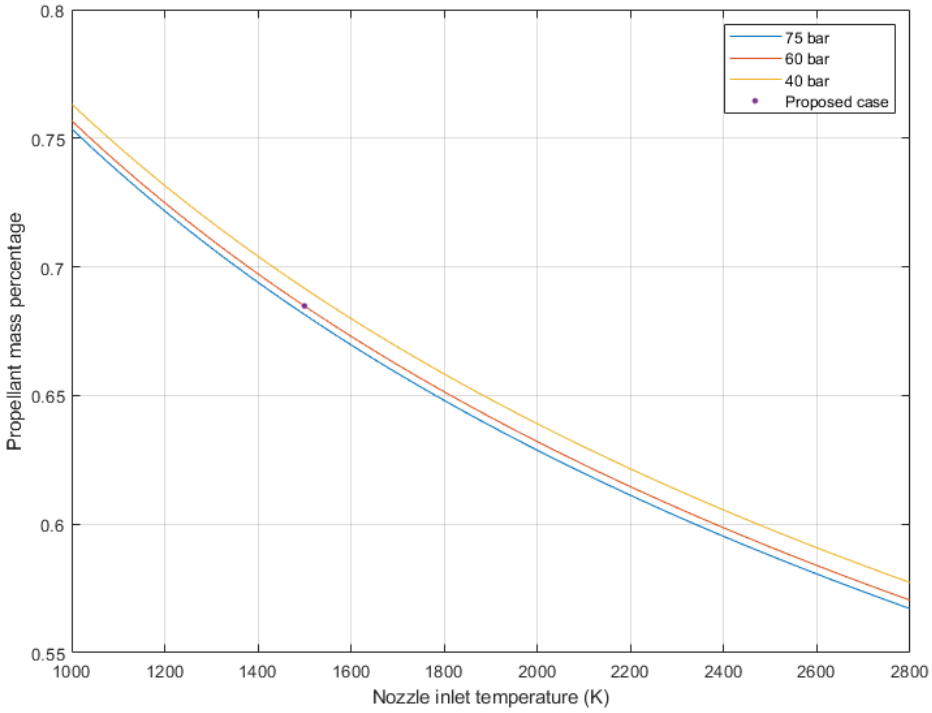

Figure 9.5: Optimum transfer from Earth to Mars (210 days): Propellant mass percentage as a function of total temperature and for different total pressures.

9.4.3 Climate effects

Another important aspect of any propulsion system is the effect on the environment. In an open loop thermonuclear propulsion system, such as the NERVA project, the refrigerant/moderator (hydrogen gas) goes through the reactor and then exits the nozzle. The problem of this design is that the hydrogen gas that is being expelled contains radioisotopes of tritium which is radioactive and has an expected decay life of 30 days. Therefore, this propulsion system should not be used at low altitudes.

Alternatively, in the thermonuclear propulsion engine based on a stirling cycle, the hydrogen gas used as a moderator and refrigerant is in a closed loop inside the reactor. Whereas, the working fluid that exits the nozzle is independent from the one used in the reactor. This means, that only hydrogen gas without radioactive isotopes is being expelled from the nozzle. This offer the possibility of using it for a launch vehicles as it produces clean emissions.

9.4.4 Costs

The process of estimating the total cost of a spacecraft powered by thermonuclear propulsion is an extremely complex process, especially as it must be considered the expenditure in the hundreds of tests that must be performed beforehand, such as a reactor pre-start-up once it is assembled, vibration tests, tests regarding the qualification of electronic equipment (must be classified as class-1E, according to IEEE-308), etc.

For these reasons, the following values are a rough estimation, obtained with the help of the co-tutor, an expert in PWR reactors.

9.4.4.1 Propellant and nuclear fuel

Regarding the cost associated with the working gas and the nuclear fuel, the results obtained in the practical case for a 40 tons spacecraft are considered. The required amount of hydrogen is approximately 27.4 tons and 60 kg of nuclear fuel are needed for the reactor to produce 1 MW.

Element	Cost per kilogram	Total cost
U-238 with 3% U-235	500 €/kg	30,000 €
Cryogenic hydrogen	36 €/kg	986,400 €

Table 9.7: Nuclear fuel and propellant costs.

9.4.4.2 Fixed mass

The term fixed mass, refers to the mass that is not propellant or nuclear fuel. The following tables summarize the estimated costs.

Element	Cost per unit	Total cost
Propellant storage tank (30-50 m^3)	250,000 €/unit	2,500,000 €
Nuclear reactor and redundancy systems	-	1,500,000 €
Control equipment	-	1,000,000 €
Valves/ sensors	-	3,000,000 €
Pipes	-	2,000,000 €
Instrumentation/Navigation equipment	-	1,000,000 €
Electronic equipment	-	1,500,000 €
Communication equipment	-	5,000,000 €
Fuselage (Al-Li alloys)	170 €/kg	2,000,000 €
Other materials (For fuselage, thermal shielding,...)	-	4,000,000 €

Table 9.8: Fixed mass costs.

9.4.4.3 Total cost

A bare minimum of €24,000,000 is estimated as the total cost. This value does not take into account the cost of the tests that must be performed due to normative nor is an accurate estimation of

the real cost of all the systems and subsystems in the spaceship. Additionally, the costs associated with the workforce or the transportation, storage and taxes are not considered.

Appendix A

Coordinate systems

A.1 Heliocentric ecliptic coordinate system

The heliocentric coordinate system is employed for interplanetary missions and it lies in the ecliptic plane with the Sun as the origin. The position is defined by means of the ecliptic latitude (λ) and the ecliptic longitude (β).

The X axis points towards a fixed point known as the Vernal equinox (γ) which corresponds to the position of the Sun when it crosses the equatorial plane the first day of spring. This point is located in the line of intersection between the equatorial plane and the ecliptic plane, known as the line of nodes or the Vernal equinox line.
The Z axis is perpendicular to the ecliptic plane and the Y axis is perpendicular to both the Z and X axis.

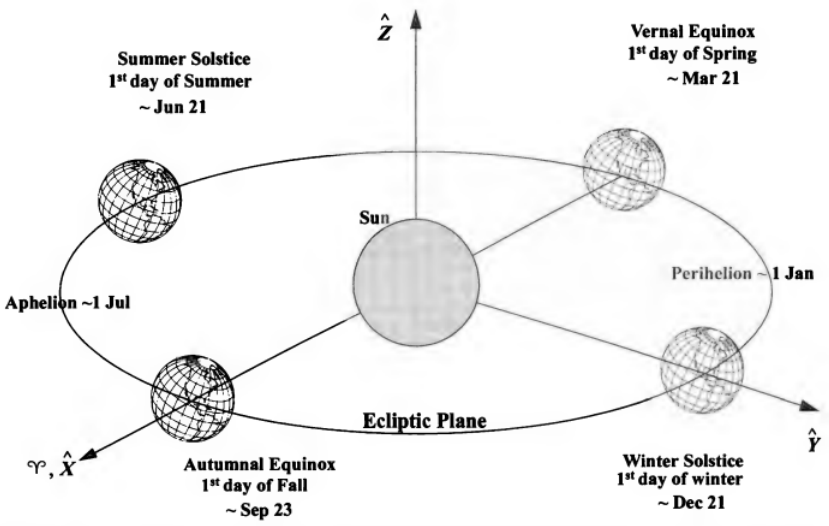

Figure A.1: Heliocentric coordinate system, source: Vallado [58].

Appendix B

Orbital parameters

In order to define an orbit it is required two parameters: the eccentricity and the specific angular momentum. Moreover, in order to locate a point in an orbit it is also needed the true anomaly. When dealing with 3D orbits, another 3 parameters are also required to described the orientation of the orbit which are the Euler angles: inclination, argument of the perigee and the right ascension.

B.1 Specific angular momentum, eccentricity and the true anomaly

The specific angular momentum is constant along the orbit and is perpendicular to the position and the velocity vectors. It is defined as the cross product of the position and velocity vectors:

$$\boldsymbol{h} = \boldsymbol{r} \times \boldsymbol{v} \tag{B.1}$$

The eccentricity allows to determine the shape of the orbit, specifically the type of conic section:

- For $e = 0$, circular orbits.
- For $0 > e < 1$, elliptical orbits.
- For $e = 1$, parabolic orbits.
- For $e > 1$, hyperbolic orbits.

The eccentricity remains constant along the orbit and its vector form can be determine as:

$$\boldsymbol{e} = -\frac{\boldsymbol{r}}{r} + \frac{\dot{\boldsymbol{r}} \times \boldsymbol{h}}{\mu} \tag{B.2}$$

The eccentricity vector (B.2) defines the apse line of an orbit, that contains the perigee and apogee, and its magnitude defines the shape of the conic.
The magnitude of the position vector can be obtained as a function of the eccentricity (e), the specific angular momentum (h), the true anomaly (θ) and the gravitational parameter (μ):

$$r = \frac{h^2}{\mu} \frac{1}{1 + e\cos(\theta)} \tag{B.3}$$

From equation (B.3) several conclusions can be made based on the value of the true anomaly:

- For $\theta = 0$, corresponds to the perigee.

- For $\theta = 180$, corresponds to the apogee.
- When $0 < \theta < 180$, the mass of an object in a given orbit is moving away from the perigee
- For $180 > \theta < 360$, the mass of an object in a given orbit is moving towards the perigee .

The specific energy of an orbit, denoted by ϵ, remains constant along the orbit which means that the specific energy at any point in the orbit is also equal to the specific energy in the perigee.

$$\epsilon = \frac{v^2}{2} - \frac{\mu}{r} = \epsilon_p = \frac{v_\perp^2}{2} - \frac{\mu}{r_p} \tag{B.4}$$

At the perigee the magnitude of the position and the velocity are equal to:

$$\begin{aligned} r_p &= \frac{h^2}{\mu}\frac{1}{1+e} \\ v_p &= v_{\perp,p} = \frac{h}{r_p} \end{aligned} \tag{B.5}$$

Returning to equation (B.4) and substituting by (B.5), the energy equation now becomes:

$$\frac{v^2}{2} - \frac{\mu}{r} = -\frac{\mu^2}{2h^2}\left(1 - e^2\right) \tag{B.6}$$

Appendix C

Reactor nominal power

For this section, a brief example will be presented on how to calculate the nominal power of the reactor and define the thermal power gradient which is used in the thermal-hydraulic design of the reactor core.

Firstly, in Tables (5.5) and (5.6) a set of typical parameters are defined for a conventional pressurized water reactor.
The number of fuel elements refers to the amount of fuel assemblies presented in the reactor core, each assembly is composed by a number of fuel rods, see Figure (5.21).

The first step is to calculate the total number of rods in the core of the reactor:

$$\text{Total Number of fuel rods} = \text{Number of elements} \cdot \text{Number of rods} = 157 \cdot 264 = 41448 \tag{C.1}$$

The next step is calculating the total length of all the fuel rods, this can be easily done by multiplying the previous results by the length of a particular fuel rod:

$$\text{Fuel rod total length} = 41448 \cdot 4.27 = 176,982.96\, m \tag{C.2}$$

With the total length defined, it is divided by the thermal power, which for a typical PWR is around 3000 Mw:

$$\text{Thermal power gradient} = \frac{3000 \cdot 10^6}{\text{Fuel rod total length} * 100} = 169.51\, W/cm \tag{C.3}$$

Appendix D

Regulatory framework

The following chapter summarizes the main normative regarding the elaboration of this final degree project as well as some important normative related with the project itself.

D.1 Real Decreto 488/1997, de 14 de abril, sobre disposiciones mínimas de seguridad y salud relativas al trabajo con equipos que incluyen pantallas de visualización. [1]

La Ley 31/1995, de 8 de noviembre, de Prevención de Riesgos Laborales, determina el cuerpo básico de garantías y responsabilidades preciso para establecer un adecuado nivel de protección de la salud de los trabajadores frente a los riesgos derivados de las condiciones de trabajo, en el marco de una política coherente, coordinada y eficaz. Según el artículo 6 de la misma serán las normas reglamentarias las que irán fijando y concretando los aspectos más técnicos de las medidas preventivas.

Así, son las normas de desarrollo reglamentario las que deben fijar las medidas mínimas que deben adoptarse para la adecuada protección de los trabajadores. Entre ellas se encuentran las destinadas a garantizar que de la utilización de los equipos que incluyen pantallas de visualización por los trabajadores no se deriven riesgos para la seguridad y salud de los mismos.

En el mismo sentido hay que tener en cuenta que en el ámbito de la Unión Europea se han fijado mediante las correspondientes Directivas criterios de carácter general sobre las acciones en materia de seguridad y salud en los centros de trabajo, así como criterios específicos referidos a medidas de protección contra accidentes y situaciones de riesgo. Concretamente, la Directiva 90/270/CEE, de 29 de mayo, establece las disposiciones mínimas de seguridad y de salud relativas al trabajo con equipos que incluyan pantallas de visualización. Mediante el presente Real Decreto se procede a la transposición al Derecho español del contenido de la Directiva 90/270/CEE, antes mencionada.

En su virtud, de conformidad con el artículo 6 de la Ley 31/1995, de 8 de noviembre, de Prevención de Riesgos Laborales, a propuesta del Ministro de Trabajo y Asuntos Sociales, consultadas las organizaciones empresariales y sindicales mas representativas, oída la Comisión Nacional de Seguridad y Salud en el Trabajo, de acuerdo con el Consejo de Estado y previa deliberación del Consejo de Ministros en su reunión del día 4 de abril de 1997.

D.1.1 Artículo 1. Objeto.

1. El presente Real Decreto establece las disposiciones mínimas de seguridad y de salud para la utilización por los trabajadores de equipos que incluyan pantallas de visualización.

2. Las disposiciones de la Ley 31/1995, de 8 de noviembre, de Prevención de Riesgos Laborales, se aplicarán plenamente al conjunto del ámbito contemplado en el apartado anterior.

3. Quedan excluidos del ámbito de aplicación de este Real Decreto:
   a) Los puestos de conducción de vehículos o máquinas.

   b) Los sistemas informáticos embarcados en un medio de transporte.

   c) Los sistemas informáticos destinados prioritariamente a ser utilizados por el público.

   d) Los sistemas llamados portátiles, siempre y cuando no se utilicen de modo continuado en un puesto de trabajo.

   e) Las calculadoras, cajas registradoras y todos aquellos equipos que tengan un pequeño dispositivo de visualización de datos o medidas necesario para la utilización directa de dichos equipos.

   f) Las máquinas de escribir de diseño clásico, conocidas como máquinas de ventanilla.

D.1.2 Artículo 2. Definiciones.

A efectos de este Real Decreto se entenderá por:

a) Pantalla de visualización: una pantalla alfanumérica o gráfica, independientemente del método de representación visual utilizado.

b) Puesto de trabajo: el constituido por un equipo con pantalla de visualización provisto, en su caso, de un teclado o dispositivo de adquisición de datos, de un programa para la interconexión persona/máquina, de accesorios ofimáticos y de un asiento y mesa o superficie de trabajo, así como el entorno laboral inmediato.

c) Trabajador: cualquier trabajador que habitualmente y durante una parte relevante de su trabajo normal utilice un equipo con pantalla de visualización.

D.1.3 Artículo 3. Obligaciones generales del empresario.

1. El empresario adoptará las medidas necesarias para que la utilización por los trabajadores de equipos con pantallas de visualización no suponga riesgos para su seguridad o salud o, si ello no fuera posible, para que tales riesgos se reduzcan al mínimo.

En cualquier caso, los puestos de trabajo a que se refiere el presente Real Decreto deberán cumplir las disposiciones mínimas establecidas en el anexo del mismo.

2. A efectos de lo dispuesto en el primer párrafo del apartado anterior, el empresario deberá evaluar los riesgos para la seguridad y salud de los trabajadores, teniendo en cuenta en particular los posibles riesgos para la vista y los problemas físicos y de carga mental, así como el posible efecto añadido o combinado de los mismos.

   La evaluación se realizará tomando en consideración las características propias del puesto de trabajo y las exigencias de la tarea y entre éstas, especialmente, las siguientes:

   a) El tiempo promedio de utilización diaria del equipo.

   b) El tiempo máximo de atención continua a la pantalla requerido por la tarea habitual.

   c) El grado de atención que exija dicha tarea.

3. Si la evaluación pone de manifiesto que la utilización por los trabajadores de equipos con pantallas de visualización supone o puede suponer un riesgo para su seguridad o salud, el empresario adoptará las medidas técnicas u organizativas necesarias para eliminar o reducir el riesgo al mínimo posible. En particular, deberá reducir la duración máxima del trabajo continuado en pantalla, organizando la actividad diaria de forma que esta tarea se alterne con otras o estableciendo las pausas necesarias cuando la alternancia de tareas no sea posible o no baste para disminuir el riesgo suficientemente.

4. En los convenios colectivos podrá acordarse la periodicidad, duración y condiciones de organización de los cambios de actividad y pausas a que se refiere el apartado anterior.

D.1.4 Artículo 4. Vigilancia de la salud.

1. El empresario garantizará el derecho de los trabajadores a una vigilancia adecuada de su salud, teniendo en cuenta en particular los riesgos para la vista y los problemas físicos y de carga mental, el posible efecto añadido o combinado de los mismos, y la eventual patología acompañante. Tal vigilancia será realizada por personal sanitario competente y según determinen las autoridades sanitarias en las pautas y protocolos que se elaboren, de conformidad con lo dispuesto en el apartado 3 del artículo 37 del Real Decreto 39/1997, de 17 de enero, por el que se aprueba el Reglamento de los servicios de prevención. Dicha vigilancia deberá ofrecerse a los trabajadores en las siguientes ocasiones:

   a) Antes de comenzar a trabajar con una pantalla de visualización.

   b) Posteriormente, con una periodicidad ajustada al nivel de riesgo a juicio del médico responsable.

   c) Cuando aparezcan trastornos que pudieran deberse a este tipo de trabajo.

2. Cuando los resultados de la vigilancia de la salud a que se refiere el apartado 1 lo hiciese necesario, los trabajadores tendrán derecho a un reconocimiento oftalmológico.

3. El empresario proporcionará gratuitamente a los trabajadores dispositivos correctores especiales para la protección de la vista adecuados al trabajo con el equipo de que se trate, si los resultados de la vigilancia de la salud a que se refieren los apartados anteriores demuestran su necesidad y no pueden utilizarse dispositivos correctores normales.

D.1.5 Artículo 5. Obligaciones en materia de información y formación.

1. De conformidad con los artículos 18 y 19 de la Ley de Prevención de Riesgos Laborales, el empresario deberá garantizar que los trabajadores y los representantes de los trabajadores reciban una formación e información adecuadas sobre los riesgos derivados de la utilización de los equipos que incluyan pantallas de visualización, así como sobre las medidas de prevención y protección que hayan de adoptarse en aplicación del presente Real Decreto.

2. El empresario deberá informar a los trabajadores sobre todos los aspectos relacionados con la seguridad y la salud en su puesto de trabajo y sobre las medidas llevadas a cabo de conformidad con lo dispuesto en los artículos 3 y 4 de este Real Decreto.

3. El empresario deberá garantizar que cada trabajador reciba una formación adecuada sobre las modalidades de uso de los equipos con pantallas de visualización, antes de comenzar este tipo de trabajo y cada vez que la organización del puesto de trabajo se modifique de manera apreciable.

D.1.6 Artículo 6. Consulta y participación de los trabajadores.

La consulta y participación de los trabajadores o sus representantes sobre las cuestiones a que se refiere este Real Decreto se realizarán de conformidad con lo dispuesto en el apartado 2 del artículo 18 de la Ley de Prevención de Riesgos Laborales.

D.1.7 Disposición transitoria única. Plazo de adaptación de los equipos que incluyan pantallas de visualización.

Los equipos que incluyan pantallas de visualización puestos a disposición de los trabajadores en la empresa o centro de trabajo con anterioridad a la fecha de entrada en vigor del presente Real Decreto deberán ajustarse a los requisitos establecidos en el anexo en un plazo de doce meses desde la citada entrada en vigor

D.1.8 Disposición final primera. Elaboración de la Guía Técnica para la evaluación y prevención de riesgos.

El Instituto Nacional de Seguridad e Higiene en el Trabajo, de acuerdo con lo dispuesto en el apartado 3 del artículo 5 del Real Decreto 39/1997, de 17 de enero, por el que se aprueba el Reglamento de los Servicios de Prevención, elaborará y mantendrá actualizada una Guía Técnica para la evaluación y prevención de los riesgos relativos a la utilización de equipos que incluyan pantallas de visualización.

D.1.9 Disposición final segunda. Habilitación normativa.

Se autoriza al Ministro de Trabajo y Asuntos Sociales para dictar, previo informe de la Comisión Nacional de Seguridad y Salud en el Trabajo, las disposiciones necesarias en desarrollo de este Real Decreto y, específicamente, para proceder a la modificación del anexo del mismo para aquellas adaptaciones de carácter estrictamente técnico en función del progreso técnico, de la evolución de las normativas o especificaciones internacionales o de los conocimientos en el área de los equipos que incluyan pantallas de visualización.

D.2 NORMATIVA DE TRABAJOS DE FIN DE GRADO Y TRABAJOS DE FIN DE MÁSTER DE LA UNIVERSITAT POLITÈCNICA DE VALÈNCIA

D.2.1 Artículo 1. Ámbito de aplicación

1. La presente normativa será de aplicación en las enseñanzas impartidas por la UPV conducentes a la obtención de los títulos de Grado y Máster Universitario de carácter oficial y validez en todo el territorio nacional (en adelante, títulos oficiales).

2. La presente normativa será de aplicación a los estudiantes de la UPV de los títulos oficiales interuniversitarios, salvo que en el correspondiente convenio o en la memoria de verificación de dichos títulos se establezcan explícitamente otras disposiciones al respecto.

3. Las Estructuras Responsables de los Títulos oficiales (en adelante ERTs) podrán establecer sus propios acuerdos de desarrollo que complementen lo que se indica en la presente Norma. Éstos no podrán contradecir lo dispuesto en esta Norma y deberán ser aprobados por la Comisión Académica del Consejo de Gobierno de la UPV con anterioridad a su entrada en vigor.

4. Las ERTs darán publicidad a la presente normativa y, en su caso, a las normativas propias complementarias, a través de los medios que consideren oportunos con el objeto de que sean conocidas por todo el estudiantado y profesorado.

5. Los TFG y TFM de los títulos oficiales que habiliten para el ejercicio de las profesiones reguladas, se regirán por lo dispuesto en la correspondiente Orden Ministerial que establece los requisitos para la verificación del título, sin perjuicio de la aplicación, con carácter complementario, de lo que se indique en la presente Normativa Marco.

6. La denominación TFG y TFM empleada en esta Normativa Marco debe entenderse de aplicación incluso en aquellas titulaciones en las que las órdenes ministeriales dispongan denominaciones alternativas para señalar módulos o materias a las que, de forma genérica, se hace referencia como TFG y TFM en el Real Decreto 822/2021, de 28 de septiembre, por el que se establece la organización de las enseñanzas universitarias y del procedimiento de aseguramiento de su calidad o norma posterior que regule esta materia.

D.2.2 Artículo 2. Naturaleza de los Trabajos de Fin de Grado y Trabajos de Fin de Máster

1. Los TFG y TFM deberán estar orientados a la aplicación y evaluación de las competencias asociadas al título.

2. Todos los TFG y los TFM de títulos que habiliten para el ejercicio de profesiones reguladas deberán tener una orientación profesional. En el resto de los casos, el TFM podrá tener orientación profesional o investigadora.

3. Los TFG y TFM consistirán en la realización de un trabajo o proyecto original en el que queden de manifiesto conocimientos, habilidades y competencias adquiridas por el estudiante a lo largo de sus estudios y, expresamente, las competencias asociadas a la materia TFG o TFM tal y como se indique en la memoria de verificación del título.

4. La originalidad del trabajo a que se hace referencia en el punto anterior debe entenderse sin menoscabo de que pueda ser parte independiente e individual de un trabajo integral desarrollado de manera conjunta entre estudiantes de una misma titulación o de diferentes titulaciones y/o ERTs. En cualquier caso, la defensa del TFG o TFM debe ser individual.

5. La materia TFG o TFM podrá organizarse mediante actividades de docencia reglada en forma de seminario, taller o similar; mediante trabajo autónomo y tutelado del estudiante; o mediante una mezcla de ambas.

6. El alcance, contenido y nivel de exigencia de los TFG y TFM deberá adecuarse a la asignación de ECTS que dicha materia haya recibido en la memoria de verificación. A tal efecto, la Comisión Académica de Titulo (en adelante CAT) velará para que el tiempo de dedicación requerido para la realización del TFG o TFM se adecúe al número de ECTS asignados al mismo y pueda ser evaluado en el periodo académico previsto en la estructura del plan de estudios.

7. Como cualquier otra materia de un plan de estudios, los TFG y TFM deberán disponer de una Guía Docente en la que, con los contenidos y alcance que determine la UPV y de acuerdo con lo indicado en la memoria de verificación del título, deberán constar todos aquellos aspectos que orienten el trabajo del estudiante. En la guía docente deberá especificarse qué parte de los ECTS asignados a la materia TFG o TFM se desarrollarán mediante docencia reglada y qué parte mediante trabajo autónomo y tutelado del estudiante. Los directores académicos del título serán los responsables de la confección de dicha guía.

D.3 MIL-STD 1568E

The following normative is focus on the requirements and standard for implementation of materials to guarantee safety, reliability and high performance. Specifically, the propulsive system presented in this project uses hydrogen gas as a propellant, therefore it is needed a set of standards to avoid hydrogen embrittlement and corrosion.

D.3.1 ASTM INTERNATIONAL

- ASTM F159. Standard Test Method for Mechanical Hydrogen Embrittlement Evaluation of Plating/Coating Processes and Service Environments.

- ASTM F945. Standard Test Method for Stress-Corrosion of Titanium Alloys by Aircraft Engine Cleaning Materials.

- ASTM G44. Standard Practice for Exposure of Metals and Alloys by Alternate Immersion in Neutral 3.5% Sodium Chloride. Solution

- ASTM G47. Standard Test Method for Determining Susceptibility to Stress-Corrosion Cracking of 2XXX and 7XXX Aluminum Alloy Products.
- ASTM G49. Standard Practice for Preparation and Use of Direct Tension Stress-Corrosion Test Specimens.
- ASTM G58. Standard Practice for Preparation of Stress-Corrosion Test Specimens for Weldments.
- ASTM G64. Standard Classification of Resistance to Stress-Corrosion Cracking of Heat-Treatable Aluminum Alloys.

D.3.2 SAE INTERNATIONAL

- SAE AMS1389. Sealing Compound, Polythioether Rubber, Light-Cured, for Integral Fuel Tanks and General Purpose, Intermittent use to 360 ºF (182 ºC).
- SAE AMS2448. Anodic Treatment of Titanium and Titanium Alloys Solution pH 13 or Higher.
- SAE AMS2759/9. Hydrogen Embrittlement Relief (Baking) of Steel Parts.
- SAE AMS3269. Sealing Compound, Polysulfide (T) Rubber, Fuel Resistant, Non-Chromated Corrosion Inhibiting for Intermittent Use to 360 °F (182 °C).
- SAE AMS3276. Sealing Compound, Integral Fuel Tanks and General Purpose, Intermittent Use to 360 °F (182 °C).
- SAE AMS3277. Sealing Compound, Polythioether Rubber Fast Curing for Integral Fuel Tanks and General Purpose, Intermittent Use to 360 °F (182 °C).
- SAE AMS3284. Sealing Compound, Low Adhesion, for Removable Panels and Fuel Tank Inspection Plates.
- SAE AMS AMS-S-8802. Sealing Compound, Fuel Resistant, Integral Fuel Tanks and Fuel Cell Cavities.
- SAE ARP1110. Minimizing Stress Corrosion Cracking in Heat Treatable Wrought Low Alloy and Martensitic Corrosion Resistant Steels.
- SAE ARP4118. Isolation and Corrosion Protection of Dissimilar Materials, Carbon Composite Structure Repair.
- SAE ARPAS6870. Nondestructive Inspection Program Requirements for Aerospace Systems.
- SAE AS12500. Corrosion Prevention and Deterioration Control in Electronic Components and Assemblies.
- SAE AS81550. Insulating Compound, Electrical, Embedding, Reversion Resistant Silicone.

D.3.3 General requirements. Corrosion prevention and control plan (CPCP)

The CPCP shall address the design, materials, and processes intended to be used on the specific system being procured including system interfaces, installation of government furnished equipment, and commercial items procured off-the-shelf. The key elements of CPC planning can be found in the Association for Materials Protection and Performance's (AMPP) Corrosion Prevention and Control Planning Standard (SSPC CPC-1/NACE-21412-2020) and in the Corrosion Prevention and Control Planning Guidebook for Military Systems and Equipment. The CPCP shall contain the following:

1. A combination of system design, engineering and manufacturing requirements, operations, logistics, and sustainment phases that mitigate corrosion throughout system life.

2. An integrated management structure that ensures ongoing, effective CPC communication and coordination among team members by defining roles and responsibilities for quality assurance, process control, materials/process engineering, manufacturing, low observables, technical writing, and Environment, Safety, and Occupational Health (ESOH) compliance.

3. Materials, processing methods, manufacturing techniques, and fabricating processes as well as the protective treatments identified in the finish specification.

4. Methods for CPC sustainability, logistics support, maintenance planning (such as methods/equipment for corrosion monitoring and non-destructive inspection), ground support and test equipment, handling, transportation, and storage of parts or assemblies, personnel training and the generation/validation/verification of technical information.

5. Performance requirements and verification methods for full stack-ups of the overall protective schemes, including low observable materials.

6. Methods to pursue compromises between conflicting requirements of corrosion mitigation, low observables, electrical grounding, environmental compliance, safety and occupational health. Life cycle costs shall be a factor in achieving compromises.

7. A requirements flow down process for suppliers, subcontractors, and sub-systems manufacturers and the procurement of commercial-off-the-shelf items that validates, verifies, and ensures their compliance with the CPC plan and finish specification.

8. Include an assessment of the planned basing and operational environments in which the system is intended to be used.

9. References to applicable specifications and standards.

D.4 Other normative

- From a mechanical standpoint, the ASME (American Society of Mechanical Engineers) standards must be followed.

- From a nuclear safety perspective, the regulation stated by the RNC (Nuclear Regulatory Commission) must be followed.

- For fire prevention safety, NFPA (National Fire Protection Association) normative must be followed.

- For electronic components, The standard IEEE (Institute of Electrical and Electronics Engineers) must be followed. The equipment must be class-1E, which must work in pristine conditions under a set of circumstances:
  - IEEE-334: For electrical motors qualification.
  - IEEE-344: Seismic qualification of the nuclear equipment.
  - IEEE-323: Environmental qualification.
    In presence of a gamma radiation source, the quality of the electronic materials is deteriorated. It is measured in rads.

$$1\ rad = 1J/kg \text{ of gamma radiation absorbed by the equipment} \tag{D.1}$$

    * Maximum total absorption: 64 Mrads.
    * Maximum hourly absorption: 1 Mrad/h.
- ISO-9001, traceability of materials and management of the constructive quality.
- Environmental management framework, ISO-14001.
- Working environment and construction safety, ISO-45001.
- Pre-nuclear test must be performed once the reactor is built.
- Vibration testing.

Appendix E

ODS

The following section is oriented in the objectives for sustainable development. These objectives consist of 17 goals proposed by the 2030 Agenda.

Figure E.1: ODS.

During the early development of thermonuclear rocket engines, specifically in the NERVA project, the refrigerant/moderator was in an open loop. This means that hydrogen gas with tritium radioactive isotopes exited through the nozzle to the outside environment. Therefore, this rocket engine could only be used at high altitudes, such as at the late stages of the launch vehicle or once in a parking orbit.

For this project a closed loop thermonuclear rocket engine has been presented. This propulsive system is characterized by the fact that clean diatomic hydrogen gas is being expelled through the nozzle. As long as at the exit of the nozzle there is no combustion process when the high temperature hydrogen gas interacts with the air molecules, there are zero emissions.

Under this circumstances the ODS-7, affordable and clean energy, and the ODS-9, Industry, innovation and infrastructure are achieved.

Appendix F

Budget

The following section should not be confused with the costs presented at the conclusion, in chapter 9. The objective is to present the cost associated with the elaboration of this final degree project.

F.1 Labor costs

The following salaries have been obtained from the management subdivision of Human Resources and Organizational structure [18] of the Polytechnic University of Valencia. The salary of the student has been considered as the one of an assistant in a research project.

Personnel	Time (hours)	Hourly salary (€/h)	Total (€)
Student	800	10.7	8565
Tutor	150	15.825	2373.75
External cotutor	200	14,68	2936
Total cost (€)			13874.75

Table F.1: Personnel salaries.

F.2 Hardware costs

The depreciation rate for electronic equipment is stated as 25 % according to the Law of 27/2014 of 27 of November, article 12 [8].

Element	Initial cost (€)	Depreciation rate	Usage (months)	Total cost (€)
Computer custom build	2000	25 %	6	250

Table F.2: Hardware usage cost.

F.3 Software costs

The software is considered as an intangible asset, whose depreciation rate is stated as 33 % according to the Law of 27/2014 of 27 of November, article 12 [8].

Software	Annual cost (€)	Depreciation rate	Usage (months)	Total cost (€)
Latex Textmaker	0	33 %	4	0
Matlab R2023b	900	33 %	4	99
Microsoft office 365	99	33%	4	10.89
Total cost (€)				109.89

Table F.3: Software usage cost.

F.4 Total cost

Element	Cost (€)
Personnel	13874.75
Hardware	250
Software	109.89
Total	14234.64

Table F.4: Total cost.

Appendix G

Future work lines

During the elaboration of this project there have been a set of ideas that could be considered and expanded for future projects.

- Study the effect of high temperature hydrogen gas with the atmosphere as it exists through the nozzle. Especially, study the possibility of a combustion process taking place at the outlet of the nozzle, as a consequence of the interaction of the high temperature hydrogen gas with the atmospheric air.
- Study the heat transfer phenomena inside the tanks, where the electric heaters are placed.
- Further develop the concept of a modified PWR with hydrogen gas as a refrigerant and moderator, and the particularities in the design for such a nuclear reactor for vacuum conditions.
- Study of the thrust performance parameters as altitude changes.

Bibliography

[1] Boe, real decreto 488/1997, de 14 de abril.

[2] Campo magnético producido por una corriente circular en un punto de su eje.

[3] Ceia-power.

[4] *Critical Facilities in Nuclear Technology.* 16, No. 12, pages 39-54 (1958).

[5] *Descripción Del Sngv Westinghouse.* Primera edición Enero de 1983. Westinghouse Nuclear Española.

[6] Horizons system.

[7] *Induction Heating.* Course 60, ASM International, Metals Park, OH, 1986.

[8] Ley 27/2014, de 27 de noviembre, del impuesto sobre sociedades.

[9] Los alamos national laboratory.

[10] *materials and processes for corrosion prevention and control in aerospace weapons systems.* department of defense design criteria standard, mil-std 1568e, 11 october 2023.

[11] Normativa de trabajos de fin de grado y trabajos de fin de mÁster de la universitat politÈcnica de valÈncia.

[12] *Pressurized Water Reactor (PWR) Systems.* USNRC Technical Training Center.

[13] *PWR Reactor Internals and Evaluation Guidelines.* USNRC Technical Training Center.

[14] *Reactor Physics Constants.* Ref. 7, Section 4.1.4.

[15] *ROMASHKA high-temperature converter-reactor.* Peaceful Uses of Atomic Energy (Proc. 3rd Int. Conf. Geneva, 1964), United Nations, New York (1965).

[16] *Transfer Function Measurement and Reactor Stability Analysis.* U. S. AEC Report ANL 6205 (1960).

[17] *U. S. AEC Report ANL 5800, 2nd Ed.* 1962, Section 10.

[18] Vicegerencia de recursos humanos y estructura organizativa.

[19] Schultz (M. A.). *Control of nuclear reactors and power plants.* McGrawHill series in nuclear engineering, second edition.

[20] Afnor. *Réacteurs à eau sous pression. Ilots nucléaires.* Paris 1992.

[21] International Atomic Energy Agency. *Proceedings of the Seminar on Codes for Reactor Calculations*. 1961.

[22] Jr. BUDEN D. Angelo, J.A. *Space Nuclear Power*. Orbit Book Company, Malabar, FL (1985).

[23] Metals Handbook ASM. *Properties and Selection: Nonferrous Alloys and Pure Metals*. ASM, Cleveland, 1979.

[24] R.R. Bate, D.D. Mueller, and J.E. White. *Fundamentals of Astrodynamics*. Dover Books on Aeronautical Engineering Series. Dover Publications, 1971.

[25] R.H. Battin. *An Introduction to the Mathematics and Methods of Astrodynamics*. AIAA Education Series. American Institute of Aeronautics & Astronautics, 1999.

[26] et al. BOGUSH, I.P. *Main goals and results of flight tests of the NPS under the TOPAZ Program*. At. Ehnerg. 70 4 (1990).

[27] V.A. Chobotov. *Orbital Mechanics*. AIAA Education Series. American Institute of Aeronautics & Astronautics, 2002.

[28] Vid. R. V. Churchill. *Modern Operational Mathematics in Engineering*. McGraw Hill Book Co., Inc., New York, 1944.

[29] D. Van Nostrand Co. *S. Glasstone y N. C. Edlung, "The Elements of Nuclear Reactor Theory"*. Princeton, N. J., 19,52, pág. 241.

[30] H.D. Curtis. *Orbital Mechanics for Engineering Students: Revised Reprint*. Aerospace Engineering. Elsevier Science, 2020.

[31] E. J. Davies. *Conduction and Induction Heating*. Peter Peregrinus, London, UK, 1990.

[32] E. J. Davies. *Induction Heating Handbook, McGraw-Hill*. New York, 1979.

[33] I. E. Dayton and G. Pettus. *The Effective Resonance Integral of Thorium and Thorium Oxide*. 286, 1958.

[34] A. D. Demichev. *Surface Induction Hardening*. St. Petersburg, Russia, 1990.

[35] R. W. Deutsch. *U. S. AEC Report GNEC 133*. 1960.

[36] L. Dresner. *Nuc. Sci. and Eng.* 1, 68 (1956).

[37] J. Appl. Phys E. Hellstrand. *Measurements of the Effective Resonance Integral in Uranium Metal and Oxide in Different Geometries*. 28, 1493 (1957).

[38] H. Etherington (Ed.). *"Nuclear Engineering Handbook"*. McGraw Hill Book Co., Inc., New York, 1958, pages 6 60 et seq.

[39] P. W. Davison et al. *U. S. AEC Report YAEC 94*. 1959.

[40] T. H. Middleham et al. *Iron and steel institute*. 187, 1 (Sept. 1957).

[41] Caillet (C.) et Carpentier (J.). *La dynamique de l'empoisonnement d'un réacteur par le xenon*. Journal of Nuclear Energy, 3 49 (1956).

[42] Furet (J.) et Garcia (A.). *Influence de l'empoisonnement xenon sur le contrôle et la sécurité des piles à haut flux.* Journal of Nuclear Energy, janvier 1962.

[43] H. Etherington. *Reactor Analysis.* McGraw Hill Book Co., Inc., New York, 1960 pages 456 et seq.

[44] M. R. Fleishman and H. Soodak. *Methods and Cross Sections for Calculating the Fast Effect.* 7, 217 (1960).

[45] J. GRAHAM. *A Vision for the Second Fifty Years of Nuclear Energy.* Visions and Strategies, International Nuclear Societies Council, 1966.

[46] ZHABOTINSKY E.E. ZRODNIKOV A.V. et al. GRIAZNOV, G.M. *Space Nuclear Power Systems with Direct Energy Conversion.* prepared by Red Star State Enterprise for the Encyclopedic Collection on Nuclear Engineering, 1999.

[47] A. Hitchcock. *Nuclear Reactor Stability.* Simmons Boardman Books, New York, 1960.

[48] Dario Izzo. Revisiting lambert's problem.

[49] Furet (J.). *Cinétique de l'empoisonnement samarium dans les piles atomiques à très haut flux.* Rapport CEA, n) 2389.

[50] Furet (J.). *Influence de l'empoisonnement xenon dans les piles à haut flux sur la vitesse des barres de contrôle.* Rapport CEA, nº 2080.

[51] Weill (J.). *Mesure de la puissance neutronique et thérmique.* Génie atomique, 2, chap. XVI. Presses universitaires de France.

[52] L. R. Shephard y J. H. Tait J. Godd. *Progress in Nuclear Energy, Series Physics and Mathematics.* Vol. 1, McGraw Hill Book Co., Inc),New York, 1956.

[53] Prof. Dr. Nader Koura. *Thermodynamics II PCE 320. Lecture 4.*

[54] A. W. Kramer. *Boiling Water Reactors.* Addison Wesley Publishing Co., Inc., Reading, Mass., 1958, pages 358 et seq.

[55] M. G. Lozinskii. *Industrial Applications of Induction Heating.* Pergamon, London,1969.

[56] Roger W. Luidens and Brent A. Miller. Efficient planetary parking orbits with examples for mars.

[57] G.M.B. Oriti M. Salvatore. *Advanced Stirling Convertor Testing at NASA Glenn Research Center.* AIAA, 2007.

[58] W.D. McClain and D.A. Vallado. *Fundamentals of Astrodynamics and Applications.* Space Technology Library. Springer Netherlands, 2001.

[59] R. V. Meghreblian and D. K. Holmes. *Reactor Analysis.* McGraw Hill Book Co., Inc., New York, 1960 pages 456 et seq.

[60] Allen Peterson Joseph VanderVeer Robert Sievers M.W. Michael Amato, Glenn Driscoll. *FLEXURE ISOTOPE STIRLING CONVERTOR (FISC) DEVELOPMENT PROGRESS.* NETS, 2019.

[61] V. Nather and W. S. Sangren. *Nucleonics.* 19, No. 11, 154 (1961).

[62] V.A. N.N., USOV. *Main results of 15,000-hour tests of the ROMASHKA high-temperature converter-reactor.* 4th US Energy Conversion Conference, Washington, 1969.

[63] USOV V.A. PONOMAREV-STEPNOI, N.N. *Conceptual design of the bimodal nuclear power system based on the Romashka type reactor with the thermionic energy conversion system.* Space Nuclear Power and Propulsion (Proc. 12th Int. Symp. Albuquerque, 1995), American Institute of Physics, New York (1995).

[64] USOV V.A. et al. PONOMAREV-STEPNOI, N.N. *Space nuclear power system based on thermionic reactor with single-cell TFEs.* 10th Symp. on Space Nuclear Power and Propulsion, Albuquerque, 1993.

[65] D.I. POSTON. *Nuclear design of the Homer-15 Mars surface fission reactor.* Nuclear News, December (2002) 36–48.

[66] D.I. POSTON. *Nuclear design of the SAFE-400 space fission reactor.* Nuclear News, December (2002) 28–35.

[67] V.Y. POUPKO. *History of Work on Nuclear Propulsion Modules for Space and Aircraft.* SSC RF-IPPE, Obninsk (2002).

[68] J.E. Prussing and B.A. Conway. *Orbital Mechanics.* Oxford University Press, 1993.

[69] Compte rendu d'une réunion de spécialistes. *In core instrumentation and reactor assessment.* Nuclear Energy Agency, Paris 1989.

[70] Georgia A. Richardson Robert B. Adams. Using the two-burn escape maneuver for fast transfers in the solar system and beyond.

[71] Horacio F.E. Rizzo y Juan José Costa. Rodolfo A. Ghelfi. *Glosario de términos nucleares.* Ed. universitaria de Buenos Aires, 1967.

[72] V. Rudnev. *Mathematical simulation and optimal control of induction heating of large-dimensional cylinders and slabs.* Ph.D. Thesis, Department of Electrical Technology, St. Petersburg Electrical Engineering University, Russia, 1986.

[73] D. Okrent y P. A. Moldauer S. Yiftah. *Fast Reactor Cross Sections.* Pergamon Press, Inc., New York, 1960.

[74] A.N. Saad and M.I. Nouh. Lambert universal variable algorithm.

[75] W. S. Sangren. *Digital Computers and Nuclear Reactors Calculations.* John Wiley and Sons, Inc., New York, 1960.

[76] Nur Adila Faruk Senan. A brief introduction to using ode45 in matlab. *University of California at Berkeley, USA*, 2007.

[77] A. E. Slukhotskii and S. E. Ryskin. *Inductors for Induction Heating.* Energy Publications, St. Petersburg, Russia, 1974.

[78] B. I. Spinrad. *Fast Effect in Lattice Reactors.* 1, 455 (1956).

[79] G.P. Sutton and O. Biblarz. *Rocket Propulsion Elements.* A Wiley Interscience publication. Wiley, 2001.

[80] C. A. Tudbury. *Basics of Induction Heating.* Rider, New York, 1960.

[81] Raievski (V.). *Effets cinétiques du xenon et du samarium.* Génie atomique, 1, chap. XII . Presses universitaires de France.

[82] Raievski (V.). *La neutronique dans les réacteurs. Effets statiques du xenon, du samarium, de la température, de la pression.* Génie atomique, 1. Presses universitaires de France.

[83] G. Vander Voort. *Atlas of Time-Temperature Diagrams for Irons and Steels.* ASM International, 1991.

[84] et al. Weichao Li. *Investigation on steam contact condensation injected vertically at low mass flux: Part I pure steam experiment.* Int. J. Heat Mass Tran. 131 (2019) 301e312.

[85] A. M. Weinberg and E. P. Wigner. *The Physical Theory of Neutron Chain Reactions.* University of Chicago Press, 1958, page 595.

[86] A. M. Weinberg and E. P. Wigner. *Reactor handbook, second edition.* Interscience Publishers, Inc., New York, 1962, Vol. III, Part A, Cap. 3.

[87] A. M. Weinberg and E. P. Wigner. *"The Elements of Nuclear Reactor Theory",.* University of Chicago Press, 1958, pág. 498.

[88] Samuel Glasstone y Alexander Sensonske. Ed. Reverté. *Ingeniería de reactores nucleares.* Barcelona, 1982.

[89] R. V. Meghreblian y D. K. Holmes. *Reactor Analysis.* McGraw Hill Book Co., Inc., New York, 1960, pages 573 et seq.

[90] Federico Goded Echeverría y Francisco Oltra Oltra. *Teoría de reactores y elementos de ingeniería nuclear. Tomos I y II.* Sección de publicaciones de la J.E.N., Madrid 1981.

[91] F. T. Miles y H. Soodak. *Nucleonics.* 11, No. 1, 66 (1953).

[92] S. Glasstone y M. C. Edlund. *The Elements of Nuclear Reactor Theory.* D. Van Nostrand Co., Inc., Princeton, N. J., 1952, pages 30 et seq.

[93] Dalin Zhang Wenxi Tian Suizheng Qiu G.H. Su Zhiwen Dai, Chenglong Wang. *Design and analysis of a free-piston stirling engine for space nuclear power reactor.*

[94] Daniel Zwillinger. *CRC standard mathematical tables and formulas.* chapman and hall/CRC, 2018.

[95] Shanqing Yan Z.Z. Guozhu Qian. *Principle and Design of Stirling Engine.* 1987.